On the Efficiency of Multi-Source Energy Harvesters

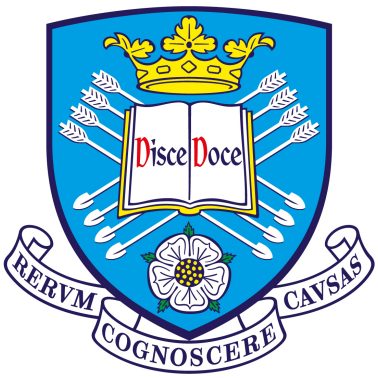

Julian Gosliga

Supervisor: Professor David Wagg

Department of Mechanical Engineering

University of Sheffield

This thesis is submitted to the University of Sheffield

for the degree of *Doctor of Philosophy*

November, 2019

To Cariad, for being there from start to finish.

Acknowledgements

First and foremost, I would like to thank Professor David Wagg for providing an incredible amount of encouragement and assistance throughout, and being a constant source of solid academic advice. The discussions during our meetings were both interesting and insightful, and if I was ever stuck, a conversation with David would always lead to a multitude of fresh ideas. I would also like to thank Dr Olga Ganilova for seeing me through my first year and providing inspiration for the project. Furthermore, I wish to thank Professor Keith Worden for his advice during a crucial period of my PhD. (One meeting in particular still stands out in my memory.) I would like to acknowledge the EPSRC for providing the funding, without which this project would not have been possible.

For their help with setting up my experiments, providing the necessary equipment and showing me how to use it, as well as practical advice on how to perform the experiment, I thank Jamie Booth, Matthew Hall and Chris Todd.

My gratitude goes out to the entire RD12b/RD14 office for helping me maintain my sanity through a seemingly endless supply of tea and Cosmos. I am grateful to the Dynamics Research Group for all their help and advice, especially these past few months. A special mention goes out to Jed, who was a close friend even before I started my PhD. Knowing that Jed would be in the office helped me to go in, even on my most difficult days.

I thank my family: my parents for their never-ending interest in my work, their support, and for teaching me to question everything; and my brother, Raymond, who arguably gave me the idea to undertake a PhD in the first place (and never let me forget it).

Alongside my family, I wish to thank my friends. The first year of my PhD would not have been the same without Jack and Dave, there were some great times in that house. Of course Sheffield life would not have been complete without Alex, Sophie, Sam, Chandy, Scottish Alex, and Ruth—a group that, by sheer coincidence, includes most of the members of General Panic, as well as most of the core fan base. To two of the finest housemates who ever lived: Simon, your ability to remain upbeat, even while working every waking hour, is something we can all learn from; and Dutt, may the Force be with you, *always*.

Abstract

Energy harvesters can be used to provide small amounts of power in remote locations. Applications include: powering wireless sensor networks and powering microelectromechanical systems. A wealth of different designs exists for harvesting energy from different sources, including designs which harvest from multiple sources simultaneously. However, there are no universally accepted metrics for assessing the performance of energy harvesters; this can make it impossible to compare designs in any meaningful way.

The first part of this thesis develops a domain-neutral framework for describing and analysing the behaviour of energy harvesters. This involves introducing a system of dimensionally consistent analogies into energy harvesting. Using this domain-neutral and dimensionally consistent framework, it is possible to come up with general expressions for the behaviour of single-source energy harvesting systems. This approach is then validated experimentally for single-source energy harvesters.

The second part of this thesis involves extending the theoretical analysis to multi-source energy harvesters. Using the system of analogies defined in the first part of the thesis it is possible to create an n-degree-of-freedom matrix representation of a multi-source energy harvester. This enables us to derive expressions which are valid for both single-source and multi-source energy harvesters. The expressions for the maximum power absorbed by an energy harvesting device are shown to be independent of the number of sources, as well as any static coupling or coupling through material effects (e.g. piezoelectric). Numerical simulations are used to explore the validity of these expressions for various system configurations driven with a mixed stochastic-deterministic input signal. From the results of these numerical simulations, a practical approach for estimating the efficiency of an energy harvester using the maximum power absorbed as a theoretical limit is described.

The third part of this thesis describes experiments which validate the theoretical analysis. These experiments are used to provide an example of how to calculate and compare the efficiency of energy harvesting designs.

Contents

List of Figures

List of Tables

1

Introduction and Literature Review

Energy harvesting refers to the conversion of energy, readily available in the environment, into useful energy to provide power for isolated systems, such as wireless sensor nodes, or small-scale systems, such as microelectromechanical systems or nanoscale devices. This is distinct from renewable energy in terms of scale and application, as renewable energy is intended for generating electricity on a large scale to power structures or even entire countries. Due to size constraints, energy harvesting devices are limited in the amount of energy they can produce. They do however possess advantages over traditional methods of power delivery, as they remove any reliance on an external power source. They also remove the need for batteries, which allows designers to create self-powered devices that can be embedded within structures. Due to this combination of advantages and limitations, energy harvesters are popular for devices with low or intermittent power requirements such as condition monitoring systems. Additionally, energy harvesting devices are popular wherever mobility or maintenance free operation is required, for example, tracking devices attached to wildlife or implantable devices.

Recently, there has been interest in harvesting energy from multiple sources as a means to improve the output and reliability of a device. This is similar to the way that solar panels and wind turbines are often used together to provide consistent power. These multi-source energy harvesters have found popularity in nanoscale devices, where the amount of energy that can be converted from any one source is limited by the size of the device. Multi-source energy harvesters are also popular in electrical engineering, where it is important that wireless sensor networks receive a steady flow of power, in spite of intermittent energy sources. However, the field of multi-source energy harvesting is currently split into these two distinct areas, which limits the development of new ideas and technology.

With the wide range of possible energy sources and operating environments, optimising energy harvesting devices is no easy task. Typically devices are optimised with respect to a specific operating condition, which limits the amount of global optimisation across the range of possible designs. Global optimisation of designs is apparent in fields such as solar and wind energy, facilitated by general expressions for the efficiency of such devices. General expressions for the efficiency—also known as effectiveness metrics—are not widely used in energy harvesting. Possible reasons for this include: the variety of different energy sources, the wide range of disciplines exploring energy harvesting, or perhaps there has previously not been sufficient motivation. The motivation for global optimisation through effectiveness metrics will be described in the following literature review, with a particular focus on the need for a general effectiveness metric for multi-source energy harvesters. The rest of the thesis will describe the development of a general effectiveness metric that is applicable across the full range of sources and disciplines.

The following sections will feature a literature review briefly covering the history of energy harvesting, through to the development of multi-source energy harvesters, with additional discussion of current energy harvester effectiveness metrics. Section 1.1 will provide a short summary of key developments in the field of energy harvesting, with a focus on vibrational energy harvesting. This section is intended to provide context and justification for the assumptions and practical decisions which feature in the rest of this thesis. Section 1.2 will include an in-depth discussion of the available multi-source energy harvesters out there, to give an idea of the wide variety of solutions available, as well as any general trends in the field. Section 1.3 will provide a critical evaluation of the applicability of existing efficiency and effectiveness metrics for energy harvesters. Section 1.4 will provide a summary of the main findings from this literature review chapter and describe the direction for the rest of the thesis.

1.1 Energy Harvesting Methods

Over the past few decades, energy harvesting has grown into a diverse field encompassing many different disciplines. This diversity is reflected in the range of topics discussed in review papers on the subject. A review paper by Harb [29] covered energy harvester theory and design, as well as circuit design. This review featured a direct comparison of 18 state-of-the-art harvester designs, utilising energy sources such as vibration, heat and radio-frequency (RF) electromagnetic radiation. As one of the main applications for energy harvesters is powering wireless sensor networks, circuit design is an important

area of discussion. A discussion of circuit design, in addtion to a taxonomy of energy hravesting sources, was included in a comprehensive review article by Shaikh and Zeadally [65]. This review compared approximately 80 harvester designs directly, incorporating sources such as: vibration, thermal, RF, solar, fluid flow and physiological sources. This shows the breadth of topics included in the field of energy harvesting.

The rest of this section will describe how vibration is one of the most widely available sources for energy harvesters; this is especially true for human-powered devices. There will be a focus on vibrational energy harvesting using piezoelectric materials. As these materials directly convert vibration into electricity,[1] they present a useful case when examining the theoretical behaviour of energy harvesters. A practical reason for choosing to focus on piezoelectric materials, is that they are easy to integrate into structures, and are generally a popular choice for vibrational energy harvesters.

Sources for Energy-Harvesting

One of the main applications for energy harvesting lies in powering wireless sensor networks. Within this theme of wireless sensor networks, monitoring a patient's health using wearable or implanted sensors has recieved significant attention [71, 47, 59]. Energy harvesting devices are well suited to this application for a variety of reasons: the human body provides a readily available source of continuous energy; the power requirements for medical implants and wireless sensor networks match the output of current energy harvesting devices; and replacing batteries may require surgery, so there is a great benefit to moving away from finite power sources.

Out of the many sources available for energy harvesting, kinetic and solar sources provide the greatest power output [60, 54]. We can, however, exclude solar energy when discussing implantable devices. Mitcheson et al. [47], Romero [59] and Sue and Tsai [71] all conclude that out of the three main sources available for energy harvesting within the human body, kinetic energy tends to be the more abundant than thermal or chemical energy. Thus the following subsection will discuss vibrational energy harvesting, due to its relative popularity and wide applicability. Additionally, as will be demonstrated, the theory used to describe vibrational energy harvesters can be used to develop a general dynamic theory, which is directly applicable to other forms of energy harvesting.

[1] The exact mechanism through which piezoelectric materials convert an applied mechanical stress into electrical charge is discussed in Section 2.1.

1.1.1 Vibrational Energy Harvesting

Here we will use vibrational energy harvesting as a catch-all term for all kinetic (mechanical) energy harvesters (with the exception of fluid flow harvesters). There are numerous methods and geometries for harvesting kinetic energy; however, the underlying physical principles for any design are largely determined by the transduction method. Traditionally, vibrational energy harvesting has focused on piezoelectric, electrostatic or electromagnetic energy harvesting [78]; whereas, more recently, developments in the manufacture of exotic materials have seen the rise of magnetostrictive, electrostrictive, and magnetoelectric devices. This can be seen by the inclusion of these devices in more recent review papers by Narita and Fox [49] and Siang et al. [67]. Whilst there is currently a wide variety of materials and methods for harvesting vibrational energy, they all fulfil the same function: converting mechanical energy to electrical energy. This subsection will discuss some of the seminal vibrational energy harvesting papers.

One of the earliest papers to discuss vibrational energy harvesting is a study by Williams and Yates [78], describing how a system driven by a harmonic source, in theory, be used to power microelectromechanical systems (MEMS) technology. The harvester proposed in this study uses electromagnetic transduction, whereby a moving magnet induces an electric current in a coil of wire. The following year, Umeda et al. [74] presented one of the first papers to discuss energy harvesting using piezoelectric materials. This study used mechanical-electrical analogies to examine the coupling between these two domains, this is in contrast to Williams and Yates [78], where only the mechanical domain was considered in detail. The first published example of an electrostatic harvester came from Meninger et al. [43], five years after it had been proposed by Williams and Yates [78]. One possible reason for this delay could be the relative complexity of such devices. An electrostatic harvester (in the voltage constrained case) relies on a varying capacitance affecting the charge held on said capacitor, whilst the voltage is held constant. To create this voltage, the capacitor must be charged initially, which is not the case for piezoelectric and electromagnetic harvesters. The complexity of maintaining the correct voltage across the capacitor at all points in the cycle whilst harvesting energy makes using some form of control circuit essential. [74, 78, 43] outline the three main transduction methods used in vibrational energy harvesting: electromagnetic, piezoelectric and electrostatic.

Later papers built these three initial designs, typically optimising and comparing the methods presented for specific applications or attempting to widen the number of practical applications for a particular design. Kymissis et al. [34] compared the effectiveness

of two different piezoelectric designs with an electromagnetic transducer for use in a shoe-based energy harvesting device. This study demonstrated that energy harvesting could be used to power useful electronics, which in this case was a radio-frequency identification (RFID) tag transmitter. Another finding of this study was that, while the electromagnetic harvester produced more power than either of the two piezoelectric harvesters, it seriously affected the gait of the user. Roundy et al. [63] build upon the design presented by Meninger et al. [43] by exploring and optimising alternative designs for electrostatic energy harvesters. Roundy et al. [63] also make use of physical analogies to consider both the electrical and mechanical domains when modelling the behaviour of the energy harvester. Work by Glynne-Jones et al. [23] developed electromagnetic energy harvesters further by proposing a four magnet generator—traditionally two magnets were used—as a method for increasing the voltage produced. Already, we begin to see the proliferation of available designs, as each study attempts to overcome the limitations of previous designs.

One of the consequences of the wide variety of operating conditions for energy harvesting devices is that there is an even wider variety of experimental conditions used when testing these devices. The inputs for an energy harvesting device can be broadly classified as *stochastic* or *deterministic*. With stochastic inputs, the forcing is random and is typically either generated numerically, or measured from a real-world environment. Deterministic inputs, on the other hand, are entirely predictable and use harmonic forcing at a specific frequency or, in the case of broadband excitation, a range of frequencies. The following examples show how the same operating environment can be used to provide both a stochastic and deterministic input for experimental results: Glynne-Jones et al. [23] attached an energy harvester directly to a car engine, which provided a source of stochastic vibrations; Sodano et al. [68] simulated a realistic operating environment, by measuring the stochastic vibrations of a car air compressor and then reproducing these using a shaker. This is in contrast to Meninger et al. [43], who measured the vibrations of a car engine, but only used a single harmonic frequency in their experiment, giving a deterministic input.

This variation in the frequency of vibrations found in the environment limited the practical application of early (linear) energy harvesting designs, as these were designed to operate at a specific resonant frequency. With linear energy harvesters, any shift in the input frequency away from the resonant frequency of the energy harvester significantly reduces the power absorbed. In practical applications, purely harmonic inputs are unlikely to exist and, if they do exist, the excitation frequency is unlikely to remain constant.

Two of the most popular solutions to this problem are: a) somehow changing or *tuning* the natural frequency of the device to match the input frequency, or b) change the design so that it has a flatter frequency response (wide bandwidth). The two main methods for tuning the natural frequency of the device are active and passive tuning, although Roundy and Zhang [62] found that the power gained from using active tuning was less than the power required to actuate the active tuning mechanism. Wide bandwidth designs are discussed in a paper by Roundy et al. [64], where it is suggested that including more proof masses—thereby increasing the number of degrees of freedom—widens the bandwidth of the devices.

It has since been discovered that by creating a device with two stable states (bistable), the bandwidth of an energy harvester can be increased. A bistable system exhibits *non-linear* behaviour. Systems which behave non-linearly typically show an increased response over a broad range of frequencies when compared to linear systems. Exploiting non-linearities to give a broadband frequency response has the advantage of not significantly increasing the size and complexity of a device. A bistable energy harvester was created by Baker et al. [5], where a beam with piezoelectric patches attached was compressed until it buckled; however, a large acceleration was required to cause the beam to *snap-through* from one stable state to another, limiting the applicability of the design. A bistable device was created by Cottone et al. [19] using magnets, where the acceleration required for snap-through to occur could be adjusted via the position of one of the magnets. A bistable composite material was created by Arrieta et al. [3], using an asymmetric lay-up of carbon fiber reinforced polymer with integrated piezoelectric patches, which required half the acceleration required in [5] to achieve snap-through. It should be noted that bistability is not the only method for creating a non-linear device with a broadband response. Duffing-type non-linearities were used by Green et al. [24] to improve the broadband performance of a mono-stable harvester, while also reducing the size of the device. Non-linear damping was used by Ghandchi Tehrani and Elliott [22] to not only expand the dynamic range of a particular energy harvester, but also improve the power output at resonance. In general, it is better to design a device to have a broadband response, unless you can be certain that there is a constant harmonic input present.

Piezoelectric energy harvesting

While the energy harvesting methods mentioned previously (electrostatic and electromagnetic transduction) each have their advantages and disadvantages, further discussion will be limited to piezoelectric energy harvesting devices. Piezoelectric devices are

useful to examine as they involve no moving parts and are mathematically simple to describe, since they directly convert mechanical strain energy into electrical energy. The theoretical behaviour of piezoelectric devices has already been accurately described in work by Sodano et al. [69], where two electromechanically coupled equations accurately predict the behaviour of a piezoeleciric harvester. A review by Anton and Sodano [2] suggests that, up to that point, piezoelectric devices had received the most attention out of electromagnetic, electrostatic and dielectric energy harvesting devices. The reason cited was that piezoelectric devices are easy to incorporate into systems, which would explain their prevalence in multi-source energy harvesters, and the continued popularity that piezoelectric energy harvesters enjoy today. This ease of integration over other devices (for example, electromagnetic devices) was first demonstrated in the study presented by Kymissis et al. [34], as the piezoelectric devices had little effect on the gait of the user. The popularity and simplicity of piezoelectric materials makes them a useful case for studying the general behaviour of energy harvesting devices.

The two main approaches to improving the conversion efficiency of piezoelectric energy harvesters are creating more efficient materials, and utilising geometric effects. Creating better piezoelectric materials usually involves improving the coupling efficiency—the proportion of mechanical energy converted to electrical energy—while simultaneously improving the durability. Both of these properties are important as coupling efficiency directly affects power output, and durability determines the lifetime of the device, as well as being indirectly linked to output. Altering these properties for piezoelectric materials is not limited to chemistry and material science: creating composite materials using piezoelectric materials in combination with other materials can also be used to achieve the desired properties. These *piezo-composite* materials are typically constructed using the piezoceramic lead zirconate titanate (PZT) and some form of epoxy resin. However, commercially available piezo-composite materials are usually designed with the aim of improving the actuation performance. Therefore, in energy harvesting applications, non-composite PZT can outperform these piezo-composite materials, particularly for stochastic inputs, as demonstrated by Sodano et al. [70]. That being said, it is possible to design piezo-composites to offer performance advantages, as in the earlier example by Arrieta et al. [3], where the authors created a piezo-composite with inherent non-linearities to improve broadband energy harvesting.

Geometric effects can improve harvesting efficiency by introducing non-linearities or otherwise changing the dynamic behaviour of the device (for example, frequency up-conversion), amplifying the stress through the piezoelectric materials, or utilising the stronger coupling modes (this will be elaborated on in Section 2.1). These geometric

effects can all be seen in the cymbal transducer design by Kim et al. [33], where the cymbal shape amplifies stress and the effective piezoelectric coefficient, while also introducing non-linear behaviour. Optimising the conversion efficiency of a piezoelectric energy harvester in practical systems will usually involve matching material and geometry to the input and size contraints on the device.

1.2 Multi-Source Energy Harvesting

Multi-source energy harvesting is a term that is not currently well-defined, and is often used synonymously with hyrbid energy harvesting. All multi-source energy harvesters are hybrid devices, but not all hybrid devices use multiple sources. Hybrid energy harvesting refers to devices which incorporate at least two energy harvesting methods, for example piezoelectric and electromagnetic transduction. Multi-source energy harvesting, on the other hand, refers to devices which incorporate at least two energy harvesting methods *and* convert energy from *at least two sources of distinct energy types*, for example heat (thermal) and vibration (mechanical).

This distinction has implications for the maximum output of an energy harvester: a hybrid energy harvester can use multiple transduction methods simultaneously to capture a larger proportion of the energy available from a single source, yet it is still limited by the total amount of energy available from that one source. The limit on the energy available to a multi-source energy harvester will instead be the sum of the energy available from all of the sources that it can utilise. This also demonstrates the importance of this distinction with respect to the reliability of energy harvesting devices: a hybrid energy harvester designed for a single source will not generate energy if that source is absent, even if it uses multiple transduction methods. Imagine instead that we have a multi-source hybrid energy harvester designed to capture both solar and mechanical energy. If this device is placed in an environment where vibration is absent, it can still generate electricity from available solar energy. From this definition of multi-source energy harvesting, we can see the advantages to utilising multiple sources of distinct energy types in terms of both output and reliability.

For this discussion on multi-source energy harvesting, we will also make a distinction between the terms *energy harvester* and *generator*. For example, we may say piezoelectric energy harvester or piezoelectric generator. The two terms, harvester and generator, are used interchangeably in the literature to mean a device which produces electrical energy. However, we will use two distinct meanings in the interest of avoiding confusion: the term energy harvester will be used to refer to the device as a whole, while

generator will refer to the component in the energy harvester which converts energy from one particular source. Using these definitions, we can say that a multi-source energy harvester is composed of individual generators. For example, a multi-source energy harvester which utilises mechanical and thermal sources might be composed of a piezoelectric generator as well as a thermoelectric generator. The term generator is synonymous with the term *cell* for certain sources, i.e. a solar cell is the same as a solar generator.

This section is designed to give an overview of the current literature regarding multi-source energy harvesting. Due to the overwhelming volume of work relating to energy harvesting in general, it was necessary to pick out key papers and studies to highlight where there was significant progress or novelty. However, since multi-source energy harvesting is a relatively new development, it was possible to perform a comprehensive review of available designs. One thing that soon becomes obvious is the lack of theoretical work in this field relating to the general behaviour of multi-source energy harvesters. To this authors knowledge, there has only been one study (Alomari et al. [1]) regarding multi-source energy harvesters to employ coupled electromechanical models—as opposed to simply using equivalent electrical models. In other words, to date, there has been no attempt to optimise, or even describe, the overall dynamic behaviour of a multi-source energy harvester. This highlights that, while energy harvesting overall is well-established as a field, the area of multi-source energy harvesting is still undeveloped. Another point to note is that the concept of multi-source energy harvesting appears to have arisen independently in two different areas of energy harvesting research. Sections 1.2.1 and 1.2.2 will discuss the developments in these two areas. Section 1.2.3 will discuss the major trends in multi-source energy harvesting as a means of concluding this section.

1.2.1 Small-Scale Multi-Source Energy Harvesting

One area where multi-source energy harvesting has become popular is nanotechnology. Research in this area presents either a physics- or chemistry-based approach to the topic. Generally speaking, energy harvesting is popular in nanotechnology as the low-power requirements of nanoscale devices match the output for current energy harvesting technologies. More specifically, in nanotechnology, size is usually a limiting factor, which in turn limits the efficiency of the device; therefore, it becomes necessary to use multiple sources. The nature of nanoscale technology means that researchers are constantly trying to make everything more compact, resulting in the incorporation of ever more sources into increasingly integrated designs. Originally, the designs

[80, 28, 40, 81, 82, 83, 86] were largely of a sandwich-style composite construction, with the individual harvesters (usually composite materials themselves) layered on top of one another. There were several attempts to integrate the harvesters into either the same layer [15, 79] or onto a single fiber [39, 52, 4, 53]. The sandwich designs for nanoscale multi-source energy harvesters are easier to design and manufacture, though less compact than integrated designs. Using the fact that piezoelectric and pyroelectric[2] effects occur within the same material, Yang et al. [81] and Zi et al. [88] were able to design harvesters combining the integrated and sandwich design. These nanoscale devices are all capable of harvesting energy from two sources *simultaneously*.

There are a wide variety of different sandwich-style designs for multi-source energy harvesting. Current designs link back to a study by Xu et al. [80]. In this study, a nanoscale device—capable of harvesting both mechanical and solar energy—was created by combining a piezoelectric zinc oxide (ZnO) nanowire-based generator (described by Wang et al. [77]) with a solar cell. To harvest mechanical and chemical energy, nanowires—this time made from the piezopolymer polyvinylidene fluoride (PVDF)—were combined with a biofuel cell (Hansen et al. [28]); however, the resulting device was deemed too large for practical applications. To create a flexible energy harvesting device, capable of harvesting both mechanical and thermal energy, a ZnO nanowire-based generator (nanogenerator) was combined with a flexible thermoelectric generator (Lee et al. [40]). It was found that this combination was synergistic: the device preserved the higher voltage output of the thermoelectric generator, along with the higher output current of the ZnO nanogenerator. A flexible energy harvester was developed by Yang et al. [81], using the piezopolymer PVDF to harvest both mechanical *and* thermal energy. This was then combined with a flexible solar cell, thus creating a device capable of havesting three different types of energy: mechanical, thermal and solar. We are at a point where these sandwich designs can be used to harvest energy from three sources simultaneously, and with further development in fabrication techniques, it is conceivable that these devices could incorporate four sources simultaneously.

We see that piezoelectric materials are a popular choice for multi-source energy harvesters; although, the piezoelectric effect is not the only method used for converting between mechanical and electrical energy on a nano-scale. Another material effect which is useful for energy harvesting is the triboelectric effect. The triboelectric effect causes certain materials to become charged through friction, and is responsible for static electricity. The combination of a triboelectric nanogenerator and an electrochemical cell

[2]Pyroelectricity is a property displayed by certain piezoelectric materials, whereby they convert thermal energy into electrical energy. A more detailed description can be found in Section 2.1.2.

was used by Yang et al. [82] to harvest mechanical and chemical energy, in a device more compact than that presented by Hansen et al. [28]. Other examples of multi-source energy harvesters which combine the triboelectric and pyroelectric effect can be found in papers by Yang et al. [83] (using PZT) and Zhang et al. [86] (using PVDF). These two devices are capable of harvesting both mechanical and thermal energy, through the triboelectric and pyroelectric effect respectively; however, since PZT and PVDF are both capable of harvesting extra mechanical energy, using these materials to only convert thermal energy leaves them under-utilised. A harvester presented by Zi et al. [88] fully utilises the PVDF by harvesting mechanical energy through both the piezoelectric *and* triboelectric effect, while also utilising the pyroelectric effect to harvest thermal energy. Referring back to Section 1.1.1, we see two other methods for converting motion into electricity: the electromagnetic and electrostatic transduction methods. These two methods are not suited to nanoscale devices due to the relative complexity of their construction.

As mentioned previously, size is a limiting factor for nanoscale devices; therefore, researchers have sought to completely integrate the various components required for nanoscale multi-source energy harvesting into a single structure. To integrate both mechanical and solar energy harvesting in a single ZnO nanowire, Lee et al. [39] coated the individual ZnO nanowires with n-type and p-type nanoparticles, thereby eliminating the need for a seperate solar cell. To create a more integrated and compact solution for harvesting mechanical and solar energy, Xu and Wang [79] improved upon their original design by directly integrating the ZnO nanowires within a solar cell. A similar solution was proposed by Choi et al. [15], where they utilised a polymer instead of glass in the solar cell, thus creating a flexible integrated harvester. By integrating both a ZnO nanowire generator and a biofuel cell onto a single carbon fiber, Pan et al. [52] overcame the size limitation of the device proposed by Hansen et al. [28]. The integration of ZnO nanowire solar cells and piezoelectric nanogenerators has been achieved using a single micro-scale plastic fiber in two different ways: the approach taken by Bae et al. [4] coated the plastic fiber with a thin aluminium film, with ZnO nanowires attached to the film and the solar cell and nanogenerator placed intermittently along the wire; this is in contrast to the approach taken by Pan et al. [53], who used a clear optical fiber to channel sunlight into a solar cell attached directly to the wire, where the solar cell was itself encased by a piezoelectric nanogenerator. One of the simplest methods for achieving integrated multi-source energy harvesting is the use of materials displaying both piezoelectric and pyroelectric effects. This approach was used by Lee et al. [38] to create a multi-source energy harvester using a single material. By using a single material,

the device could harvest both thermal and mechanical energy, whilst also being flexible and highly stretchable. Integrated designs to date have only included two sources, this is possibly due to the relative difficulty in fully integrating more effects into a single device.

There are three devices that fit into this area of research, but are not necessarily designed for nanoscale operation. The first device, presented by Guo et al. [27], was a solar cell and thermoelectric generator combination, designed to improve the overall efficiency of the solar cell. Some of the light that hits a solar cell is converted into heat instead of electricity. This heat further degrades the performance of the solar cell. Including a thermoelectric generator in this design not only removes some of this heat, but also converts it into useful electrical energy. The second device, presented by Alomari et al. [1], is a piezoelectric-pyroelectric cantilever. In describing this device, the author modelled the dynamics of the beam and included them in an electromechanical analysis; despite this, the author stopped short of modelling the complete thermo-electrico-mechanical system. The third device, presented by Zhong et al. [87], used a graphene based solar cell to capture solar energy, as well as harvesting energy from water flow. Both the first and third device mentioned here need to be illuminated for their secondary energy harvesting effects to become active—these effects are thermal gradients or charge transfer, respectively. This leaves the question of whether or not these two devices truly fit the definition of multi-source energy harvesters open to debate.

1.2.2 Power Management for Multi-Source Energy Harvesting

Another area where multi-source energy harvesting has become popular is electrical engineering. Here we propose two main reasons why multi-source energy harvesting has become a topic of interest in electrical engineering: firstly, multi-source energy harvesters may present an interesting case for studying the design of power management circuits, as integrating the inputs from many varying and unpredictable sources is not straightforward; secondly, there has been interest in developing self-powered wireless sensor nodes, where the transmitter, sensors and energy harvesting are all fully integrated into a single device. Multi-source energy harvesting lends itself well as a solution for creating self-powered wireless sensor nodes as it offers greater reliability.

Interestingly, the topic of of dealing with power input from multiple sources is not new to electrical engineering, with research on combining the output of macro-scale wind and solar sources going back to a study by Borowy and Salameh [10]. However, these earlier studies are distinct from energy harvesting as they deal with renewable energy.

The first paper to deal with multi-source energy harvesters was a design presented by Park and Chou [55] which combined wind and solar energy on a small scale. For energy harvesters, the design constraints and applications are very different to the considerations for macro-scale renewable energy production—for example, energy harvesters, unlike renewable energy, can be used indoors. The challenges presented by energy harvesters operating indoors, was described in a paper by Tan and Panda [72]; where, not only is the power available from artificial light much less than from the sun, the power is only available during business hours.

The use of separate circuits for each source is a common feature in the majority of the electrical engineering research on multi-source devices. The device proposed by Park and Chou [55] has a separate conditioning circuit for each source, whereas for the nanoscale devices described in Section 1.2.1, the output from the two sources was usually combined directly. Separate circuits are used for each source in order to: a) convert alternating current (AC) sources into direct current (DC) sources, and b) to ensure that the impedance of the source matches the impedance of the energy harvesting device. Impedance matching is important for achieving maximum conversion efficiency from a source, and DC current is required for charging batteries and capacitors. The use of separate circuits results in a heavy focus on improving the circuit architecture, rather than the materials or geometry used.

These multi-source energy harvesters again feature vibration as a popular energy source, with several designs featuring piezoelectric cantilevers in their design. In several designs, piezoelectric generators were combined with solar cells: in work by Colomer et al. [17], a micro-scale hybrid energy harvester used a Quick Pack PZT cantilever as the piezoelectric generator; a design by Guilar et al. [26] featured energy storage (using capacitors) directly incorporated into an energy harvester ; and in work by Yu et al. [84], one of the sources was an arrary of PZT cantilevers (as opposed to having a single cantilever) and the harvester used only one power conditioning circuit for both sources. These three designs represent various methods for combining mechanical and solar sources. Mechanical and solar sources were also combined with a thermal source by Colomer-Farrarons et al. [18] through the use of a thermoelectric generator; this design had circuitry integrated onto a single chip. This same combination of sources (mechanical, solar and thermal) was used by Bandyopadhyay and Chandrakasan [6], where the use of a novel *maximum power point tracking* scheme improved the conversion efficiency of the circuit. Into this combination of mechanical, solar and thermal sources, Dini et al. [20] introduced yet another source: ambient radio-frequency (RF) radiation. In this study, a rectifier (AC to DC converter) was used with the mechanical (piezoelectric)

input, while maximum power point tracking was used for solar, thermal and radio-frequency sources. A piezoelectric generator was used by Vankecke et al. [75] to overcome the limitations of using a thermoelectric generator on its own. This study found that the temperature gradients required for the thermoelectric generator were not always present, therefore a piezoelectric generator was used to supplement the power output.

Harvesting energy from ambient RF radiation has received interest for multi-source energy harvesting. An early design for harvesting both RF and thermal energy was proposed by Lhermet et al. [41], although this device could not operate both sources simultaneously—instead switching between the two sources and the battery, depending on which one was providing the most power. For harvesting both RF and solar energy, researchers have often combined antennas with solar cells. The idea of combining antennas and solar cells was initially reported by Tanaka et al. [73], where the main goal was to save space by integrating radio transceivers with the solar panels of a satellite. This idea was then used by Georgiadis et al. [21] to form a multi-source energy harvester by using the antenna to harvest energy as opposed to transmitting signals. The design for an energy harvester utilising both RF and solar energy was further optimised by Collado and Georgiadis [16], through the use of more detailed simulations and experimental measurements. This combination of RF and solar energy is also explored by Niotaki et al. [51], where an improved circuit is used to increase the efficiency of the device; this paper also examines the application of the proposed harvester. One of the limitations with RF energy harvesting, is that these harvesters have a *dead-zone*, where the device cannot produce a sufficient voltage to power the rectifying devices. To overcome this limitation, a piezoelectric generator was used by Nguyen et al. [50] to provide the necessary voltage to power the rectifying circuits, thus extending the effective range of the RF harvester.

1.2.3 Trends in Multi-Source Energy Harvesting

Of the 33 devices examined, 25 use piezoelectric materials for either vibrational or thermal energy harvesting. In comparison, 20 of the devices examined use some form of solar energy harvesting. Due to their overwhelming popularity in multi-source energy harvesters, piezoelectric materials will form the basis for the theoretical and experimental work presented in this thesis.

All of the above devices have shown increased power output through combining multiple sources, but there remains the question of which combination of sources—or hybridisation—is the most effective for a given application? Due to the large number

of possible combinations, it would be inefficient to design devices through trial and error. Additionally, comparing the effectiveness and efficiency of these combinations is made more complicated by the introduction of multiple forms of energy. To facilitate the comparison of these possible combinations, it would be useful to develop a general effectiveness metric. Using such an effectiveness metric, it would be possible to identify the optimal combination of sources for a given application.

Due to the interdisciplinary nature of multi-source energy harvesting, any framework would need to remain domain-neutral—using terminology that is common across disciplines. This requirement for domain-neutrality is further demanded by the fact that there are two very distinct areas where multi-source energy harvesting is of interest. Each of these two areas has its own terminology and methods for describing multi-source energy harvesters. However, there is common ground between these two areas, as the physics underlying any approach to multi-source energy harvesting is the same, regardless of the terms used to describe the system. The general dynamic behaviour of these devices—described using domain-neutral terminology and analogous mathematical expressions—could form the basis for a theoretical framework for describing the overall behaviour of multi-source energy harvesters. This theoretical framework could also provide a means of describing the general behaviour of the entire energy harvesting device, including any attached circuitry. This would open up more opportunity for the optimisation of multi-source energy harvesters.

1.3 Energy Harvester Efficiency

It is not possible to say with confidence that the effectiveness of energy harvesters has increased with time. The reason for this is that review papers in the field of energy harvesting often compare energy harvesting designs using their power output. While at first this may seem logical, simply using the power output to compare designs completely neglects the fact that the input conditions for harvesters can vary considerably. This may explain that, while examining the references in Table 3 in the review by Harb [29], it would appear that there has been little to no progression in the effectiveness in energy harvesters, with earlier designs often exceeding the power output quoted for more current designs. This trend may, however, instead be due to more conservative estimates of the energy available to these devices, and represent more accurate methods of characterising the inputs for energy harvesters. In addition, the size of energy harvesters affects the power output, and we would naturally expect a large device (with the same efficiency) to harvest more energy than a smaller device. The size (volume) for devices is included

alongside their power output in Figure 23 in the review by Narita and Fox [49], but this still does little to help us determine which design is actually more effective— and, if we look more closely we see that more recent designs do not always have higher outputs. Again this may simply be because modern devices are designed for nano or micro scale operation. In either case, we can see that *it remains unclear* whether or not energy harvesters have improved over time. This leads to a myriad of available energy harvesting designs, but no clear idea as to which designs are worth developing further.

This is in stark contrast to renewable energy, where there is clear development and an obvious convergence of designs for wind turbines or solar panels. One key difference between the fields of renewable energy and energy harvesting is that, in renewable energy, there have been efficiency metrics available for a long time—with Betz [8] providing an efficiency metric for wind turbines and Shockley and Queisser [66] providing an efficiency metric for solar panels. While we cannot say for definite that the existence of an efficiency metric is the sole factor which led to a convergence of designs in renewable energy, we *can* say that (without resorting to trial and error) it is not possible to globally optimise designs without some form of comparison framework. It would, therefore, be reasonable to suggest that the development of a universal effectiveness metric has the potential to positively impact the development energy harvesters. It would, at the very least, enable us to state that energy harvesting technology has progressed over the years.

This of course raises the question: why are effectiveness metrics not widely used in energy harvesting? One possible reason could be that the amount of different disciplines where energy harvesting is of interest (mechanical engineering, materials, electrical engineering, physics, MEMS, nanoscale) makes it difficult to find a common language with which to express these metrics. A further reason could be the variety of inputs for energy harvesters. The inputs for solar and wind turbines are similar across all devices—the sun in one country can be modelled in the same way as the sun in another, with the main difference being intensity; the same is true for the wind. However, an energy harvester inside the human body will experience vibrations of a different nature to a harvester attached to a machine. Therefore, it is often the case that expressions for the efficiency of a device are limited to one specific application or design.

Despite these challenges, there have been attempts to develop more general effectiveness metrics for energy harvesters. The remainder of this section will evaluate the various metrics and limits on harvester performance which have been developed. Typically these metrics employ sets of assumptions on the system (linear or non-linear) and the input (stochastic or deterministic). The first attempts at developing effectiveness metrics focused on linear systems driven by deterministic inputs, as resonant energy harvesters

were popular at the time. However, these metrics became obsolete as energy harvesting solutions progressed to non-linear and stochastic systems. The selected effectiveness metrics have been developed for vibrational harvesters; although, as we will see in the remainder of this thesis, these expressions can be applied to any dynamic system. This thesis attempts to define a dimensionless metric—using efficiency as a basis—which has applicability across the full range of system types, inputs and combination of sources.

1.3.1 Linear Effectiveness Metrics

Linear effectiveness metrics are typically based around the maximum power absorbed at resonance by a linear system. There are two main approaches for developing these linear effectiveness metrics: dynamics based and electrical-mechanical analogy based. The dynamics-based approaches stem from the findings presented by Williams and Yates [78]: the generated power (electrical output power) of a vibration-driven device is proportional to

$$P_{out} = \frac{m\zeta_t Y_0^2 \left(\frac{\omega}{\omega_n}\right)^3 \omega^3}{\left[1 - \left(\frac{\omega}{\omega_n}\right)^2\right]^2 + \left[2\zeta_t \frac{\omega}{\omega_n}\right]^2} \tag{1.1}$$

where Y_0 is the amplitude of the input vibration, ω is the frequency of input vibration, ω_n is the natural frequency of the device, ζ_t is the damping factor of the transducer used, and m is the oscillating mass. This expression is normalised by Mitcheson et al. [45] with respect to the maximum displacement of the device with the aim of adapting the expression for the specific case of velocity-damped electrostatic energy harvesters. An alternative expression for a non-resonant form of harvester is presented by Mitcheson et al. [45], although this is still proportional to $Y_0^2\omega^3 m$. This result was used to form the basis for a review by Mitcheson et al. [44], in which this normalised expression is used as the basis for a performance metric for comparing vibrational energy harvesters operating at resonance. We can see that for harmonic harvesters, the term $Y_0^2\omega^3 m$ clearly possesses some universality. These approaches develop an expression for the maximum mechanical power available, and then examine how the power is split over the electrical and mechanical impedances.

The electrical-mechanical analogy based approach models the entire system as an equivalent circuit, and directly derives the conversion efficiency, rather than the mechanical power available. The expression for the conversion efficiency is typically

expressed in terms of the coupling coefficients and quality factor.[3] An equivalent electrical-mechanical circuit model was used by Richards et al. [58] to develop an expression for efficiency based entirely around the electromechanical coupling coefficient k and quality factor Q. A through-and-across electrical-mechanical analogy was used by Roundy [61] to develop a general effectiveness metric. This general metric was successfully applied to electrostatic, electromagnetic and piezoelectric energy harvesters, giving the following effectiveness e:

$$e = k^2 Q^2 \frac{\rho}{\rho_0} \frac{\lambda}{\lambda_{max}}, \tag{1.2}$$

where ρ is the density of the design, ρ_0 is some reference density, λ is the actual transmission coefficient, and λ_{max} is the maximum transmission coefficient. The maximum transmission coefficient is itself related to the electromechanical coupling efficient. The issues with this as an approach are: firstly, it requires some calculation of density, which is not always obvious for energy harvesters due to the differences in geometry; secondly, it does not have a maximum limit, and so it is impossible to determine how close the performance of a device is to the optimum. However, this effectiveness metric does represent an attempt to develop a metric that is independent of the particular design of the device as well as the input, which is important for comparison between devices.

The potential usefulness of effectiveness metrics was demonstrated by Mitcheson et al. [46], where an expression for the maximum power was used to normalise the power output for a range of harvesters found in the literature. This use of effectiveness metrics to normalise the power outputs made it possible to examine trends in harvester effectiveness over time. Normalising the power output of the device with respect to the maximum power available to the device gives the efficiency. Any measure of efficiency is effectively normalised to that particular design and hence independent of the particular details of the system. This in turn enables a wide range of vibrational energy harvesting devices to be compared. Normalised power was also used by Beeby et al. [7] to examine trends in energy harvesters. In this study, the reported power for the harvesters was normalised with respect to the volume of the harvester in an attempt to give a power density which is independent of the size of the device. The reported power was also normalised with respect to the input by dividing the reported power by the square of the input acceleration. This author would argue that normalising with respect to the maximum output power—incorporating the input amplitude and frequency, as well as the mass of the device—is a

[3] The quality factor, or Q factor, describes the level of damping present in a harmonic oscillator, as well as the bandwidth of the oscillator.

more thorough approach than using volume and acceleration squared. This is due to the fact that this expression for maximum power already incorporates the size (mass) and input of the device, and derives directly from the physics.

A review paper by Mitcheson et al. [47] attempts to improve upon the effectiveness metric presented in [46]. This review shows the trend in energy harvesting output using a different effectiveness called the *volume figure of merit*. In this paper, similar metrics to [46] are utilised, except this time the maximum power is proportional to $\frac{1}{2}Y_0 Z_l \omega^3 m$, where Z_l is the internal motion amplitude. This expression for the maximum power includes the actual internal or relative motion of the device, and so can be considered as closer to the actual performance. An attempt is made to normalise this result to an arbitrary reference case, which is a linear harvester with the same volume and with a proof mass made of gold occupying half of this volume. The rationale given in the paper is that simply using the maximum power does not differentiate between devices with different proof mass densities or geometry. They also introduce the idea of a bandwidth figure of merit to give some idea as to how the device will perform under broadband excitation.

In some of the later attempts to develop effectiveness metrics, it is common to see the device output normalised with respect to volume. The use of volume for normalising the power output of a device has a key limitation: the volume of a device is not always easy to define. This can lead to confusion, as authors do not always define the dimensions or geometry of their device, and there is no consistent way in which this is done. Calculating the volume of a device requires several decisions to be made about which dimensions to use. For example, does the volume of a vibrational harvester include the volume displaced by the proof mass? Should only active components be included in volume calculations? Should the harvesting circuitry also be included? It is easier to find either the total mass or the proof mass of a design; this is also simple to report: 'The total mass of the device was...'

The use of a reference case is an attempt to differentiate between designs of different geometry and proof mass. A possible rationale could be that devices which are larger, tend to have a higher efficiency; therefore, using a reference case when developing an effectiveness metric may reduce the dependence of said metric on the size of the device. This author would argue that this relationship between size and efficiency is important, as it highlights the limitations on energy harvesters presented by miniaturisation. Furthermore, all of the effectiveness metrics discussed show that the power output of the device depends on the mass, whether this is directly in the expression or through the Q factor. This is because the mass determines how much mechanical energy a harvester

can absorb, which limits the amount of energy that can be converted into electricity. For these reasons, it makes the most sense to normalise the reported power output of energy harvesters with respect to mass, and not volume or a reference case.

1.3.2 Non-linear Effectiveness Metrics

We now move on to effectiveness metrics for non-linear energy harvesters. The effectiveness metrics presented by Richards et al. [58], Roundy [61] and Beeby et al. [7] rely on damping coefficients and Q factors, which limits them to linear systems. The effectiveness metric presented by Mitcheson et al. [44] can be used for non-linear systems. This highlights an advantage of using the maximum mechanical power available: it requires fewer assumptions regarding the behaviour of the mechanical system. The effectiveness metrics that calculate the electrical power directly all require some assumptions about the nature of the mechanical system, as well as any coupling present. A review on bistable energy harvesting by Pellegrini et al. [57] noted this and proposed the following non-dimensional performance metric

$$I = \frac{P_{\text{rms}}\omega}{ma_{\text{rms}}^2} \tag{1.3}$$

where P_{rms} is the root mean square (RMS) electrical output power, ω is the frequency, m is the mass, and a is the acceleration. Since the terms ma_{rms}^2/ω makes no assumptions regarding the underlying signal, we can assume that this expression generalises effectively across harmonic vibrational energy harvesters. The authors of [57] suggest taking the average over a range of frequencies

$$I_{a-b} = \frac{\int_b^a I \, \mathrm{d}\omega}{b-a} \tag{1.4}$$

where a and b are specific frequencies, and $b - a$ is the bandwidth of operation.

We now have some idea what the general performance metric for both linear and non-linear harmonic energy harvesters might look like, but not all inputs are harmonic and deterministic. There has been recent work concerning the performance of energy harvesters with purely stochastic inputs [35, 36, 37]. These papers build on a general dynamic theory presented by Langley [35], which shows that the power dissipated by a single-degree-of-freedom linear oscillator with a stochastic input is

$$P_{out} = \frac{\pi S_0}{2}, \tag{1.5}$$

where S_0 is the spectral density of the white-noise input. Further analysis by Langley [36] demonstrates that this expression for the maximum power absorbed applies to *all* linear and non-linear systems—with the power dissipated in this case being proportional to

$$P_{out} = \frac{\pi m S_0}{2}. \tag{1.6}$$

This paper also highlights an interesting approach for dealing with these coupled systems, whereby the coupled system equations can be treated separately when formulating the problem. The coupled system equations are then combined using a single state-space vector. Langley [37] extends this analysis to an n-degree-of-freedom system using Lagrangian mechanics, as well as covering both wideband and narrowband stochastic excitation. These works provide an expression for the maximum mechanical power available from a stochastic source, which we can use as the basis for an effectiveness metric for stochastic energy harvesters.

Of course, in reality, stochastic inputs are not always white noise. In reality, signals could contain a mix of stochastic and deterministic signals. A thesis by Hawes [30] explores the applicability of the limits developed by Langley [37] to non-white noise and systems with mixed inputs. However, Hawes states that the assumptions used in the Wiener theory limit the practical applicability of this approach to systems where the energy harvester has no significant effect on the base vibration. Therefore, to develop an effectiveness metric with wider practical applicability, it is necessary to seek novel methods for deriving these power bounds. Hawes [30] also discusses methods for predicting the probabilistic trajectories of non-linear systems driven by mixed stochastic and harmonic inputs. As mentioned in said thesis, knowledge of the entire joint probability density over the system response is often not required for energy harvesting applications. For the sake of developing a general effectiveness metric valid for non-linear systems with mixed stochastic and harmonic inputs, we will assume that both the power output and input excitation are measured. This allows us to simply use the mean square average of the input when developing expressions for the maximum power absorbed. A further reason for measuring the average power absorbed is that it does not require prior knowledge of the nature of the system response.

1.4 Conclusions

Energy harvesting is a popular choice for powering wireless sensor nodes as it allows them to be embedded in structures, and reduces the amount of maintenance required. Of all the energy harvesting sources available, vibrational sources are the most popular for human-powered and indoor applications. Energy harvesters utilising vibrational sources started off as linear harmonic oscillators, using either electromagnetic, electrostatic or piezoelectric transduction methods to convert mechanical energy into electrical energy. While these systems work well when excited at resonance, any shift away from resonance dramatically reduces the power output. Since in real environments, the frequency of vibrations rarely stays fixed, there was a pressing need to develop devices with a broadband response. The requirement for a broadband response led to non-linear systems being utilised in energy harvesting.

However, there are limits on the amount of power available from any one source, regardless of the energy harvester design. Therefore, once a design is well-optimised in terms of efficiency (or where efficiency is limited), the only way to improve the output of a device is to utilise additional sources. Utilising additional sources has the added benefit of improving the reliability of an energy harvester. There have been various experimental and simulated realisations of the concept of multi-source energy harvesters; however, there is no general framework for describing either the behaviour or performance of multi-source systems. This limits the amount of optimisation possible.

A universal effectiveness metric would enable the global optimisation of energy harvesting designs. This author proposes that some form of efficiency (similar to those used in solar and wind energy) is the most logical choice, as efficiency is a dimensionless measure, normalised (and hence independent) of the particular energy harvester design. Using such an effectiveness metric would enable a wide variety of energy harvesting technologies to be compared with one another, clearly highlighting the best designs. There have been various attempts to develop general effectiveness metrics for vibrational energy harvesters. Several of these generalise effectively across linear harmonic energy harvesters. However, the rise of stochastic and non-linear energy harvesting has led to these effectiveness metrics becoming obsolete.

There has been recent research developing expressions for the maximum power available for non-linear vibrational systems, with either stochastic and deterministic inputs. We see that for both stochastic and harmonic energy harvesters, there exist effectiveness metrics that are applicable to both linear and non-linear systems. However,

due to fundamental differences in the underlying assumptions, there currently exists no effectiveness metric universal to both stochastic and harmonic systems.

The task now becomes: firstly, to extend this expression to other domains (electrical, thermal, etc.) and secondly, to develop these expressions for multi-source energy harvesters. The first part of this will require demonstrating that a mathematically analogous form of this expression exists outside of the mechanical domain. The theoretical framework for developing these expressions will be discussed in Chapter 2. The theoretical and practical work to derive and verify these expressions will be discussed in Chapter 3. The second part will require theoretical analysis of systems coupled in at least three domains, described in Chapter 4. Lastly, it is important to experimentally verify any assumptions used in the derivation of these expressions, as described in Chapter 5. A summary of these results, along with their significance and implications, will be discussed in Chapter 6.

2

Theory and Background Information

This chapter aims to provide background, context and an explanation of the key concepts found in the rest of the thesis, namely: the piezoelectric and pyroelectric effects, and the method of physical analogy. This chapter will also define the system of analogies—and corresponding terms—that will be used throughout the thesis to provide a generalised approach to describing energy harvesters. A futher aim of this chapter is to provide an understanding of the advantages and limitations of this generalised approach for describing energy harvesters.

The key to understanding energy harvesters is understanding how they convert one form of energy into another, and how the energy is subsequently stored and dissipated within the system. Section 1.1 briefly outlined some of the methods used in energy harvesting to convert various forms of energy. However, it is useful to have a further understanding of the physics governing particular energy harvesting materials and methods. Due to their ease of integration, piezoelectric materials are useful in multi-source energy harvesting due to their ability to simultaneously convert both mechanical and thermal energy into electricity. For this reason, the theoretical and practical work described in Chapters 3 to 5 focuses on the use of piezoelectric materials.

As such, a discussion of how the piezoelectric and pyroelectric effects manifest themselves physically is included in Section 2.1. We will see that, despite the differences in the physics governing the coupling behaviour, these two effects can be described in a similar way mathematically. This will be discussed in Section 2.3.4.

Section 2.2 will detail existing analogies for describing electrical, mechanical and thermal systems in equivalent terms. This is motivated by the difficulties that arise when trying to describe multi-source harvesters using the particular language associated with each of these domains. Existing analogies all have their particular method of converting from one domain to another: mobility analogies are designed to preserve the topology of

system schematics, at the cost of physical analogy; impedance analogies are designed to preserve the physical relationships; and bond graphs provide both mathematical and physical analogy, alongside accurate network graphs, but at the cost of added graphical complexity. There is always some trade-off when choosing analogies, and it comes down to where the greatest clarity and ease of analysis is required.

It is necessary to define an comprehensive list of analogies when discussing multi-source energy harvesters. Otherwise, complications arise, since there are typically at least three distinct types of energy present in any one harvester. Further complications when describing multi-source energy harvesters come from the different boundary conditions constraining each system (this will be discussed in Section 2.3.1). Finally, in multi-source energy harvesters, there can be various forms of coupling (e.g. dynamic, static) between the different domains (discussed in Section 2.3.4). Section 2.3 will define the system of analogies that will be used throughout the remainder of the thesis. To define the system of analogies, it was important to choose variables and parameters that provide *mathematical* analogy in all cases. These definitions are intended to describe the general dynamic relationships for multi-source energy harvesters, as the range of possible devices and configurations available (as discussed in Section 1.2) limits the applicability of more specific approaches. Providing a more detailed description of the behaviour of a particular design of energy harvester requires additional assumptions that limit any resulting model or expression to that specific case. Nevertheless, as will be demonstrated in Chapters 3 and 4, it is possible to use specific realisations of energy harvesters to verify these general physical relationships for practical systems.

The definitions found in this chapter are intended to create a system of analogies that use domain-neutral language, and use variables and parameters that provide a physical (as well as a mathematical) analogy. It is hoped that the language used in these definitions will give an intuitive understanding of the effect that each parameter has on the physical behaviour of the system. Using these definitions to describe energy harvesting systems has the potential to provide a common language to researchers designing multi-source energy harvesters. Furthermore, use of these definitions and analogies could create the possibility for energy harvesting solutions that exist in one domain to be transferred to another—for example, through analogy, methods for analysing the dynamic behaviour of electrical circuits have been successfully applied to mechanical systems and vice versa.

And so, this chapter will begin with a description of the piezoelectric and pyroelectric effects, along with a discussion of the distinction in the coupling provided by these two effects. Section 2.2 will provide a description of physical analogies, starting off with mechanical-electrical analogies, on to more general analogies, and eventually bond

graphs. Section 2.3 will detail the definitions of equivalent variables and parameters that will be used in the rest of the thesis. Using these analogies we define the variables and equivalent parameters in such a way that the expressions for instantaneous power, along with the system equations appear identical regardless of the domain.

2.1 Background on Piezoelectric Materials

Small-scale energy harvesting devices have become more viable due to the growing development and applications of smart materials. Smart materials act as transducers, converting one form of energy to another, making them useful for the purposes of harvesting energy. Smart materials have benefits such as repeatable, predictable behaviour, and no moving parts. Certain (dielectric) materials are useful in energy harvesting as they can convert both mechanical and thermal energy into electrical energy (and vice versa).

This section will briefly describe the material structure and physics behind the piezoelectric and pyroelectric effect, together with a general mathematical description. This includes a description of the mechanism through which piezoelectric materials convert mechanical energy into electrical energy. The pyroelectric effect is displayed by a certain sub-class of piezoelectric materials, possessing a similar crystal structure, but with key differences in their polarisation behaviour. Pyroelectric materials are useful in energy harvesting as they provide a means of converting thermal energy into electrical energy.

2.1.1 The Piezoelectric Effect

Physical description

This sub-section provides a summary of the physical mechanism that causes piezoelectric materials to exhibit the piezoelectric effect, as described by Vives [76]. Piezoelectric materials are ionically bonded, consisting of atoms with positive and negative charges. These atoms are arranged in a repeating lattice structure, known as a crystaline structure, with each piezoelectric crystal being made up of the same basic atomic structure called a unit cell. The unit cell for lead zirconate titanate has the atomic structure shown in Fig. 2.1. The unit cells in a crystal are usually symmetrical, however in piezoelectric materials, these unit cells lack central symmetry. This asymmetry leads to a positive and negative charge across each unit cell which creates dipole moments. These dipoles form regions where each dipole has the same alignment as their neighbours.

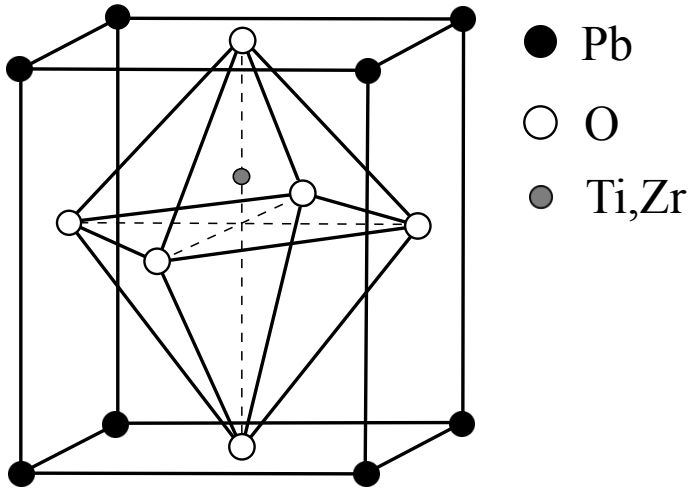

Figure 2.1: Diagram of the unit cell of a piezoelectric material, showing the asymmetric arrangement of the atoms.

Much like the magnetic fields found within ferrous metals such as iron, the regions within the piezoelectric material are initially randomly orientated within the material. This random orientation results in a lack of strong overall polarisation. This lack of strong overall polarisation within the material means that the material exhibits a negligible piezoelectric effect. To create a material which displays a strong piezoelectric effect, it is necessary to artificially impose this polarisation by subjecting piezoelectric material to an extremely strong electric field. The strong electric field orients all the dipoles in the same direction, called the poling axis. When the electric field is switched off, most of the dipoles remain in the same alignment. This alignment can be reversed and the material can be *de-poled* if heated above its Curie temperature, or if subjected to a strong electric field in the opposite direction.

Ordinarily, a piezoelectric material is neutrally charged—the dipole moments cancel each other out. However, the material becomes charged when a stress is applied. When a stress is applied, it upsets the balance of the charges (by forcing the dipoles to rotate) and a net potential difference (voltage) occurs across the material. When a piezoelectric material becomes charged due to an applied stress, this is called the direct piezoelectric effect. This effect describes how electricity is generated when a force is applied, as shown in Fig. 2.2. The opposite is also true—when there is a potential difference applied to the material, the dipoles change their position, generating internal stresses which deform the material. This is known as the inverse piezoelectric effect.

Piezoelectric materials have a different coupling efficiency based on whether or not the force is acting along the poling axis. The coupling efficiency defines what percentage

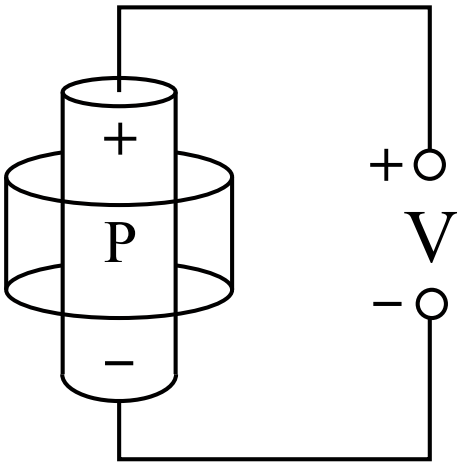

Figure 2.2: A voltage is generated (denoted by V) as the piezoelectric material is deformed. The voltage is generated in the same direction as the poling direction (marked here with P).

of the mechanical energy in a piezoelectric material is converted into electrical energy. When the material is deformed, the voltage is generated along the poling axis, which is conventionally defined as the 3-axis. This is most efficient when the force is applied in the same direction as the poling axis; this is called the 3-3 coupling or *stack* mode. Another commonly utilised coupling mode is the *cantilever* or bending mode, and occurs when a perpedicular force is applied to the end of a piezoelectric cantilever. The perpendicular force causes bending, which results in forces (compression and extension) along the 1-axis of the piezoelectric cantilever, perpendicular to the poling direction in the 3-axis; therefore, this is called the 3-1 coupling mode. These coupling modes are demonstrated in Fig. 2.3. Both of these modes have different piezoelectric coefficients associated with them. The stack mode is associated with the strongest d_{33} coefficient, and the cantilever mode is associated with the weaker d_{31} and d_{32} coefficients. For most piezoelectric materials, the d_{31} and d_{32} coefficients considered to be the same. This is because piezoelectric materials are often transversely isotropic—Moheimani and Fleming [48] state that this is true for piezoelectric ceramics —so the 3-2 coupling mode is approximately the same as the 3-1 mode.

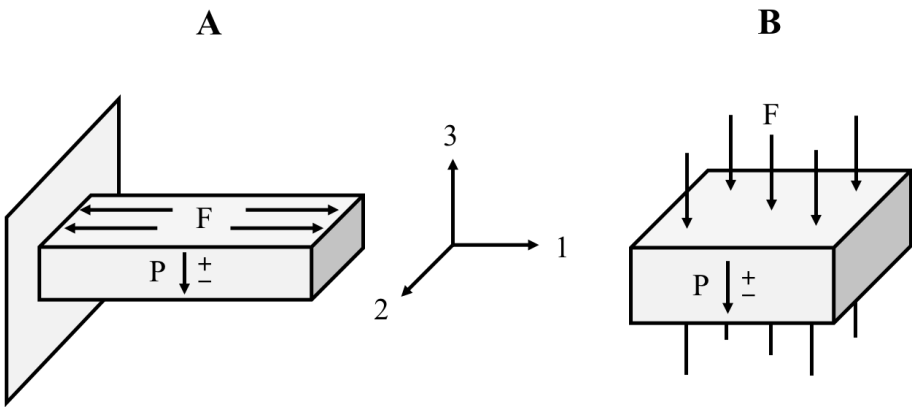

Figure 2.3: The two main piezoelectric coupling modes. Plot A shows the 3-1 mode (cantilever). We can see that the force F is acting along the 1-axis, while the poling direction P is in the 3-axis. Plot B shows the 3-3 mode (stack). The force and poling direction are both acting along the 3-axis.

Mathematical description

Jaffe et al. [32] provide a general description for the combined linear piezoelectric effect which typically has the form

$$\begin{pmatrix} D \\ S \end{pmatrix} = \begin{pmatrix} \epsilon^{\sigma} & d \\ d^{T} & s^{E} \end{pmatrix} \begin{pmatrix} E \\ \sigma \end{pmatrix} \tag{2.1}$$

where D is a vector of electric displacements; S is the vector of material engineering strains; ϵ is the permittivity matrix; d is the matrix of the piezoelectric coefficients; s is the compliance matrix; E is vector of the electric field strength; σ is the vector of material stresses; the superscript E indicates the coefficients measured under a zero, or constant, electric field (e.g. short-circuit); the superscript σ indicates the coefficients measured under a zero, or constant, stress field; and the superscript T indicates the transposition of a matrix.

The piezoelectric material properties are described by several matrices. The matrix of piezoelectric coefficients relates the mechanical strain to the applied electrical field and vice versa. If we assume that the material is poled along the 3-axis and is transversely isotopic, the piezoelectric coefficients appear as follows

$$d = \begin{pmatrix} 0 & 0 & 0 & 0 & d_{15} & 0 \\ 0 & 0 & 0 & d_{15} & 0 & 0 \\ d_{31} & d_{31} & d_{33} & 0 & 0 & 0 \end{pmatrix}, \tag{2.2}$$

where the subscripts 1 and 3 refer to the directions shown in Fig. 2.3, while 5 refers to the transverse direction (not shown). These coefficients define the coupling modes between the mechanical and electrical systems. The matrix of the permittivities is symmetrical and relates the electric displacement and the electric field:

$$\epsilon^{\sigma} = \begin{pmatrix} \epsilon_{11}^{\sigma} & 0 & 0 \\ 0 & \epsilon_{11}^{\sigma} & 0 \\ 0 & 0 & \epsilon_{33}^{\sigma} \end{pmatrix}. \tag{2.3}$$

The compliance matrix is also symmetrical due to isotropy in the 1 and 2 directions. These terms relate the stress and strain and can be written as

$$s^{E} = \begin{pmatrix} s_{11}^{E} & s_{12}^{E} & s_{13}^{E} & 0 & 0 & 0 \\ s_{12}^{E} & s_{11}^{E} & s_{13}^{E} & 0 & 0 & 0 \\ s_{13}^{E} & s_{13}^{E} & s_{33}^{E} & 0 & 0 & 0 \\ 0 & 0 & 0 & s_{55}^{E} & 0 & 0 \\ 0 & 0 & 0 & 0 & s_{55}^{E} & 0 \\ 0 & 0 & 0 & 0 & 0 & s_{55}^{E} \end{pmatrix}. \tag{2.4}$$

These matrices are defined for piezoelectric materials with 3-dimensional spatially distributed properties. To better facilitate the use of analogies, this thesis deals with 1-dimensional lumped element models instead. Assuming a 1-dimensional system means that the matrix of piezoelectric coefficients becomes a single coefficient. The lumped element assumption removes the dependence on strains and permittivity. As we will see in Chapters 3 and 5, these simplified models are sufficient for the purposes of predicting the power absorbed by energy harvesters.

2.1.2 The Pyroelectric Effect

Physical description

Some piezoelectric materials display an additional smart material effect, called the pyroelectric effect. Both the piezoelectric and pyroelectric effect rely on an asymmetry in their crystal structure that leads to polarisation; however, some piezoelectric materials have a symmetry which prevents spontaneous polarisation. For the pyroelectric effect to be present, the cystal needs to exhibit spontaneous polarisation, even in the absence of an electric field. These are called polar materials, and their crystals attract free electrons and ions—also known as depolarisation charges—which cancel out the internal electric field.

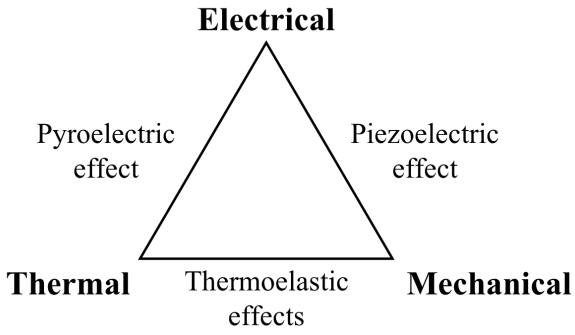

Figure 2.4: The piezoelectric effect couples the mechanical and electrical domains, while the pyroelectric effect couples thermal and electrical domains. Thermal energy is converted to mechanical energy through thermal expansion (thermoelasticity).

Similar to the behaviour of a piezoelectric material under stress, a change in temperature causes a change in the positions of the atoms within the piezoelectric crystal, creating a flow of charge at the surfaces of the material. Unlike in a piezoelectric material, where the net potential remains until the force is removed, in a pyroelectric material this polarisation is only temporary. In a pyroelectric material, the depolarisation charges will eventually adjust their position and re-balance the polarisation of the crystal structure. This is why, unlike the piezoelectric effect, the pyroelectric effect is generally considered to require a fluctuating thermal gradient to generate power. However, we could also say that a piezoelectric material requires a fluctuating force to provide constant source of power. This becomes more obvious when we consider the similarity in the mathematical description of both effects, which will be discussed in more detail in Section 2.3.4.

The difference in the piezoelectric and pyroelectric effects in a system with electrical, thermal and mechanical energy can be illustrated by representing the system as a triangle, shown in Fig. 2.4, with credit to Buchanan [13]. One side of this triangle describes the conversion of mechanical energy into electrical energy through the piezoelectric effect. The other side of this triangle gives us the conversion between thermal and electrical energy through the pyroelectric effect. The remaining side represents usual thermoelastic effects, which take care of the energy conversion between thermal gradients and mechanical stress. This shows us why piezoelectric materials are useful in multi-source energy harvesting: in a single material we can harvest from at least two sources of distinct energy types simultaneously.

Mathematical description

As presented by Zahra El Fatnani et al. [85], the general mathematical description for the pyroelectric effect is similar in form to Eq. (2.1), except that it is expressed in terms of the derivatives

$$\begin{pmatrix} \mathrm{d}D \\ \mathrm{d}S \end{pmatrix} = \begin{pmatrix} \epsilon^{\theta} & \rho \\ \rho^{T} & C_s \end{pmatrix} \begin{pmatrix} \mathrm{d}E \\ \mathrm{d}\theta \end{pmatrix}, \tag{2.5}$$

where θ is the vector of the temperatures; and the superscript θ indicates the coefficients measured under a constant temperature. Other differences include using the matrix of *pyroelectric* coefficients ρ; and instead of compliance we now have the thermal equivalent—entropy capacity C_s. The need to use entropy capacity instead of heat capacity will be discussed in Section 2.3.2. The derivatives in Eq. (2.5) will be taken with respect to time. Again due to the 1-dimensional and lumped mass assumptions used, we can reduce the matrices containing the system parameters (ϵ, ρ, C) to single constants. Also the vectors $(dD, \mathrm{d}S, \mathrm{d}E, \mathrm{d}\theta)$ will become scalar variables.

2.2 Physical Analogies

Being thoughtful when choosing system parameters and variables allows us to develop analogies between different systems. When developing analogies, the concepts of energy and power are useful, as all physical systems can be described in these terms. This provides us with a common language to describe the behaviour of these systems. There are many fields, such as physics and control systems theory, where employing analogies has long been common practice. Electrical-mechanical analogies are particularly popular.

Analogies help us to understand and explain crucial ideas regarding multi-source energy harvesters by giving us a common basis, which allows us to simplify how we describe these systems. An expanded form of the impedance analogy will form the basis for the theoretical work presented in this thesis.

The expanded impedance analogy has also formed the basis for bond graphs. Bond graphs use the idea of generalised forces (effort variables) and generalised velocities (flow variables) to form bonds which represent the flow of energy.

Mechanical-electrical analogies are used to represent mechanical systems as electrical networks, or vice versa. These analogies were originally conceived by Hermann von Helmholtz and James Clerk Maxwell to describe electrical phenomena in the mechanical terms they were accustomed too. However, as theoretical techniques for examining electrical networks developed, these analogies were used in reverse, so that techniques

for analysing circuits could be applied to mechanical systems. Mechanical-electrical analogies have obvious use in systems with electromechanical coupling, by allowing the equations for both systems to be expressed in the same way, simplifying the analysis. These analogies seek to define a set of variables from each domain, where the mathematical relationships between variables within each set are the same for both domains. Typically these variables are either power conjugate variables or Hamiltonian variables.

While a wide variety of analogies are theoretically possible, two popular choices are the impedance and mobility analogies. In the mobility analogy, the topology of the network diagrams is preserved—i.e. the layout of mechanical network remains the same when converted to a circuit diagram. Whereas, in the impedance analogy, the definition of the impedance as the ratio of the power conjugate variables is preserved—i.e. force/velocity gives mechanical impedance, voltage/current gives electrical impedance.

This section aims to outline and describe existing analogies that form the basis for the theoretical work of this thesis. To introduce what may possibly be considered the origin of mathematical analogies in physics, we begin with a brief description of Hamiltonian and Lagrangian mechanics. We then briefly examine the impedance and mobility analogies, before exploring how the impedance analogy can be extended to include further energy domains. This extended impedance analogy is used as a basis for bond graphs, so we will briefly discuss bond graphs and their advantages with regards to describing multi-physics systems. While bond graphs will not be used in this work, they include useful concepts and illustrate ideas that will be expanded upon in Section 2.3.

Hamiltonian and Lagrangian Mechanics

It would be remiss to discuss physical analogies and energy-based methods without briefly discussing the relevance of Hamiltonian and Lagrangian mechanics to the development of physical analogies. The Lagrangian $\mathcal{L}$ can be interpreted as an energy based re-formulation of Netwon's laws and provides us with a physically and mathematically analogous framework, as they can be used to describe exactly the same phenomena. However, unlike Newtonian mechanics, the Lagrangian formalism is not restricted to an inertial reference frame and generalised coordinates can be used instead—making it possible to choose coordinates in such a way as to simplify the analysis. More importantly to this work, the coordinates used in the Lagrangian do not necessarily need to be spatial, as will be demonstrated in Chapter 4.

Hamiltonian mechanics are derived from the Lagrangian formulation. The Hamiltonian formalism introduces the canonical coordinates of position and momentum, whereas the Lagrangian uses only the position and time derivatives thereof. The canonical coordi-

nates can be used to create phase-space representations of a system's behaviour, where its time history is plotted as a trajectory on a graph. The Hamiltonian $\mathcal{H}$ can be said to describe the total energy of the system—incorporating the Lagrangian—and is a function of generalised coordinates and momentum:

$$\mathcal{H}(\mathbf{q}, \mathbf{p}, t) = \mathbf{p} \cdot \dot{\mathbf{q}} - \mathcal{L}(\mathbf{q}, \dot{\mathbf{q}}, t), \tag{2.6}$$

where $\mathbf{q}$ is the vector of generalised displacements, $\mathbf{p}$ is the vector of the generalised momentum for each coordinate, t is the time, and a dot over the variable represents differentiation with respect to time.

Hamiltonian and Lagrangian mechanics can be interpreted as methods of analogy, although the motivation behind them is largely mathematical. As a consequence, these methods focus more on mathematical formalism, and less on the physical embodiement of the systems they describe. However, the ideas included in these formalisms are invaluable in the development of meaningful physical analogies.

The Lagrangian and Hamiltonian both relate to the potential and kinetic energy in the following ways:

$$\mathcal{L} = T - V, \tag{2.7}$$

and

$$\mathcal{H} = T + V \tag{2.8}$$

where we define T here as the kinetic energy of the system, and V as the potential energy. Therefore, we can interpret the Lagrangian as describing the balance of energy stored in a conservative system, while the Hamiltonian describes the total energy stored in a system. Dissipative and non-conservative forces can also be included.

2.2.1 Mobility Analogy

The mobility analogy is formulated in such a way that the network diagram remains the same between mechanical and electrical systems. This analogy is formulated by considering the quantities which are the same through elements connected in series: the force through series mechanical elements (except masses) is the same, while the current through series electrical components is the same. This analogy is not immediately intuitive, but allows theorists to apply analysis based on Kirchoff's Laws to mechanical systems, which is useful for certain applications.

2.2.2 Maxwell or Impedance Analogy

Maxwell originally developed his analogy to describe the behaviour of electrical systems in familiar terms; however, it soon became apparent that the method of physical analogy could serve as an analytical tool in and of itself. According to Bokulich [9], Maxwell believed that physical analogy served as a middle ground between physical equations as a form of pure mathematics (the Lagrangian and Hamiltonian formalisms) and equations relating to the precise and particular physical behaviour of a specific system. He believed that you could describe the general dynamic behaviour of systems in such a way that one could substitute in a number of different physical systems. Maxwell thought that, through this method of physical analogy, you could infer general physical laws, provided that you did not mistake these physical analogies for explanations of the true physical nature of the system.

The Maxwell (or impedance analogy) is constructed using power conjugate variables, described as flow and effort variables, leading to the following system of analogies:

- Velocity, angular velocity and current are flow variables.
- Force, torque and voltage are effort variables.

We can see that this analogy preserves the physical relationships between the variables and parameters in each system: for example, a spring and a capacitor (relating effort to the integral of flow with respect to time) both concern the potential energy of the system. As the name would suggest, the impedance analogy also preserves the impedance relationship as the ratio of effort over flow.

The Maxwell or impedance analogy is useful as it allows us to develop a framework for describing energy harvesters which is independent of any particular design. Following these ideas, this work attempts to provide a framework that can be used to describe the general physical behaviour of any energy harvester. Much like Maxwell's analogy, this framework is expressed using a system of definitions that does not change with different domains (energy types). The framework presented in this chapter adopts and adapts Maxwell's analogy which allows us (in Chapter 4) to derive general theoretical expressions that can be applied to a wide range of energy harvesting devices.

Power conjugate variables

Power conjugate variables are variables whose product has the units of power. While this is a relatively loose definition that gives a wide choice of possible variables sets in each domain, we can narrow down the options by restricting ourselves to variables

that are easy to measure. The variables chosen in the electrical domain are traditionally current and voltage. In the mechanical domain, the variables chosen are usually velocity or force, or the rotational equivalent.

To use these variables to fully define an analogy, it is necessary to specify the association between the variables from each domain: for example, in the impedance analogy, voltage is associated with force, and current with velocity; whereas, in the mobility analogy, current is associated with force, and voltage with velocity. We can see that, by reversing these associations, we can move between analogies. In other words, the impedance and mobility analogies are *duals* of one another. By changing the associations used in the analogy and using this idea of duality, we can find analogous expressions regardless of whether the system is described in terms of flow or effort.

2.2.3 Expanded Impedance Analogy

The impedance analogy was originally designed as a mechanical-electrical analogy. Despite this, it is possible to extend this analogy by finding equivalent variables for other types of systems, such as thermal and chemical, as described by Busch-Vishniac [14]. Here we define the equivalent (effort and flow) variables for a wide range of systems in domain neutral terms; examples can be found in Table 2.1. In this table, we have also included the Hamiltonian variables of generalised momentum and generalised displacement.

The power conjugate variables mentioned so far for mechanical and electrical systems are those that we commonly use. However, for thermal systems, the product of the two most common variables—heat flow and temperature—does not have the dimensions of power. To give the pair of power conjugate variables for thermal systems, entropy flow must be used instead of heat flow. According to Busch-Vishniac [14], the main reason that power conjugate variables are not typically used to describe thermal systems, is that entropy flow cannot be directly measured. While entropy flow may not be the most intuitive variable for describing thermal systems, to continue using the impedance analogy, we must use power conjugate variables.

Using entropy flow instead of heat flow also requires a modification of the parameters used to describe the thermal system. Using the common parameters of heat capacity and thermal resistance along with entropy flow results in dimensional inconsistencies. To give the correct dimensions, the heat flow and the system parameters must all be divided by the absolute temperature. Section 2.3.2 discusses the necessary change of parameters

Table 2.1: Flow, effort, generalised displacement and generalised momentum variables used in the expanded impedance analogy, defined for common domains

Domain	Flow	Effort	Generalised displacement	Generalised momentum
Electrical	Current	Voltage	Charge	Magnetic flux linkage
Mechanical translation	Velocity	Force	Displacement	Momentum
Mechanical rotation	Angular velocity	Torque	Angular displacement	Angular momentum
Thermal	Temperature	Entropy flow	Entropy	
Chemical	Chemical potential	Molar flow	Number of moles	

in greater detail. The steps required to form a proper thermal-electrical analogy are also described by Bosworth [12].

Bond graphs

Bond graphs will be briefly discussed because the terminology and relationships captured in these graphs are useful for describing multi-physics systems. As described by Borutzky [11], bond graphs use the same ideas as the expanded impedance analogy to provide a domain neutral graphical representation of the system. Bond graphs can be considered an impedance analogy since the power conjugate variables are related to each other through the same impedance relationship, regardless of the type of system being examined.

In the original lectures on bond graphs, Paynter [56] represents the relationship between these sets of variables in a diagram known as the tetrahedron of state, shown in Fig. 2.5. The physical relationships captured in this diagram are: the generalised momentum and flow are related by the inertance (Newton's second law), the generalised displacement and effort are related by the compliance (inverse Hooke's law, charge on a capacitor), and the flow and effort are related by the resistance (Ohm's law and mechanical damping). This diagram also shows how the system parameters relate the variables to one another. As would be expected, by integrating the power conjugate

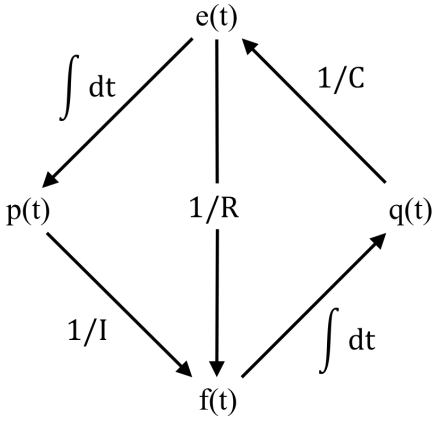

Figure 2.5: The tetrahedron of state that is formed by the relationships in a bond graph. To move from effort to generalised momentum, or from flow to generalised displacement, you need to integrate with respect to time. Dividing the generalised momentum by intertance gives flow. Dividing the generalised displacement by compliance gives the effort variable. Dividing the effort by the resistance gives the flow variable.

variables with respect to time, we obtain the Hamiltonian variables—which relate to the energy of the system.

So we see that bond graphs provide a physically intuitive method for describing the relationships between system variables and parameters in a domain neutral way. Using these ideas essentially reduces a multi-physics system to a single physics system, as we can now describe all the subsystems in a consistent manner, regardless of their domain.

Causality in bond graphs

Each bond in a bond graph is written as a link between *elements* with the effort variable indicated above and the flow variable indicated below. These bonds represent an exchange of energy between elements in the system and have the dimensions of power, where the direction of the flow of power is indicated using half-arrows.

For each bond, a stroke can be used to indicate causality, determining whether a port *causes* a flow or an effort: for example, a pure flow or effort source (analogous to a pure current or voltage source) *causes* a flow or effort respectively. This notion of causality is included to preserve physical analogy, as opposed to simply using analogous equations. When examining the causality of elements in the system, we must consider the physical behaviour of the element in question. For example, a capacitor *causes* an effort because it cannot be charged instantly and therefore requires any elements connected in parallel

to have the same voltage (effort). In the same way, an inductor *causes* a flow because it cannot change flux instantaneously and so requires any elements in series to have the same current (flow). The causality relationship is symmetrical; a bond cannot have two sides which cause the same thing. When one side of the bond determines (causes) the instantaneous flow, the other side determines the instantaneous effort.

2.3 Definition of Equivalent Terms

This section will define the equivalent terms for the system of analogies used throughout this thesis. Each of the sub-sections will provide extra clarification of the physical significance of the definitions used. For example, while the main aim of Section 2.3.1 is largely to provide a list defining the equivalent variables used, this sub-section also provides further discussion of some of the key concepts: the first part of this sub-section discusses one of the major themes of Chapter 3—the difference between describing systems as constrained by effort or flow—before moving on to discuss the concepts of generalised momentum and displacement along with their physical significance; and then, finally, how the concepts of duality and causality are captured in this system of analogies. Section 2.3.2 provides similar insight with regards to the equivalent parameters used in this work. Since this work is primarily concerned with energy harvesting, Section 2.3.3 describes how we can use these equivalent variables and parameters to develop expressions for the instantaneous power in the system. And finally, Section 2.3.4 will discuss various forms of coupling using the system of analogies defined in the rest of this section.

Analogies built around energy flow provide an intuitive approach to thinking about these systems. We can define physical systems in terms of kinetic and potential energy, as well as the energy into and out of the system. Using the definitions for kinetic and potential energy, as well as dissipated energy, we can think of physical systems as having some form of compliance, some resistance term and some form of inertia. By describing systems in terms of compliance, resistance and intertia we can parameterise systems using these terms. Using the definitions for the energy in a system, we can naturally find corresponding variables. Additionally, using these analogies to describe the energy flow within subsystems, between subsystems, and between any subsystem and its environment allows us to break complex systems into simpler subsystems.

When defining any set of parameters or variables in an analogy, it is essential to be mathematically consistent. It is equally important to ensure that the analogous parameters and variables represent physical reality. So, while we can attempt to parameterise all

physical systems in terms of their compliance, resistance and inertia, we must realise that certain systems—namely thermal and chemical—lack any form of momentum or intertia. Momentum, inertia and kinetic energy terms have no real physical significance when applied to these systems; we therefore need to avoid using these analogous terms when describing thermal and chemical systems. This author would suggest that this may be due to the fact that thermal and chemical systems are in fact abstractions of underlying atomic behaviour, based on underlying electrical and mechanical principles: for example, a particle may have mass and a charge, and so these descriptions have a real physical meaning. The voltage is related to the electromotive force acting upon the particle, and the velocity describes the actual motion of the particle. However, chemical potential is related to the electromotive force experienced by *all* particles which form the molecule, and temperature is an average of the velocity of particles within a substance.

It is easy to mistake mathematical analogy with actual physical analogy. Within the impedance analogy, the mathematical relation between mass, force and displacement is identical to the relation between the inductance, voltage and charge. However, the physical mechanism that causes a mass to build up kinetic energy differs from that which causes an inductor to store electrical energy. Analogies do not directly provide a physical explanation of phenomena. Maxwell [42] himself warns that the similarity in the mathematical form of certain phenomena does not imply that the physics governing such phenomena are the same.

This work aims to construct theoretical models which capture the important dynamic behaviour of multi-physics systems, while attempting to avoid obscuring differences in the physical manifestation of these systems. To capture the dynamic behaviour of these systems, we seek to model physical systems as coupled differential equations, by treating each energy type as a seperate and single degree of freedom. Representing these systems using a similar system equation enables us to see clearly whether or not we expect two systems to behave in the same way—behaviour in this sense meaning linear or non-linear, and resonant or non-resonant.

Energy-based analogies have a wide use in science and engineering, and they are particularly useful when analysing energy harvesters. Using the general language of these analogies would aid designers in moving away from only considering a limited range of harvesters (vibrational, thermal, chemical, etc.) for a given application. In addition, describing these systems in a generalised fashion would hopefully allow designers to see the wider applicability of their work.

2.3.1 Equivalent Variables

One of the primary reasons for using equivalent variables is that we can combine multiple energy types in the same system. For this work in particular, it allows us to convert the coupled system equations for the various domains (mechanical, electrical, thermal) into a single domain-neutral system equation. Representing a whole range of different subsystems in one system equation allows us to perform analysis as if it truly were a single system, which will become very important in Chapter 4.

The use of equivalent variables not only simplifies analysis, but also allows for a clearer description of general dynamic behaviour by eliminating domain-specific terminology. Using domain-specific terminology only confuses matters, since we wish to focus on the mathematical relationships within and between the various systems. This allows us to develop a framework that will enable the theoretical discussion of multi-source energy harvesters, in addition to simplifying the language used.

In this work, we use a selection of the variables from the expanded impedance analogy as described in Section 2.2.3. The definitions for the variables used in this work can be found in Table 2.2. This table also includes a description of their units and dimensions. Examining the dimensions of each of the variables illustrates the difference in how each variable relates to the physical world. Another motivation for including the dimensions is that we can see how the displacement and momentum in each case combine to give energy (dimensions L^2MT^{-2}), and how the flow and effort multiply to give power (dimensions L^2MT^{-3}).

Effort and flow

To enable us to effectively employ the method of physical analogy, we will describe the energy harvesters using the domain-neutral language of effort and flow. We define effort variables in Table 2.2 as: electrical potentials in electrical systems, forces in mechanical systems, and temperature gradients in thermal systems. These variables do not describe a change of energy or movement themselves, but represent the potential for a system to generate a flow. An unbalanced effort in a system will necessarily produce a flow; however, no energy will have been exchanged *until* the flow occurs.

A flow describes the change in the position or displacement of the system with respect to time—often in reference to an equilibrium position. This change in position is velocity for mechanical systems and current in electrical systems. If we use this idea

[1] An analogous form of generalised momentum does not exist for thermal systems. However, we can speculate what units and dimensions such a quantity would have.

Table 2.2: Physical definitions for the generalised displacement, flow, effort and generalised momentum variables

Panel A: Generalised Displacement - q			
Domain	Name	Units	Dimensions
Mechanical	Displacement	meters	L
Electrical	Charge	Coulombs	Q
Thermal	Entropy	Joules/Kelvin	$L^2MT^{-2}\Theta^{-1}$
Panel B: Flow - f			
Domain	Name	Units	Dimensions
Mechanical	Velocity	m/s	LT^{-1}
Electrical	Current	A	QT^{-1}
Thermal	Entropy flow	W/K	$L^2MT^{-3}\Theta^{-1}$
Panel C: Effort - e			
Domain	Name	Units	Dimensions
Mechanical	Force	F	LMT^{-2}
Electrical	Voltage	V	$L^2MT^{-2}Q^{-1}$
Thermal	Temperature	K	Θ
Panel D: Generalised Momentum - p			
Momentum	Name	Units	Dimensions
Mechanical	Momentum	$F \cdot s$	LMT^{-1}
Electrical	Magnetic flux linkage	Wb ($V \cdot s$)	QT^{-1}
Thermal[1]		$K \cdot s$	ΘT

we can see that we can describe all physical systems in terms of either flow or effort variables—the common choice of variable varies depending on the system in question. Electrical or thermal systems are usually described using their effort variable. Chemical systems are often described in terms of molar flow. Mechanical systems are commonly described in terms of their displacement, which is the flow integrated with respect to time. Describing systems in terms of their displacement is useful when we wish to know the energy of a system, but less so when we want to know the instantaneous power transfer.

By keeping the dimensions consistent, we can always ensure that we are using power conjugate variables. Using power conjugate variables means that, whatever the type of system, we are always describing the system in terms of power (energy exchange differentiated with respect to time). This makes finding expressions for the instantaneous power easier: if you have a system equation written using the flow or effort variable then to find the instantaneous power transfer within the system, you simply need to multiply the expression by the corresponding conjugate variable. This will result in an expression where each term represents the instantaneous power flow for each element in the system (e.g. masses, springs, resistors).

This requirement, that the product of the flow and effort variables has the dimensions of power, explains why it is necessary to use entropy flow instead of heat flow in thermal systems. Multiplying the heat flow by the temperature difference would instead give the dimensions of $L^2MT^{-3}\Theta$, which has the dimensions of power multiplied by temperature. Dividing through by the temperature (to give entropy flow instead) gives us the correct dimensions. Changing from heat flow to entropy flow requires changing the commonly used system parameters (heat capacity and thermal resistance) to keep the mathematical relationships consistent.

Momentum and displacement

Momentum describes the tendency for a system to remain either in motion or at rest when some effort is applied. Generalised momentum takes the concept of linear and angular momentum and applies it to generalised coordinates, allowing the concept of momentum to be used in Hamiltonian and Lagrangian mechanics. The concept of generalised momentum can be applied—through analogy—to electrical systems. The generalised momentum is defined here as the product of the inertance (analogous to mass or inductance) and the flow. From the tetrahedron of state shown in Fig. 2.5, we can also see that it is the effort variable integrated with respect to time.

The generalised displacement is the position of the system described in one of the generalised coordinates. The displacement is usually taken with equilibrium being chosen as $q = 0$, where the equilibrium is the point where the system has no potential energy. The generalised displacement is the product of the compliance (analogous to the mechanical compliance or electrical capacitance) and the effort. The derivative of the generalised displacement with respect to time is the flow.

The product of the generalised momentum and displacement has the units of energy. The Hamiltonian—expressed in terms of generalised momentum and displacement—represents the total energy in the system. Since power P is energy E differentiated with respect to time

$$P = \frac{\mathrm{d}E}{\mathrm{d}t} = \frac{\mathrm{d}\mathcal{H}}{\mathrm{d}t}. \tag{2.9}$$

Therefore, to find the instantaneous power of the system, it is necessary to differentiate both the generalised displacement and momentum with respect to time. The instantaneous power for each element in the system is given by

$$P = \dot{p}\dot{q} = \frac{\partial p}{\partial t}\frac{\partial q}{\partial t}. \tag{2.10}$$

Since $\dot{p}$ is equivalent to the effort variable and $\dot{q}$ is equivalent to the flow variable, Eq. (2.10) again demonstrates that taking the product of the flow and effort gives the instantaneous power.

Duality

Sometimes it is convenient to switch between describing the system in terms of the effort variable or in terms of the flow variable. An example of this would be using electrical duality to switch from using current to describe a system, to using the voltage instead. Duality can be used to switch between using an impedance or mobility analogy; we can therefore describe these analogies as being duals of one another. When we use duality to switch the variable used to describe a system, we use the same values for the system parameters, but their relation to the system variable changes—this is required to keep the dimensions consistent. For example, if we were to change the system variable used to describe a simple undamped oscillator

$$m\ddot{x} + kx = F \tag{2.11}$$

from displacement x to force F, we need to invert[2] the relationship between the system parameters (stiffness k and mass m) and the variable used to describe the system

$$m^{-1} \iint F \, \mathrm{d}t \, \mathrm{d}t + k^{-1} F = x. \tag{2.12}$$

(It is not common practice to describe the state of a mechanical system using forces instead of displacement, but it is possible.) If you want to exchange the variables used to describe the system equation from flow to effort—or vice versa—it is necessary to invert the relationship between the system variable and parameters. Using duality to switch how a system is described in this way results in an expression that is mathematically analogous, but not necessarily physically analogous. The equation will describe the same system and the same behaviour, but the nature of energy transfer is particular to whether you are dealing with a flow source or an effort source.

Causality

Similarly to bond graphs, causality is determined by the instantaneous changes that an element can experience. In a bond graph causality is indicated explicitly using 'causal strokes'; however, in this framework, causality is instead determined by the order of the time derivative of the system variable associated with that element. For example, in a system described in terms of the effort variables, the effort source is associated with the first time derivative of the effort. The capacitor is also associated with the first time derivative of the effort. The inductance is linked to the integral of the effort with respect to time (generalised momentum). We could say then that elements linked to the first derivative of the effort with respect to time are causal in these systems. This makes physical sense: if an element is associated to a higher order time derivative of the system variable, it will naturally experience a change *before* the other elements in the system, and elements associated with the same order time derivative experience changes *simultaneously*.

[2]Not only are the operations relating the coefficients to the system variables inverted, but also the temporal dependency.

2.3.2 Equivalent Parameters

Using these equivalent variables to describe systems allows us to define a set of equivalent parameters. This not only simplifies analysis, but also the description of the dynamic behaviour of these systems. Having separate names for mass and inductance only confuses things when describing the general dynamic behaviour of systems.

There are natural differences and similarities in the language used to describe these systems. In both the electrical and thermal case, the term describing how much energy is dissipated is called the resistance. There is also thermal and electrical capacitance, and the argument has been made by Bosworth [12] for including thermal inductance. Since thermal inductance has questionable physical significance, we will exclude it from our system of analogies. Possibly due to the nature of the mathematical analogies used to describe these systems, the language used to describe thermal and electrical systems is similar.

When we move to mechanical systems, everything is in terms of mass, stiffness and damping. This is possibly because a lot of the terms used to describe mechanical systems existed before physical analogies were invented and are derived from common language, with no relation to the underlying mathematical relationships. Some mechanical terms do have counterparts that can be described using a similar language to thermal and electrical systems, for example: frictional resistance, wind resistance, viscous resistance and a variety of other dissipation mechanisms. Through analogies we can see that inductance and mass are similar—both are related to the second time derivative of the displacement. In addition, we can show that the compliance (inverse of stiffness) of a mechanical system is analogous to the capacitance of an electrical system. We can see that the natural way of describing these systems is by no means the most rational, and so we are forced to abandon common language if we wish to clearly describe multi-physics systems.

Through analogy we can show that there are three main classes of parameter used to characterise dynamic systems which, in this thesis, are described as compliance terms C, resistance terms R, and inertance terms I. In practical systems, these may be some combination of other parameters—in mechanical systems these parameters are often determined by geometry—however, their relationship to the energy in the system remains the same. The absence of any of these terms immediately tells you something about the behaviour of the sytem: if either the compliance or inertance is not present, the system is non-resonant; alternatively, if the resistance term is missing, then the system has no energy dissipation.

Table 2.3: Equivalent parameters for each type of energy

Parameters	Compliance C	Resistance R	Inertance I
Mechanical $_m$	Compliance k^{-1}	Damping c	Mass m
Electrical $_e$	Capacitance C_e	Resistance R_e	Inductance L_e
Thermal $_t$	Capacity C_t	Resistance R_t	

Table 2.4: Constitutive relationships linking the equivalent parameters and variables for both the linear and the general case

Parameters	Compliance C	Resistance R	Inertance I
Linear	$q = C \cdot e$	$e = R \cdot f$	$p = I \cdot f$
General	$q = \mathbb{C}(e)$	$e = \mathbb{R}(f)$	$p = \mathbb{I}(f)$

Table 2.3 shows the equivalent parameters for each energy type, along with their analogous definition. In this table (and throughout the rest of this thesis) we use the subscripts m, e, and t to denote the type of energy—we take these separate energy domains as the generalised coordinates. This is similar to the use of subscripts 1, 2, 3, ... to denote the generalised coordinates in Lagrangian mechanics. We can combine the system parameters with the system variables to form the constitutive relationships between the power conjugate variables. The nature of these relationships is determined by the system which they describe. The specific example of a linear system is given in Table 2.4, along with the general case.

Thermal parameters

Thermal systems represent a case where using the common parameters of heat capacity and thermal resistance results in dimensional inconsistencies, as heat flow and temperature difference are not power conjugate variables. Instead of using heat flow, we need to use entropy flow as a variable. This requires us to divide the heat capacity and the thermal resistance by the absolute temperature. This results in the thermal capacitance (analogous to electrical capacitance) C_t and thermal Ohm R_t, as described in [12]. The thermal capacitance does not measure the amount of heat that the system can transfer, but rather the increase in entropy possible for the system. If the system and surroundings were allowed to reach a uniform temperature, the entropy of the system and the

surroundings would increase by

$$\int_0^{\theta} C_t \, \mathrm{d}\theta, \tag{2.13}$$

where C_t is the thermal capacitance, and θ is the temperature difference between the system and its environment. The thermal resistance is now analogous to the electrical resistance, giving the rate at which heat is converted into entropy and therefore can no longer perform useful work. This is similar to the way heat is dissipated in an electrical circuit—any energy dissipated as heat in through an electrical resistance can no longer perform work in the circuit.

2.3.3 Expressions for Power

The instantaneous power describes the instantaneous flow of energy into and out of a system. When looking at the dynamic behaviour of a system, the energy and the rate of change of energy in the system relates directly to its state. This makes energy and power incredibly useful for describing general systems. When it comes to energy harvesters in particular, directly examining the power dissipated by systems has obvious advantages.

The question arises, why not examine the energy dissipated? Energy can flow into and out of a system, and for practical systems, this change must happen over *time*. If we were to look at the energy dissipated, we would have to introduce time as an extra dimension and so the duration over which you measure the energy dissipated would become a factor. However, in a stationary system—for example, a system at steady state—we can assume that, over long durations, the ensemble-averaged power dissipated is constant and therefore independent of time. In fact for a number of initial conditions, a system will settle down to the same value for the ensemble-averaged power dissipated, and this will be dependent on the boundary conditions. By measuring instantaneous power, it is possible to estimate the ensemble-averaged power dissipated which, as we will see in Chapter 4, is useful when examining stochastic systems.

We introduce two further definitions to make this easier to follow: kinetic energy is proportional to the flow variable squared multiplied by the inertance, and potential energy is proportional to the effort variable squared multiplied by the compliance. Therefore, the kinetic and potential instantaneous powers will be the time derivative of the kinetic and potential energy respectively. This allows us to construct Table 2.5, showing the kinetic, dissipated and potential instantaneous power for a system described using the flow variable and also for a system described using effort.

Table 2.5: Linear expressions for power

Constraint	Potential	Dissipated	Kinetic
Flow	$P_p = C^{-1} f \int f \, \mathrm{d}t$	$P_d = Rf^2$	$P_k = I\dot{f}f$
Potential	$P_p = C\dot{e}e$	$P_d = R^{-1}e^2$	$P_k = I^{-1}e \int e \, \mathrm{d}t$

Generalised system equations

Using these equivalent parameters it is possible to write the mathematically analogous expression for any system. For a system described in terms of the flow variable

$$\frac{\mathrm{d}}{\mathrm{d}t}\mathbb{I}(f) + \mathbb{R}(f) + \int \mathbb{C}^{-1}(f) \, \mathrm{d}t = e \tag{2.14}$$

and for a system described in terms of the effort variable

$$\frac{\mathrm{d}}{\mathrm{d}t}\mathbb{C}(e) + \mathbb{R}^{-1}(e) + \int \mathbb{I}^{-1}(e) \, \mathrm{d}t = f. \tag{2.15}$$

For linear systems

$$I\dot{f} + Rf + C^{-1} \int f \, \mathrm{d}t = e, \tag{2.16}$$

$$C\dot{e} + R^{-1}e + I^{-1} \int e \, \mathrm{d}t = f. \tag{2.17}$$

2.3.4 Forms of Coupling

Two systems which exchange energy and interact with each other are said to be coupled. There are a wide variety of mechanisms through which energy can be transferred between systems. When we define a system for the purposes of modelling its physical behaviour, we limit the modes of coupling to the most significant. This section will cover the four forms of coupling that are most relevant to this thesis: dynamic and static coupling, and pyroelectric and piezoelectric coupling.

Dynamic and static coupling

When dealing with a linear mechanical system with more than one degree-of-freedom (DOF), it is convenient to express the system equations in a matrix form:

$$\mathbf{M}\ddot{\mathbf{x}} + \mathbf{C}\dot{\mathbf{x}} + \mathbf{K}\mathbf{x} = \mathbf{F}, \tag{2.18}$$

where **M** is a matrix containing the masses associated with each degree of freedom, **C** is a matrix of the damping coefficients, **K** is defined here as a matrix of the stiffnesses, **F** is a matrix of the input forces, and **x** is a vector of the displacements. For a damped, forced, uncoupled, 2-DOF system:

$$\begin{pmatrix} m_{11} & 0 \\ 0 & m_{22} \end{pmatrix}\begin{pmatrix} \ddot{x}_1 \\ \ddot{x}_2 \end{pmatrix} + \begin{pmatrix} c_{11} & 0 \\ 0 & c_{22} \end{pmatrix}\begin{pmatrix} \dot{x}_1 \\ \dot{x}_2 \end{pmatrix} + \begin{pmatrix} k_{11} & 0 \\ 0 & k_{22} \end{pmatrix}\begin{pmatrix} x_1 \\ x_2 \end{pmatrix} = \begin{pmatrix} F_1 \\ F_2 \end{pmatrix}, \tag{2.19}$$

where the subscripts 1 and 2 represent the generalised coordinate directions.

As well as describing the exchange of energy between systems, coupling can describe an exchange of energy between the degrees of freedom in a system. The nature of the coupling is determined by the elements in the system which exchange the energy. If the energy exchange is due to inertial or damping effects, this is known as *dynamic* coupling, and we see the coupling terms in the mass matrix. If the energy is exchanged via springs or other elastic effects, this is known as *static* coupling, and we see this in the stiffness matrix. However, for a forced, damped, dynamically and statically coupled mechanical system:

$$\begin{pmatrix} m_{11} & m_{12} \\ m_{12} & m_{22} \end{pmatrix}\begin{pmatrix} \ddot{x}_1 \\ \ddot{x}_2 \end{pmatrix} + \begin{pmatrix} c_{11} & c_{12} \\ c_{12} & c_{22} \end{pmatrix}\begin{pmatrix} \dot{x}_1 \\ \dot{x}_2 \end{pmatrix} + \begin{pmatrix} k_{11} & k_{12} \\ k_{12} & k_{22} \end{pmatrix}\begin{pmatrix} x_1 \\ x_2 \end{pmatrix} = \begin{pmatrix} F_1 \\ F_2 \end{pmatrix}, \tag{2.20}$$

where, in this example, the terms c_{12} and m_{12} define the dynamic coupling and the term k_{12} defines the static coupling. These forms of coupling can be generalised and applied to systems with different domains.

Piezoelectric and pyroelectric effects

When dealing with piezoelectric and pyroelectric materials, there are additional coupling effects—these materials couple different energy domains. The coupling between the thermal and the electrical domain is represented by the pyroelectric coefficient ρ, while the coupling between the mechanical and the electrical domain is represented by the piezoelectric coefficient d.

While in Section 2.1, the physical manifestation of these two effects was discussed, here we shall discuss the mathematical description of these two effects. The piezoelectric effect relates the mechanical displacement x to the voltage v (electrical effort); for the one-dimensional case

$$x = dv. \tag{2.21}$$

The pyroelectric effect relates the current i (electrical flow) to the time derivative of the temperature gradient θ (thermal effort)

$$i = \rho\dot{\theta}. \tag{2.22}$$

By integrating Eq. (2.22) with respect to time, using power conjugate variables, and re-arranging the expressions, we can begin to see the mathematical analogy between these two effects:

$$e_e = d^{-1} \int f_m \, \mathrm{d}t, \tag{2.23}$$

$$e_t = \rho^{-1} \int f_e \, \mathrm{d}t. \tag{2.24}$$

So we can see that even though these two effects are governed by different physical mechanisms, they exhibit analogous behaviour. Both of these effects link the effort in one domain to the time integral of the flow in another through some experimentally determined constant.

Interpreting this physically, we see that piezoelectric materials rely on constant variation in either temperature, or deformation, in order to generate a steady current: if a piezoelectric material is held at a constant deformation, the voltage (and hence charge) dissipates, however it needs to be connected to a circuit first; and if a pyroelectric material is held at a temperature gradient, the accumulated charge quickly dissipates, regardless of whether or not it is connected to a circuit. Still, they are not perfectly analogous. Due to the difference in the physical nature of the two effects, the pyroelectric effect can be considered as a source of electrical flow, while the piezoelectric effect represents a source of electrical effort.

2.4 Conclusions

Hopefully, through this chapter, the reader has gained an appreciation for how the pyroelectric and piezoelectric effects arise in certain materials. Alongside this, the reader has been provided with a mathematical description of these effects that will be used throughout the remainder of this work. The analogous aspect of these effects has also been highlighted, demonstrating that the mathematical relationships governing the effects are equivalent, while their physical behaviour is not.

This links to the idea of physical analogy which has been discussed at length in this chapter. By now it is hoped that the reader will have an idea of how physical analogies are formulated and the advantages to using analogous descriptions of systems. The advantages that can be gained when using analogies to describe multi-physics systems have been highlighted, as well as their limitations. These analogies allow us to express systems of any domain using the same form of equation which allows us to apply the same analysis. However, the analogy between systems is limited to their overall behaviour, described using the particular parameters and variables chosen when defining the analogy. The analogous behaviour of two systems does not imply that the physics governing the two systems are the same.

The definitions for the generalised variables and parameters have been provided, along with definitions of their relationships, not only to each other, but to the power and energy of the system. These definitions and relationships will be used in Chapter 3 to find a domain-neutral expression for the maximum power absorbed by a single-source stochastic energy harvester. They will also be utilised extensively in Chapter 4 to extend these expressions to multi-source stochastic energy harvesters—a task which would have been impossible without a comprehensive set of analogies.

3

Single-source Energy Harvesters

The work described in this chapter focuses on using the analogies presented in Chapter 2 to extend the expressions for the theoretical maximum power absorbed by mechanical systems to electrical systems. In the previous chapter we defined a system of analogies using equivalent variables and parameters. We can now use these analogies to describe the general dynamic behaviour of energy harvesting systems, which allows us to compare mechanical and electrical systems. In order to compare the behaviour of mechanical and electrical systems, we derive the system equation for an electromagnetic energy harvester, and check that the analogies defined in Chapter 2 hold for specific examples.

One of the main aims of this thesis is to develop expressions for the theoretical maximum power absorbed by multi-source energy harvesters. It is therefore logical to first show that these expressions for the maximum power absorbed can be extended across all single-source energy harvesters. The expression for the maximum power absorbed by a system driven by an electrical displacement can be found by simply using equivalent parameters and the system equation for a mechanical harvester driven by displacement. However, there are differences in the physical behaviour depending on whether a system is driven by a displacement or a potential.

When we describe a system as being driven by flow, we are saying that its boundary conditions are described in terms of flow. We can also say that it is *constrained* by flow. We can also describe boundary conditions and constraints in terms of effort, examples include force-controlled fracture testing, or using temperature gradients as boundary conditions. When we examine the physics, we see that our choice of constraint largely creates the apparent difference in behaviour and not the domain of the system. Therefore, the analysis would have been the same if a thermal system driven by temperature fluctuations was chosen instead of an electrical system driven by a changing voltage, since both are constrained by effort variables.

Since we wish to use lumped-mass models, performing the initial analysis on an electrical system makes sense. Electrical systems are often described in terms of idealised components with their properties located at a point in a network, similar to how we describe dynamic mechanical systems. In a practical sense, the variables that we deal with in electrical systems are easier to measure and control than in thermal systems: it is relatively simple to achieve a precise input voltage, whereas achieving a steady temperature gradient is far more challenging.

Section 3.1 describes how we can use the system of analogies defined in Chapter 2 to find the system equations for various boundary conditions. Section 3.2 describes the experiment that was performed to validate the analogies used. Section 3.3 provides a summary of the main findings from this chapter.

3.1 Deriving the System Equation

Finding equivalent variables and parameters enables us to find mathematically equivalent expressions for systems constrained by flow and effort. This simplifies the analysis of such systems, particularly when there is some form of coupling present. On the other hand, there are differences in how we interpret the system equations, depending on how the boundary conditions are described. The boundary conditions imposed on a system constrained by flow result in different physical behaviour than when the system is constrained by effort. Even though the system equations end up as *mathematically* analogous expressions regardless of the boundary conditions, care must be taken when interpreting these as they are not *physically* analogous.

3.1.1 Systems Constrained by Flow

For a system constrained by a flow (for example a circuit driven by a current source or a mechanical system driven by vibration), we have the following system equation

$$I\dot{f} + Rf + C^{-1}q = 0, \tag{3.1}$$

where I is the inertial coefficient (inertance), analogous to either the mass or inductance of the system; R is the resistance, analogous to damping or electrical resistance; C is the compliance, analogous to mechanical compliance or electrical capacitance; f is the flow variable; and $q = \int f \, \mathrm{d}t$ as the general displacement. The first term in this equation (the inertance term) is related to the first derivative of the flow with respect to

time—the mechanical acceleration. We can also interpret this term as the derivative of the generalised momentum with respect to time, which gives us effort. The second term in Eq. (3.1) is the resistance term, and this is directly related to the flow, again giving effort. The third term is the compliance term, and is related to the integral of the flow with respect to time, the generalised displacement—this effort is analogous to the force on a spring, or charge across a capacitor.

By examining the system equation in more detail, we can develop an idea of how kinetic energy transfer is related to changes in the generalised momentum of the system. The generalised momentum is defined as

$$p = If \tag{3.2}$$

for the linear case. The corresponding kinetic energy V is given as

$$V = \frac{1}{2} p\dot{q}. \tag{3.3}$$

This tells us that a change in the kinetic energy of a system requires either a change in the generalised momentum or flow of a system. However, since the momentum and flow are both associated with the derivative of the displacement with respect to time, the change in momentum and flow must occur simultaneously.

Differentiating the generalised momentum with respect to time gives us the effort variable. In a system constrained by flow, this gives an expression relating the effort to the inertia of the system

$$e_V = I\dot{f} = \dot{p}, \tag{3.4}$$

where e_V represents the interial effort (relating to kinetic energy). Eq. (3.4) is equivalent to Newton's law stating force equals mass times acceleration, since $I\dot{f} = I\ddot{q}$. We can define the other efforts in the system in a similar way

$$e_R = Rf = RI^{-1}p, \tag{3.5}$$

$$e_U = C^{-1}q = C^{-1}I^{-1}\int p\,\mathrm{d}t, \tag{3.6}$$

where e_R represents the resistive effort (relating to dissipated energy); and e_U represents the compliant effort (relating to potential energy). We can see that in Eq. (3.4), the momentum is differentiated with respect to time; whereas, in Eq. (3.5) the momentum is not differentiated with respect to time, and in Eq. (3.6) the momentum is integrated with respect to time. Referring back to the ideas of causality described in Section 2.3.1,

we can infer that a change in momentum with respect to time *causes* the change in momentum experienced by the system. Therefore, kinetic energy into the system must come from the inertial effort, and is thus linked with the flow differentiated with respect to time.

This can also be demonstrated if we examine the Hamiltonian $\mathcal{H}$—representing the total energy of the system—for a conservative system. We can write the system equation in terms of general displacement

$$I\ddot{q} + C^{-1}q = 0, \tag{3.7}$$

where the sum of the kinetic and potential energy is

$$\mathcal{H} = \tfrac{1}{2}I\dot{q}^2 + \tfrac{1}{2}C^{-1}q^2, \tag{3.8}$$

allowing us to re-write Eq. (3.7) as

$$I\frac{\mathrm{d}}{\mathrm{d}t}\frac{\partial \mathcal{H}}{\partial p} + \frac{\partial \mathcal{H}}{\partial q} = 0. \tag{3.9}$$

Only the first term—and hence kinetic energy—is explicitly dependent on time; therefore, any instantaneous change in energy must come from a change in flow with respect to time. It is true that flows and displacements within the system will change the distribution of energy in the system, but these are always preceded by a base acceleration. If the system is displaced and allowed to reach equilibrium (Eq. (3.6) is a constant) then there is no change in momentum (or energy) over time. Equally, if the system has a constant flow (dynamic equilibrium) then Eq. (3.5) is a constant and $\dot{p} = 0$ so there is no change in energy over time.

For systems attached to the base, there needs to be a change in the relative displacement or flow between the system and the base for energy exchange to occur. If both the flow or displacement of the base is increased by an equal amount, and this is done over a long duration, or the system is allowed to reach equilibrium after this initial increase, then there will be no internal effort. Effort (forces, potentials) require an energy flow to be present in a system, otherwise they are balanced and so there is no net effort.

These are symmetry conditions; if both the base and the system are transformed by the same amount (in the dimensions of displacement or flow), there is no energy exchanged. For a mechanical system, when you change the distance or velocity of the base in a quasi-static fashion, there are no internal forces produced. In an electrical system, this is the same as increasing the charge of the ground and the charge on a

capacitor simultaneously—no voltage will be produced. In other words: increasing the displacement or flow of the entire system produces negligible internal effort, provided this change takes place over a sufficiently long duration. In theory, this duration would have to be infinite, but it works as an approximation for real systems.

We can use these ideas to derive the system equation for a general system driven by flow. We can express the internal effort of the system as a function of the flow $\mathrm{g}(f, q)$. Since there is no energy transfer in the system at equilibrium, and hence no net effort

$$\mathrm{g}(f, q) = 0. \tag{3.10}$$

Introducing $r = f + \mathcal{F}$ as the new equilibrium point after an increase in the base flow $\mathcal{F}$, we can also say that $\mathrm{g}(r, \int r \, \mathrm{d}t) = 0$. Hence

$$\mathrm{g}(r, \int r \, \mathrm{d}t) = \mathrm{g}(f + \mathcal{F}, q + \int \mathcal{F} \, \mathrm{d}t) = \mathrm{g}(f, q) = 0. \tag{3.11}$$

Since we are assuming that this change happens over an infinite duration, $\dot{p} = I\dot{f} = 0$. We can also see from this that if f and q are both constant, then $\dot{f} = 0$. Currently, in the system as we have described it, the relative flow f does not change. However by introducing

$$I\dot{r} = I\dot{f} + I\dot{\mathcal{F}}, \tag{3.12}$$

we can re-write Eq. (3.1) as

$$I\dot{f} + Rf + C^{-1}q = -I\dot{\mathcal{F}}. \tag{3.13}$$

We can see that this is both mathematically and physically equivalent to the system equation for vibrational harvesters found in [36], which has the following expression for the maximum power absorbed

$$P = \frac{\pi S_0 \, m}{2}. \tag{3.14}$$

It should be noted that Eq. (3.14) is only valid for white-noise systems. Therefore, applying the same analysis will yield an expression for the power-bound for a system driven by a white-noise input

$$P = \frac{\pi S_{\dot{\mathcal{F}}} I}{2}. \tag{3.15}$$

Using the analogous terms, we can quickly find the power-bound for electrical systems

$$P = \frac{\pi S_0 \, L_v}{2}. \tag{3.16}$$

If we wish to find these expressions for any other system, then we can use the equivalent parameters relevant to that system. This demonstrates the usefulness of analogies: we can now extend this analysis to any system that is driven by flows.

3.1.2 Systems Constrained by Effort

Re-arranging familiar expressions for mechanical systems and comparing these with electrical system equations allows us to easily demonstrate that these systems are analogous. If we so desired, we could re-write the equation for a mass-spring-damper system

$$m\ddot{x} + c\dot{x} + kx = 0 \tag{3.17}$$

in terms of effort (forces), instead of displacement. This gives rise to the following expression

$$k^{-1}F + c^{-1}\int F\,\mathrm{d}t + m^{-1}\iint F\,\mathrm{d}t\,\mathrm{d}t = 0 \tag{3.18}$$

where k is the stiffness, c is the damping, m is the mass, F is the force, and x is the mechanical displacement. This expression does not satisfy the requirement for using power conjugate variables, as the terms give the generalised displacement—whereas we require flows (velocities) and effort. Therefore, we need to differentiate Eq. (3.18) with respect to time, giving

$$k^{-1}\dot{F} + c^{-1}F + m^{-1}\int F\,\mathrm{d}t = 0. \tag{3.19}$$

This is not a familiar expression; it is rare that we describe mechanical systems in terms of effort. We do however frequently think about electrical systems in terms of their effort variable

$$C_v\dot{v} + R_v^{-1}v + L_v^{-1}\int v\,\mathrm{d}t = 0, \tag{3.20}$$

where C_v is the capacitance; R_v is the electrical resistance; L_v is the inductance; and v is the voltage. Comparing Eq. (3.20) to Eq. (3.19) allows us to see that these system will display analogous behaviour. Electrical duality allows us to re-write this equation as

$$L_v\ddot{q}_e + R_v\dot{q}_e + C_v^{-1}q_e = 0, \tag{3.21}$$

(q_e is the electrical displacement) confirming the equivalence of these systems, as this closely resembles Eq. (3.17). So we can be satisfied that, theoretically at least, these systems are analogous.

Again, using ideas about the change in generalised momentum for a system, we can begin to examine what happens when we drive a general system with an effort. First, it is useful to first examine the conditions required for the system to reach equilibrium. Writing Eq. (3.20) in the general form gives

$$C\dot{e} + R^{-1}e + I^{-1}\int e\,\mathrm{d}t = 0. \tag{3.22}$$

Examining the case where

$$\dot{e} = 0 \tag{3.23}$$

and starting from an equilibrium state ($e = 0$) we see that any change in the effort variable e will produce a flow and so

$$R^{-1}e + I^{-1}\int e\,\mathrm{d}t \neq 0. \tag{3.24}$$

In fact, if e remains constant, this flow will continue to increase indefinitely—imagine the velocity of a mass accelerating under a constant force in space. This shows us that while there is a net effort present (i.e. unbalanced forces or potentials) the system will not reach a static or dynamic equilibrium. For a system constrained by effort, equilibrium implies that there is some equal, opposing effort $\mathcal{E}$, such that $e = -\mathcal{E}$. In the case where these two efforts are equal there is no energy transfer present and so the energy in the system remains constant. We can also understand this in terms of momentum change in the system. The momentum of the system—as well as its energy—depends on the initial displacement and flow of the system. The momentum of the system will remain the same indefinitely, provided there is no net effort, as $e + \mathcal{E} = \dot{p} = 0$. Some physical examples of this principle include: a hot item left in a room will achieve a temperature in balance with a room; to maintain a constant voltage across a circuit we need to apply power constantly; and when the chemical potential energy in a battery is depleted, there can no longer exist any voltage across it.

Now that we understand what equilibrium looks like for a system driven by effort, we can explore how potential energy is transferred to the system. For a system in equilibrium, the only way energy transfer can occur is if there is an instantaneous change in the constraining effort variable. For physical systems, this change must occur with respect to time, which will create an instantaneous imbalance. This instantaneous imbalance leads to a change in the potential energy of the system, before this is dissipated

or converted to kinetic energy. For a system at equilibrium, this implies

$$C\dot{e} + C\dot{\mathcal{E}} = 0, \tag{3.25}$$

since energy (and in this particular case, charge) must be conserved. Combining Eqs. (3.22) and (3.25) gives

$$C\dot{e} + R^{-1}e + I^{-1}\int e\,\mathrm{d}t = -C\dot{\mathcal{E}}. \tag{3.26}$$

Now that we have the system equation for a system driven by an effort, given by Eq. (3.26), we can find an expression for the maximum power absorbed by this system. Following a similar analysis to the systems constrained by flow, the power-bound for a system constrained by effort is shown to be

$$P = \frac{\pi S_{\dot{\mathcal{E}}} C}{2}. \tag{3.27}$$

Using the equivalent parameters for an electrical system gives

$$P = \frac{\pi S_{\dot{\mathcal{E}}_e} C_e}{2}, \tag{3.28}$$

which, through electrical duality, we can show as equivalent to

$$P = \frac{\pi S_{\dot{\mathcal{F}}_e} I_e}{2}. \tag{3.29}$$

Performing dimensional analysis confirms that these have the dimensions of power. It is clear that Eq. (3.27) is mathematically analogous to Eq. (3.15); they are duals of one another. Eq. (3.15) relates to the kinetic energy absorbed, while Eq. (3.27) relates to the potential energy absorbed.

3.2 Experimental Verification

In order to validate the measurement and post-processing procedure that will be used in Chapter 5, an experiment was set up using a linear circuit. Since the behaviour of such a system is already well understood, we would expect the experimental results to match the theoretical expressions for the maximum power absorbed by a system driven by an effort source (for example, an electromagnetic energy harvester).

For the experiment, it was necessary to measure the capacitance as well as the voltage (effort) to calculate the time averaged power absorbed. Post-processing the experimental results allows us to estimate the time derivative of the input voltage. Once we have found both the voltage and its time derivative, the time averaged power absorbed can be calculated using Eq. (3.27). S_0 in this case has been estimated from the root mean square average of the input signal $\dot{\mathcal{E}}_e(t)$. Once the time averaged power absorbed by the system has been calculated, it can be plotted against the measured capacitance. If the experimental results show a linear relationship between the time averaged power absorbed and the capacitance, then this gives us confidence in both the measurement and the post-processing procedure.

3.2.1 Setup

The energy harvesting system was represented using a simple circuit, shown in Fig. 3.1. In this circuit, various capacitors and a single $1 \times 10^5\Omega$ resistor are attached in parallel. The actual circuit varied from this theoretical setup, as can be seen in Fig. 3.2. For the actual circuit, it was necessary to attach a resistor in series with the capacitor as otherwise it would have short-circuited the voltage source, producing large currents that may damage the capacitor. This can still be considered as a parallel capacitor with a parasitic resistance. The voltage across both of these components will be regarded as the voltage across the capacitor. To provide the circuit with a stochastically varying input voltage, an NI USB-6002 data acquisition (DAQ) card is attached in parallel. The DAQ has an output range of $\pm$10V, with an output current drive of $\pm 5 \times 10^{-3}$A. The absolute accuracy (no load) in the output voltage is 8.6×10^{-3}V typical at full scale.

A GDS-2000A oscilloscope (Fig. 3.3) was used to measure and record the voltage across the circuit. The oscilloscope was connected in parallel as shown in Fig. 3.2 using a BNC cable. The attenuation on the oscilloscope was set at 1x. For the purely electrical testing, the alternating current (AC) grounding setting of the oscilloscope was used. Since the oscilloscope is connected in parallel with the other components, the voltage across all of them is the same, therefore only one channel is needed. The oscilloscope itself has a capacitance of 16×10^{-12}F and a resistance of $1 \times 10^6\Omega$. The voltage waveforms from this oscilloscope can be saved as a .csv file with a voltage resolution of 2×10^{-3}V and selecting full bandwidth gives 5000 samples per waveform. The 'Single' mode was used to record the data. In this mode the oscilloscope records data until all samples are full and then stops. Since the oscilloscope will always take 5000 samples, changing the sampling frequency changes the duration over which the

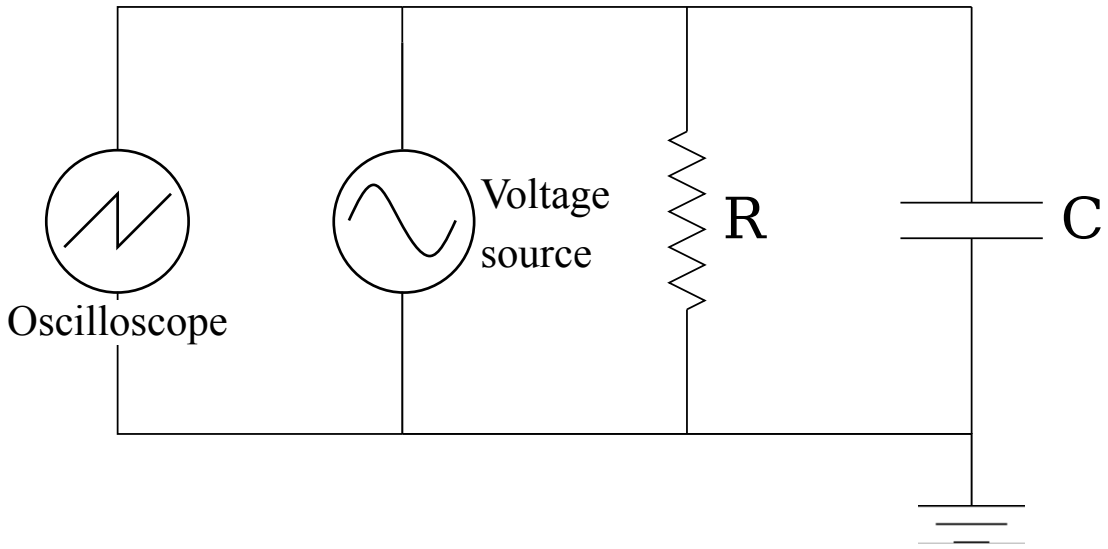

Figure 3.1: Schematic of the parallel resistor-capacitor (RC) circuit used in the single-source experiments. The resistor shown represents R_e, and the capacitor shown represents the electrical capacitance C_e of the system. The analog output channel from the DAQ is connected in parallel with the system components and provides the stochastic voltage source. The oscilloscope is also connected in parallel.

sample is taken, for example a sampling frequency of 1000 Hz requires 5 seconds to generate 5000 samples.

3.2.2 Procedure

The electrical noise was generated using the waveform function in LabView (Fig. 3.4), which generates a discrete approximation of a white noise zero-mean Gaussian signal. The amplitude of the generated signal is controlled by changing the standard deviation σ of the signal in LabView, which can range from 0 to 2. A value of 1 was used for this experiment. This white-noise signal is then converted into an output voltage using the DAQ. This voltage is applied in parallel to the circuit shown in Fig. 3.2.

The value of the capacitance (C in Fig. 3.1) was changed by physically swapping the capacitor used in the circuit. The values of the capacitors (measured values for C_e) used were (0.08, 0.21, 0.47, 0.66, 0.89, 2.35 and 3.01) $\times 10^{-6}$ F. For each capacitor, the circuit was driven by the white-noise input and the electrical effort e_e across the circuit was recorded using the oscilloscope. The electrical effort was also measured when there was no capacitor in the circuit. Since the electrical source is in parallel, the electrical effort $\dot{e}_e$ in this case was equal to the input effort $\dot{\mathcal{E}}$. By measuring this effort, the power absorbed at each capacitance can be calculated using Eq. (3.27).

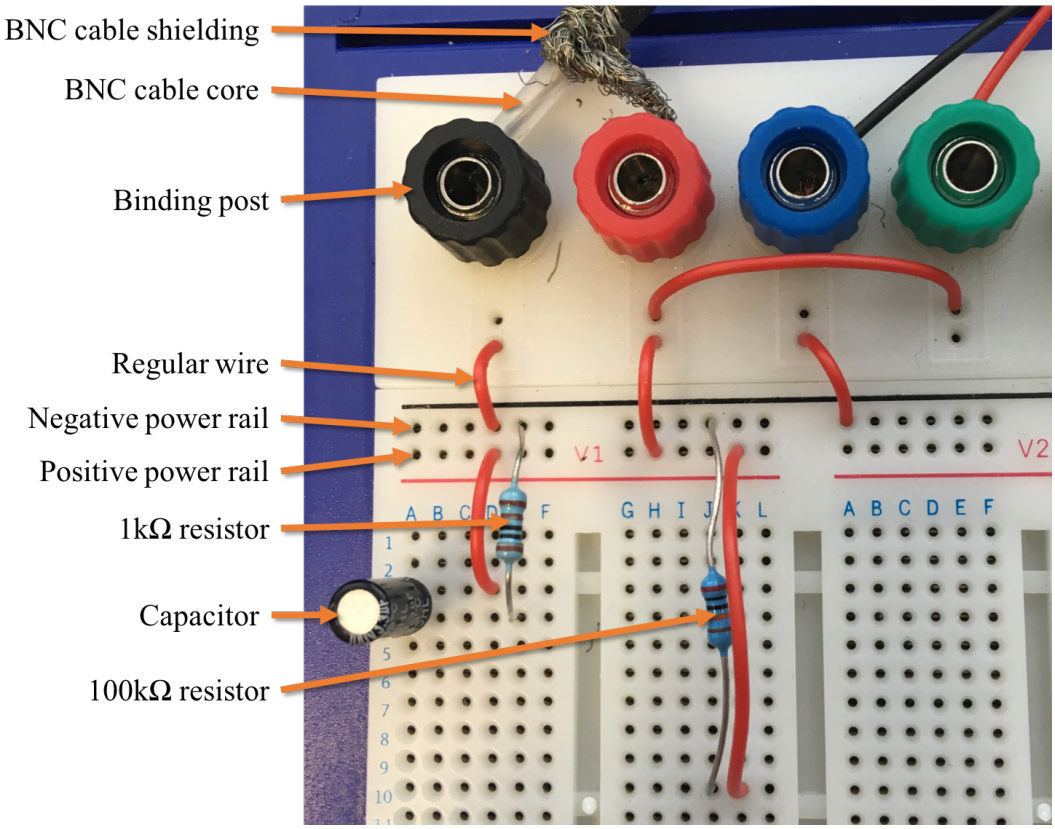

Figure 3.2: Photograph of the physical circuit. In the top left we can see the core of the BNC cable (oscilloscope active) attached to the black binding post; this is then connected to the negative power rail (black). The shielding from the BNC cable (oscilloscope ground) is attached to the red binding post; this is then connected to the positive power rail (red). The active wire (black) leading from the analog output channel of the DAQ is attached to the blue binding post; this is then connected to the negative power rail. The ground wire (red) from the DAQ analog output channel is connected to the green binding post. This is directly connected to the ground of the oscilloscope. The circuit components are placed so that they form a bridge between the two power rails, creating a parallel circuit.

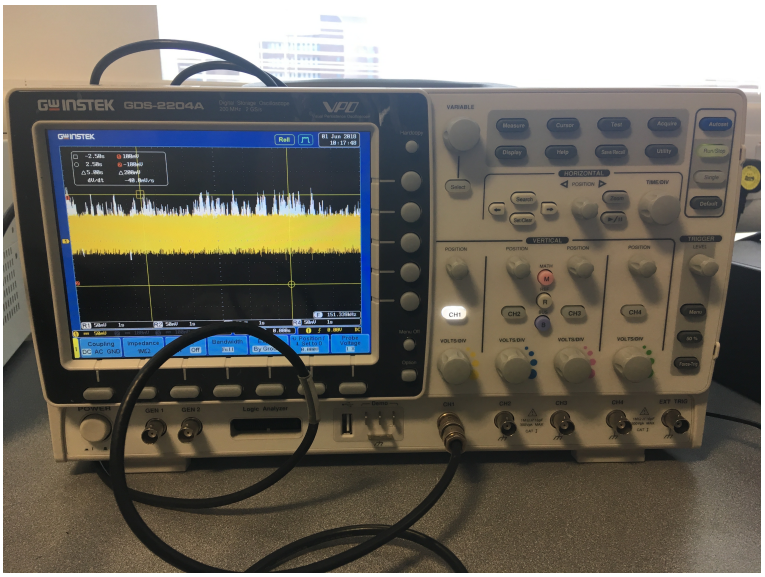

Figure 3.3: Photograph showing the oscilloscope used in the experiment. Only a single channel was required, as there is only one voltage of interest. The yellow waveform is the waveform that is currently measured by Channel 1. The white waveform is a waveform that has been previously saved, and has been recalled so that it is visible.

Transferring files

The time history of the electrical effort is saved onto the oscilloscope as a waveform. The waveform for each capacitor was saved onto the oscilloscope as a .csv file. After all of the waveforms were saved—8 in total—they were recalled and displayed on the oscilloscope. Up to 4 waveforms at a time can be displayed on the oscilloscope. The displayed waveforms were then saved in a combined .csv file onto a USB drive (there were 2 files containing 4 waveforms each). These combined .csv files were then imported into MATLAB, with each waveform as a seperate variable. Once in MATLAB, these waveforms were combined into a single array and the headers (cells at the beginning of each file containing information about the oscilloscope settings) were removed from each waveform. This procedure produced an array containing the time history of the electrical effort for all of the capacitors.

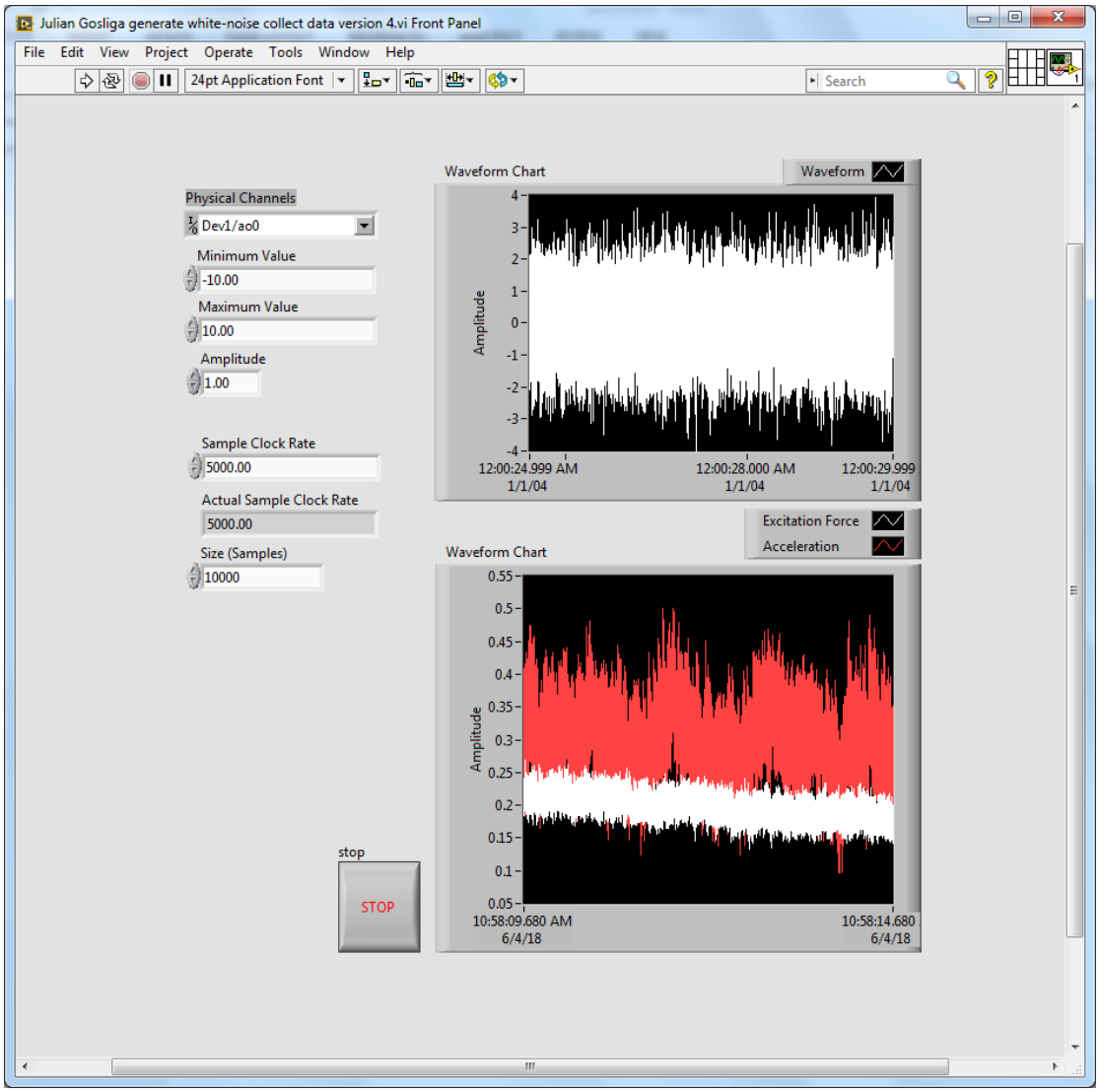

Figure 3.4: Screenshot of the front panel for the LabView virtual instrument (VI) used to generate the white-noise signal. Using this front panel, the standard deviation of the signal can be altered, as well as the maximum and minimum values for the output voltage. Other settings to determine the sample rate and buffer size can be adjusted. The generated signal is then sent via a USB cable to the DAQ, which applies the corresponding voltage across the circuit.

3.2.3 Post-Processing

Calculating the power absorbed by the capacitor requires us to use the time derivative of the electrical effort variable $\dot{e}_e$. Since the electrical effort e_e is a stochastic white noise process, any samples measured on the oscilloscope are uncorrelated; as such, its derivative is not defined in the same way as a normal function. Therefore, it is necessary to fit a smooth function to the data before evaluating the time-derivative.

Here we will compare a selection of different post-processing methods. The results from various filtering and post-processing methods will be considered against results obtained by using the forward finite difference method with the raw data. While the time derivative may be undefined for a stochastic process, we can see the forward difference method as in some way giving a linear fit to the data points. We can assess the validity of the post-processing methods by examining how closely their time history and frequency content matches the raw data. The frequency content of both the original signal and its derivative (obtained using forward difference method) are close to what we would expect to see for a white-noise signal, which makes the forward difference method appropriate as a benchmark. We would also expect that the phase angle between the signal and its time-derivative will be 90°.

Savitzky-Golay filtering

Savitzky-Golay filters provide a linear least squares fit to successive data points. This meets the first criterion of providing a differentiable function which approximates the stochastic process e_e. It is also possible to directly obtain an estimate for the derivative using the coefficients generated by the Savitzky-Golay filter. The Savitzky-Golay filter not only provides a smooth function which fits the original data, but also an estimate for its derivatives.

The width of the window used with the Savitzky-Golay filter has an effect on the power of the processed signal. Increasing the width of the window (for example 101,103) gives a higher estimate for the power. However, there is a limit on how wide the window can be before the filtered signal no longer resembles the original signal. The effect of changing the window width is shown in Fig. 3.5, where an excessively wide window gives a sparser response with higher amplitude peaks, which does not match the raw data; whereas, a narrow window gives a response that more closely matches the raw data. This shows that choosing the correct window length is vital to obtaining a physically representative estimate of $\dot{e}_e$ when using the Savitzky-Golay filter. The window length

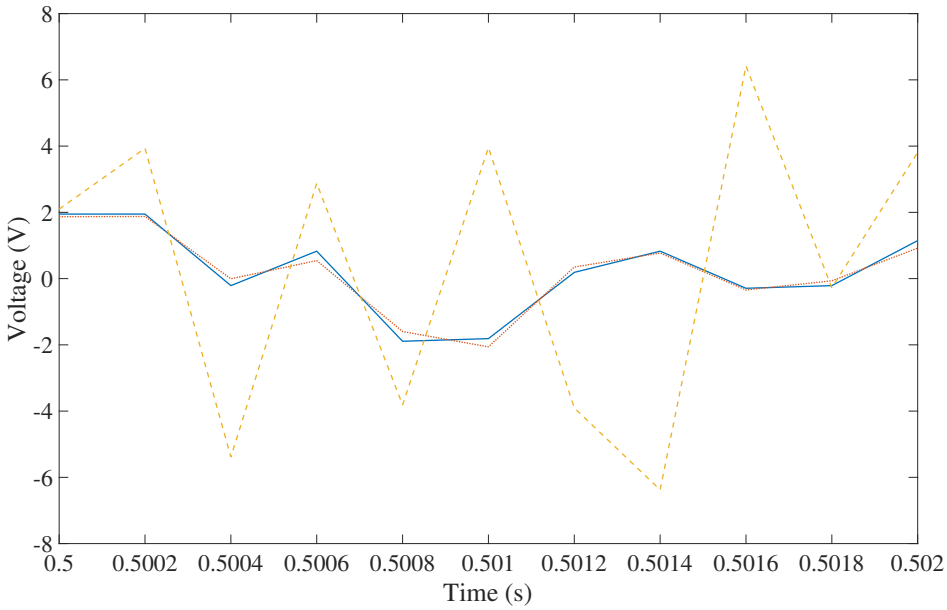

Figure 3.5: Time history of the raw data (solid blue line) compared with the Savitzky-Golay filter using a wide window (orange dashed line) and using a narrow window (red dotted line). The Savitzky-Golay filter using the narrow window shows close agreement with the raw data, while using the wide window does not resemble the raw data.

can also be adjusted to a point where the results are essentially unfiltered, which of course matches the original signal exactly.

When we examine the phase between the filtered signal and its derivative we see a 180° difference. This tells us that these signals are not representative of the physical case. The signals produced using the Savitzky-Golay filter could be interpreted as giving us a surrogate signal, with similar statistical properties to the original, but with different time-domain behaviour.

Interpolation smoothing

The interpolation smoothing method takes the initial samples and interpolates a smooth function between them. This smooth function is then differentiated using the forward difference method.

This method involves upsampling the measured data, and then interpolating between the data points to fill the new samples. First, a new time vector is created that is the length of the original sampled time vector. The length of the new time vector is then scaled by an integer value to increase or decrease the sampling rate. For example, to

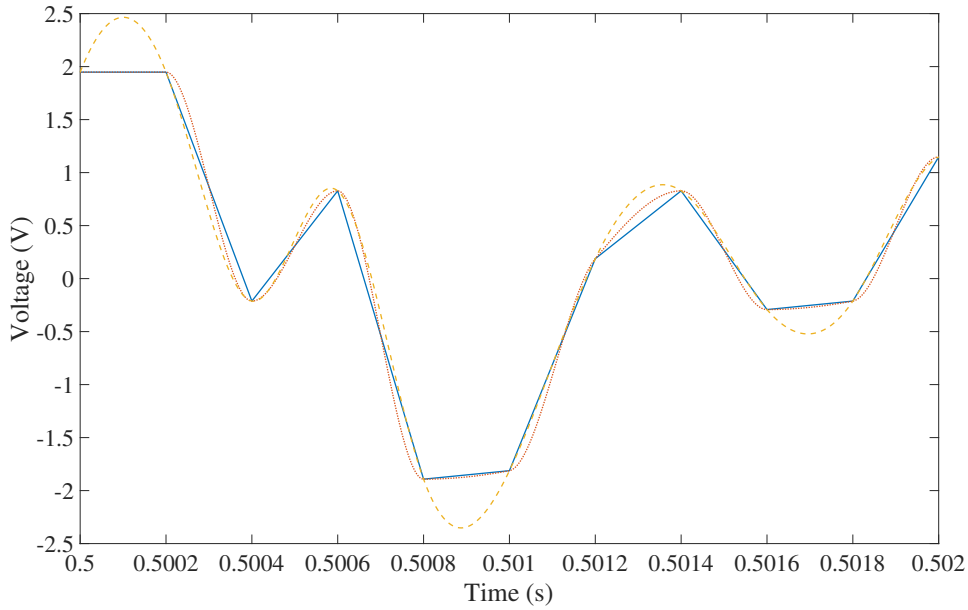

Figure 3.6: Time history of the raw data (blue solid line) and smooth interpolated function using the spline method (orange dashed line) and using the pchip method (red dotted line). The linear interpolation method is not shown as it follows the raw data exactly. These methods all show good levels of agreement.

double the sampling rate, the length of the time vector must be doubled. This scaling process creates extra time steps between the measured data points. To generate the extra data points, the 1-dimensional interpolation function in MATLAB is used to interpolate between the measured data points.

The results of applying various interpolation methods can be seen in Fig. 3.6. Using the linear interpolation method results in an identical signal to the raw data, but with a higher sampling rate. The pchip interpolation method preserves the flat sections in the signal, while rounding edges slightly, giving essentially the same result as linear interpolation. Using the spline method creates a signal that is arguably closer to what we might expect the true behaviour of the system to look like. In the true physical response of the system, we would expect to see rounded peaks, rather than sharp points or flat sections.

In a physical system, we would expect the time derivative to be 90° out of phase with the signal. Applying this sanity check to the post-processed results gives us some sense of their validity. We see that most of the time the phase difference is 180° when using

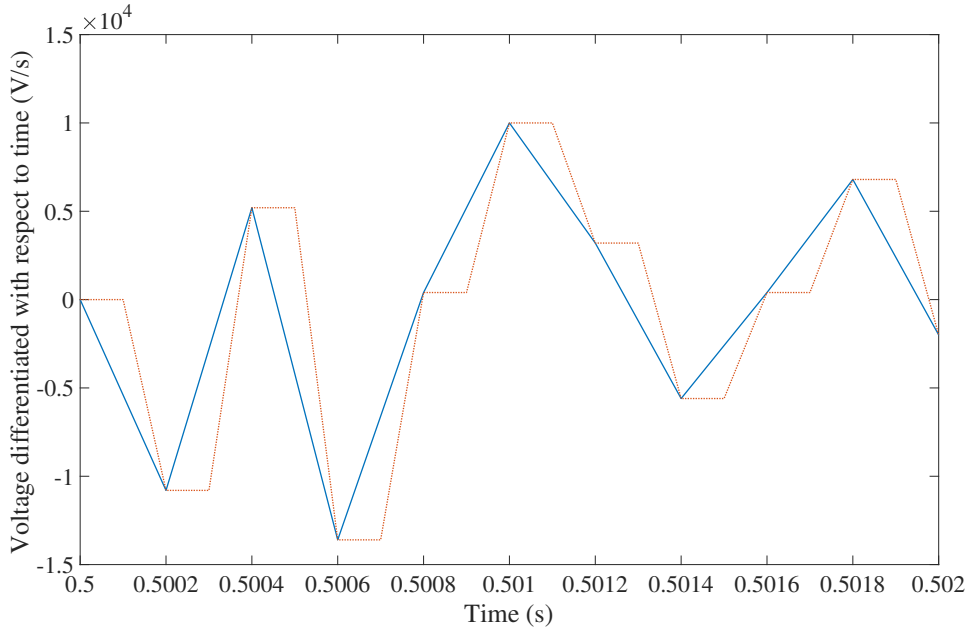

Figure 3.7: The time derivative of the voltage estimated from raw data (blue solid line) and linear interpolation (red dotted line).

the spline or pchip methods. The method that best preserves the phase-difference is the linear interpolation method.

However, care must be taken when using the linear interpolation method to upsample the data. It follows the raw voltage data exactly, but there is a stepping effect seen when we take the time derivative of the signal. This stepping behaviour is shown in Fig. 3.7, where it is compared against the estimate of the time derivative obtained with no upsampling. We would not expect to see stepping behaviour like this in the physical system, and so whilst the phase difference obtained using the linear interpolation method is physically representative, the time derivative is not.

Sampling frequency

Adjusting the sampling frequency used for the oscilloscope has two important effects. Firstly, increasing the sampling frequency increases the measured power, since the sampling frequency gives the cut-off frequency for the oscilloscope: any energy at frequencies higher than the sampling frequency will not be recorded by the oscilloscope. Secondly, the sampling frequency affects the duration over which the signal is recorded since the oscilloscope can only record a maximum of 5000 samples. Therefore, the sampling period (inverse of the sampling frequency) affects the overall duration. If

the duration over which the signal is recorded becomes too low, then we see excessive variability in the results. To find the optimal sampling frequency, the results for the experiment will be recorded at a range of sampling frequencies.

Chosen post-processing method

We can see from Fig. 3.8 that all of these post-processing methods distort the frequency content in some way. The Savitzky-Golay filter (plot B) has the same maximum frequency as the raw data (plot A), but we see that it filters out a certain frequency range. Also, using the Savitzky-Golay filter, we see distortion in the higher frequencies possibly resulting from edge effects. The linear (plot C) and spline (plot D) interpolation methods avoid distorting the frequency content below half the original sampling frequency (5000Hz), although there is distortion above this frequency. We can avoid this distortion by using an interpolation method and keeping the sampling frequency the same.

The methods were assessed on the mode of the phase angles calculated between the electrical potential and its time derivative. The phase angles in radians are shown for the various methods in Fig. 3.8, where the value should be 90° or 1.57 radians . While there is some variation in the phase angles due to the stochastic nature of the system, in the majority of cases, the phase angles for the raw data and the linear interpolation method (shown in plot E) match with the theory. The mode of the phase angles is 180° in the case of the spline interpolation and Savitzky-Golay filtering method (shown in plot F), suggesting that the results generated using these methods are not representative of the underlying physical behaviour. Distortion of the phase angle is particularly important when examining the energy and power of a dynamic system, as it often features in calculations.

In the end, the interpolation method with a linear fit and without any upsampling was chosen. The linear interpolation method will give us a differentiable function, which is essentially the same as the recorded signal. Based on the results shown in Fig. 3.8 the linear interpolation method is the best option to avoid distorting either the frequency content or the phase angle. Other methods (spline interpolation and Savitzky-Golay filtering) are better suited to signals where there is some underlying harmonic signal with unwanted noise as they are primarily designed to remove noise from a signal. However, in the case where the signal is purely white noise, there are no additional benefits to these methods.

While there are a wide variety of numerical differentiation methods available, we will use the forward difference method. We can assume that the error from the forward difference method $O(h)$ is reasonably small, due to the small step sizes used ($h = 1/5000$

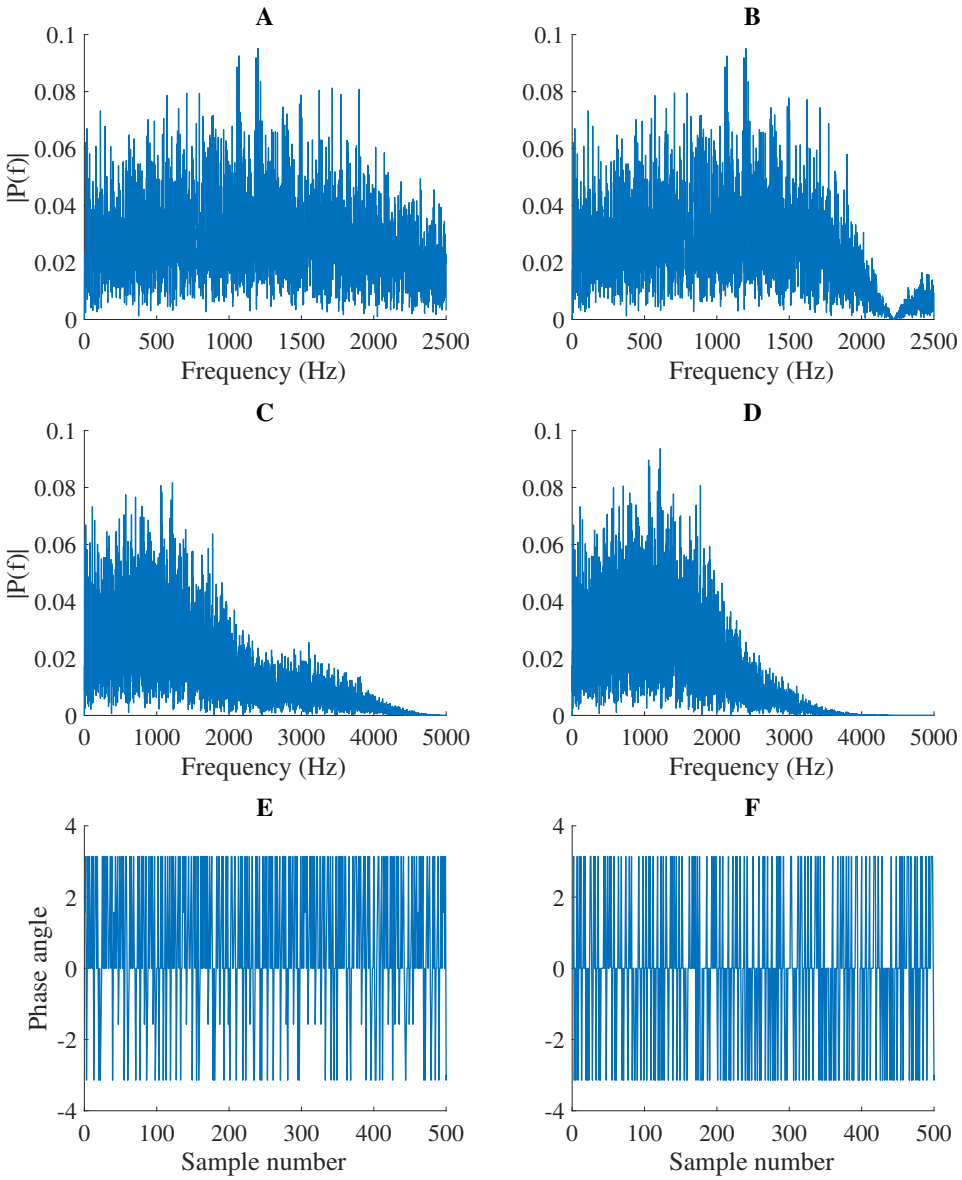

Figure 3.8: A series of plots showing the frequency content for: A) the raw voltage data, B) the voltage estimated using a Satizky-Golay filter, C) the linear interpolation method, and D) the spline interpolation method. The final two plots show a comparison of the phase angle between the voltage and its time derivative for each sample.

or 5000 samples over the whole duration). In addition, according to Grossman et al. [25], finite difference methods are a widely dominant solution for solving partial differential equations, and so should be well suited to this application. Finally, it is easy to understand how this method works, which makes the post-processing steps transparent and avoids masking the physical significance.

3.2.4 Results

The experimental results for the power absorbed by the system vary linearly with the electrical capacitance, as shown in Fig. 3.9; this matches with the theoretical prediction given by Eq. (3.28). From these results, we can also see that recording the results for an overall duration of less than 1 second causes excessive variation in the results, obscuring the trend. We can see in Fig. 3.10 that as the sampling frequency increases, the time averaged power absorbed convergences to some value. This demonstrates that there is some practical limit on the amount of energy that can be absorbed from the source by the system, which is as expected.

3.2.5 Discussion

Eq. (3.27) can be used to calculate the power absorbed by an energy harvester driven by an effort source—and hence the maximum useful power available. The equivalent expression for mechanical harvesters, given by **??**, has already been verified by Hawes [30] and Langley [35, 36]. The results shown in Fig. 3.9 confirm that mathematically analogous expressions can be applied to systems driven by an effort source—in this case an electromagnetic harvester. As discussed in Section 2.2, the expressions for the power absorbed Eqs. (3.15) and (3.27) can be applied regardless of whether systems are described in terms of mechanical or electrical energy; they are domain-neutral expressions. As such, we can assume this expression is valid for physical systems that we can define in terms of power conjugate variables. The chosen type of energy simply determines which set of parameters or variables appear in these expressions.

We find the only major difference between Eqs. (3.15) and (3.27) (the expressions for the power absorbed by a general energy harvester) is the parameters used in the expression for the power absorbed. Depending on the constraints of the system—flow or effort—the power absorbed is related to the system's capacity to store kinetic or potential energy respectively. The way the constraints are described changes the system parameter used in the expression for the power absorbed. For systems constrained by flow this parameter is generalised inertance, while for effort-constrained systems, the generalised

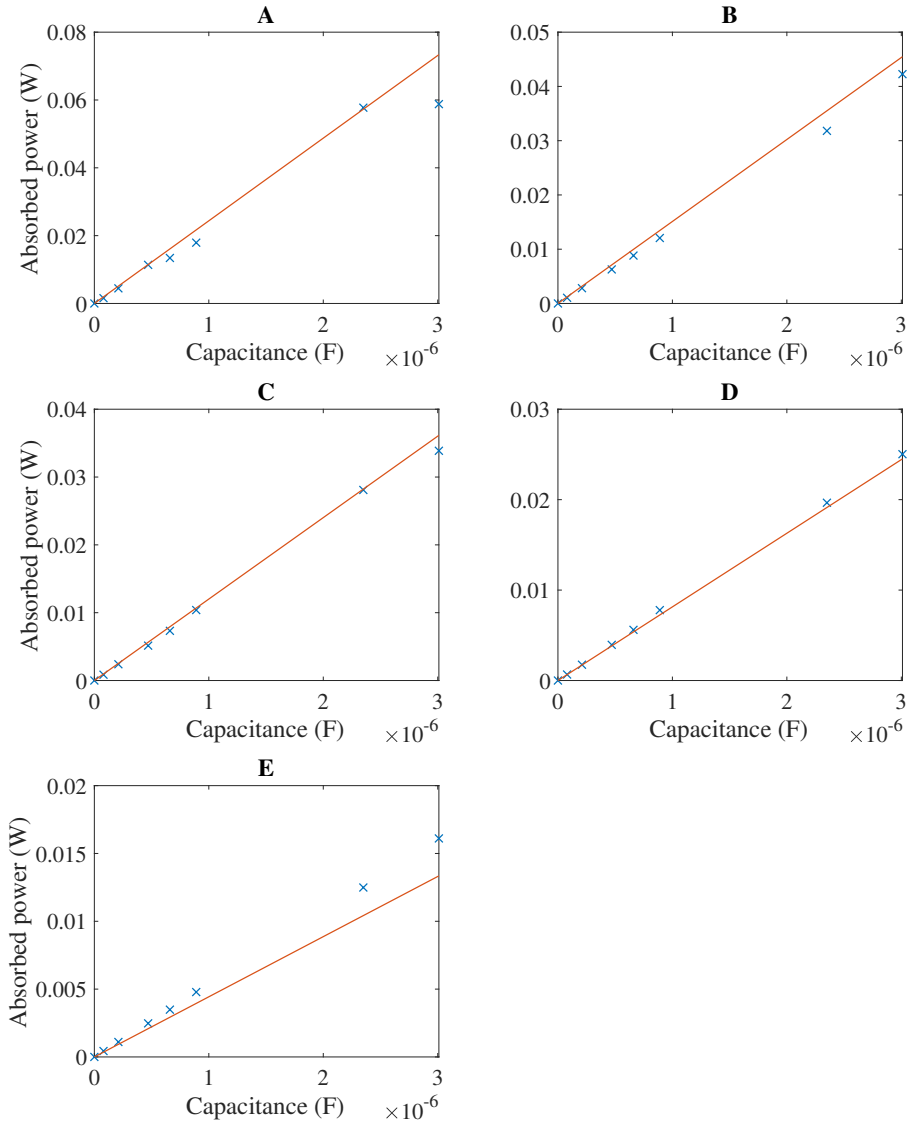

Figure 3.9: Experimental results (blue crosses) compared with the theoretical prediction (solid red line) given by Eq. (3.27). In all cases, both the experimental results and theoretical predictions show a linear relationship between the power absorbed and the capacitance, with C and D giving the closest agreement between the experimental results and the theoretical prediction. The duration over which the results were recorded—and therefore the sampling frequency—was varied. The experiment was run with a: A) 0.2 second duration at 25,000 Hz, B) 0.5 second duration at 10,000 Hz, C) 1 second duration at 5,000 Hz, D) 2 second duration at 2,500 Hz, and E) 5 second duration at 1,000 Hz. We can see increased variance with A and B, where the linear relationship becomes less clear.

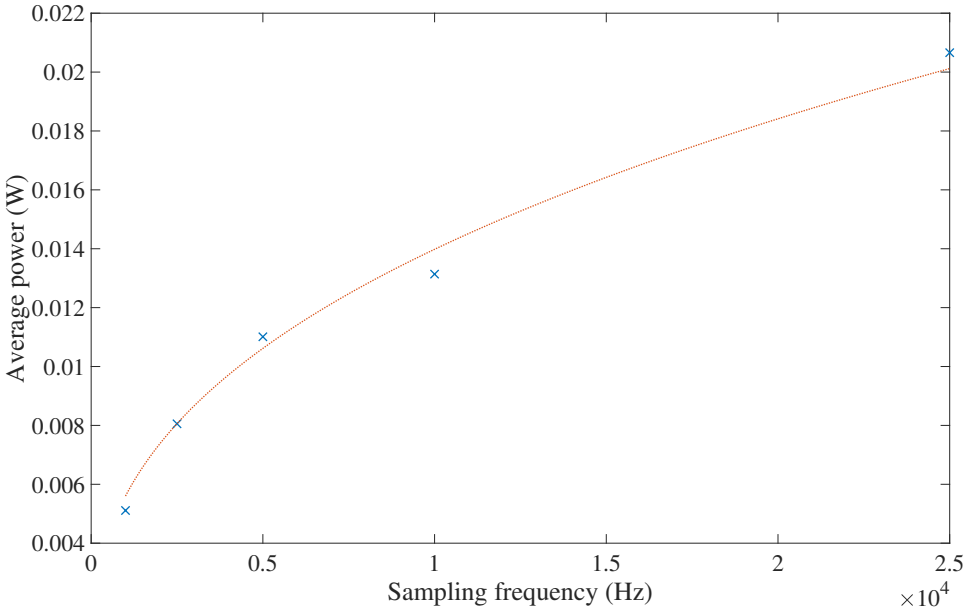

Figure 3.10: The average measured power for all values of the capacitance (blue crosses) is shown as a function of sampling frequency. The reason for averaging across all values of the capacitance is to represent the power absorbed as a function of sampling frequency. There is an approximately logarithmic relationship (red dotted line) between the measured power and the sampling frequency. We would expect the value for the average power absorbed to approach some limiting value as higher frequencies are included. This limiting value arises as practical systems can only transfer a finite amount of power.

compliance is used. Since all boundary conditions are some combination of flow or effort (or their time derivatives) we can postulate that this expression is valid for all boundary conditions. The universality of this approach for single-source systems gives confidence that we can use this approach for multi-source systems.

Implications

In Chapter 1 we saw that while there are a vast number of different designs available, there is a lack of a single metric for assessing the performance of energy harvesters. We have now developed a universal expression for the maximum theoretical power available from any single-source energy harvester, thereby allowing us to compare the performance of any single-source energy harvester using the same metric. The expressions Eqs. (3.15) and (3.27) for the power absorbed do not violate existing efficiency metrics, such as Betzs law. They need not replace existing efficiency metrics and are intended to provide researchers with an additional tool to effectively and quantitatively assess a large number of different designs.

The universality of this approach, and the ease with which it can be verified experimentally, provides a useful analysis tool for people studying general multi-physics systems. While the motivation behind this work is energy harvesting, there is nothing in this approach that limits it to energy harvesting. The approach is based on energy transfer, which is present in any dynamic system. In theory, this approach could be used to find the efficiency of any engineering component, provided the boundary conditions can be measured.

Significance

According to Eq. (3.15), for flow-constrained systems, the power absorbed increases linearly with inertance; and according to Eq. (3.27) for effort-constrained systems, the power absorbed increases linearly with compliance. This in itself has immediate practical significance. For example, in an environment where the input closely approximates an effort source, you would want to design a harvester with high compliance. In an environment where the available energy resembles a flow source, a high inertance would be desirable.

Langley [36] states that the maximum output of a vibrational harvester constrained by displacements is independent of anything other than its mass. This is further supported by work conducted by Green et al. [24], who found that changing the stiffness had no effect on the output for an energy harvester driven by a flow source. Examining **??** would

give us an idea why, with the caveat that it does not give a complete picture as the power dissipated is related to impedance. More detailed power bounds provided by Hawes [30] showed that changing the resistance can increase the percentage of the power absorbed that is dissipated electrically. Ghandchi Tehrani and Elliott [22] showed analytically and numerically that non-linear damping can also improve the power output for a device, although both the non-linear and linear device have the same output at resonance—this suggests that at resonance they both hit the same theoretical maximum as the impedance approaches zero. Therefore, we can say that for all single-source mechanical systems, there exists a maximum power available which is dependent on only the input and the mass. We can see, through the theoretical analysis performed in Section 3.1, that the equivalent statement is true for electrical systems (where the appropriate parameter is selected depending on the input). Describing this result in a general way allows us to extend these expressions beyond mechanical systems. We can now say that for *any* single-source system, the power absorbed depends only on the input and a single system parameter, and is independent of the configuration of the system.

These expressions are independent of the system configuration because they examine the power absorbed. Examining the power absorbed involves studying energy flowing into the system, rather than energy contained in the system. You can see how much power is absorbed by measuring the input to the system directly; you do not need to know exactly what the system is doing. While examining the power absorbed may not enable you to predict the specific state of the system, you may be able to infer information about how the system is behaving. For example, the power absorbed may limit a non-linear system to certain states: when driven with a low power, a bistable system is limited to intrawell behaviour. With sufficient power input, the system will begin to behave chaotically, or even display interwell oscillations.

Examining the power absorbed will not be able to tell you directly what the amount of useful power out of a system is. It is necessary to measure the power out of the system or calculate this separately for the specific case you are examining. Fortunately, this is a step that is normally carried out when designing or testing an energy harvester, as the useful power out is of primary concern. If you can measure the power into the system, along with the desired power out, you can calculate how efficient the system is. For stochastic and non-linear systems, the power in and power out can be a lot easier to measure than the actual state of the system.

Future work

A possible future addition to this work, requiring in-depth electrical engineering knowledge, would be to try and find circuits that might not obey Eqs. (3.15) and (3.27). This is motivated by the fact that this study only employed a single circuit design. This is in contrast to work performed by Hawes [30], where the expression for mechanical harvesters was verified for various mechanical configurations. If the expression for mechanical harvesters can be shown to be independent of the system configuration, we can infer that the same is true in the electrical case. That being said, it is always preferable to verify these statements. If possible, it would be interesting to use a non-linear capacitance to examine the applicability of Eq. (3.27). Lastly, it would be interesting to use real electromagnetic energy harvesting devices—especially devices described in the literature—to further interrogate these limits.

The physics would suggest that this form of analysis and analogy would be valid for chemical and thermal systems. This presents an opportunity for further work to test the validity of this method for a wider range of different energy types. For this thesis however, it was not possible to find a system that invalidated these expressions for the maximum power absorbed.

3.3 Conclusions

Past work had shown that the expression for the maximum power absorbed by a mechanical energy harvester from a white-noise input was independent of the configuration of the harvester. This chapter demonstrates that such expressions for the maximum power available to an energy harvester are independent of the type of system (mechanical or electrical). This chapter also demonstrates that different boundary conditions (flow or effort) require the use of different—albeit mathematically analogous—expressions. For systems where the boundary conditions are described in terms of flow or effort, Eqs. (3.15) and (3.27) show that the maximum power absorbed from a white-noise input is a function of the inertance or compliance respectively.

Since all physical systems can be described using power, we can assume that all physical systems—and all boundary conditions—can be described using power conjugate variables. Since the expressions Eqs. (3.15) and (3.27) only require that a system is described in terms of power conjugate variables, these expressions apply to all physical systems. Experimentally, these expressions were shown to be valid for electrical systems constrained by potentials. Past work has already shown that the equivalent expressions

for the maximum power absorbed are valid for mechanical systems constrained by displacements. The universal applicability of the concepts of power and energy allow us to postulate that these expressions apply to all practical systems driven by white-noise inputs. There is further work required to experimentally demonstrate that this is true for chemical and thermal systems, however, the theoretical foundation has now been laid.

The expressions Eqs. (3.15) and (3.27) have important practical applications as they can be used to immediately predict the maximum possible output for an energy harvester, provided the intensity of the white-noise input is known. These expressions can further guide the design process by showing which system parameter determines the maximum power available. Furthermore, these expressions for the maximum theoretical power can also be compared against the actual output for a specific application to create an efficiency metric. Such an efficiency metric is useful because it is universal for all energy harvesters. These expressions are not only helpful in the design of a specific harvester, but in a wider context to compare and review a wide variety of single source harvester designs.

The universal nature of Eqs. (3.15) and (3.27) gives confidence to the idea that a similar approach could be used for multi-source energy harvesters driven by white-noise. Using the same domain-neutral approach opens up a realm of further work into how multiple sources interact and combine. The application of this approach to energy harvesters incorporating multiple sources will be covered in Chapter 4. Up until this point, there has not been any significant work on the theory of multi-source energy harvesters. For multi-source systems, we will examine how the maximum power available relates to the actual power harvested. We will then experimentally verify any theoretical predictions for the behaviour of multi-source harvesters in Chapter 5.

4

Theoretical Analysis of Multi-source Harvesters

As described in Chapter 1, there are some clear benefits to harvesting energy from multiple sources, namely improved output and reliability. The ability to harvest energy from more than one source allows designers to improve the output of a device without greatly increasing its size. Harvesting energy from multiple sources also allows a self-powered device to continue functioning when one source is absent. For these reasons, multi-source energy harvesters have become popular for powering wireless sensor networks and nanodevices. The concept of multi-source energy harvesting has been realised experimentally; however, there is a lack of theoretical work describing the overall dynamics of these devices.

In Chapter 3, the analogies described in Chapter 2 were used to develop general expressions for the power absorbed by a single-source energy harvester, irrespective of the type of energy harvested. Equivalent expressions for the power absorbed were found for systems where the boundary conditions were described in terms of either flow or effort variables. Using a similar approach, it will be shown here that equivalent expressions can be found which describe the maximum amount of power that can be harvested from multiple sources simultaneously.

The following sections will describe several approaches for deriving an expression for the maximum power absorbed by a non-linear system with thermal, electrical and mechanical inputs. Section 4.1 will describe the system equations for a multi-source energy harvester combining the piezoelectric and pyroelectric effects for harvesting mechanical and thermal energy. Electrical energy is also included to represent an additional electromagnetic source, for example, an attached antenna. This system will be expressed as a set of coupled equations, where each domain is taken as a separate degree-of-freedom. These equations will be written using the analogous parameters and variables, as defined in Sections 2.3.1 and 2.3.2. In Section 4.2, these equations

will be used to derive expressions for the maximum power absorbed by a multi-source energy harvester with stochastic inputs ()Section 4.2.1). Section 4.2.2 will discuss the application of these expressions for the maximum power absorbed to more general systems. Section 4.2.3 provides an alternative derivation for a system with stochastic inputs and arbitrary system equation. In Section 4.2.4, the system equation for a multi-source energy harvester will be derived using the Lagrangian. Section 4.3 will simulate the response of a system to a mixed stochastic-deterministic input to provide numerical validation of the approach for calculating the input power from Section 4.2.2. Section 4.4 will provide reflection on how each derivation differs, and how this affects our interpretation of the resulting expressions. As well as providing a brief summary of the chapter, Section 4.5 will include the proposed efficiency metric for multi-source harvesters, along with suggestions for how this can be implemented practically.

4.1 System Equations for a Piezoelectric Device

As mentioned in Section 1.2, piezoelectric materials are a popular choice to examine for multi-source energy harvesters. Through the piezoelectric and pyroelectric effect, certain piezoelectric materials can simultaneously convert both mechanical and thermal energy directly into electrical energy. Therefore it is possible to make a multi-source energy harvester simply by exposing a single piece of piezoelectric material to both vibrations and fluctuating temperature gradients. Energy harvesters based on piezoelectric materials also require fewer moving parts than, say, electromagnetic energy harvesters; often the piezoelectric material can be included as a simple cantilever.

Piezoelectric materials are also interesting from a theoretical point of view as they incorporate two different types of coupling: in the pyroelectric case, the induced electrical flow f_e is linked to the time derivative of the temperature gradient (thermal effort e_t); and in the piezoelectric case, the induced voltage (electrical effort e_e) is linked with the integral of the velocity (mechanical flow f_m) with respect to time. While there are differences in the physical coupling behaviour, these effects are mathematically analogous. Including two different forms of coupling in our analysis gives us increased confidence that the resulting expression can be generalised across different forms of coupling.

The thermo-electro-mechanical system equations (written in common parameters) for a material displaying both piezoelectric and pyroelectric coupling at equilibrium are

as follows

$$C_s\dot{\theta} + R_s^{-1}\theta - R_s^{-1}\rho^{-1}\int R_v^{-1}v\,\mathrm{d}t = 0, \tag{4.1}$$

$$C_v\dot{v} + R_v^{-1}v + L_v^{-1}\int v\,\mathrm{d}t + \rho\dot{\theta} - R_v^{-1}d^{-1}x = 0, \tag{4.2}$$

$$m\ddot{x} + c\dot{x} + kx + kdv = 0, \tag{4.3}$$

where C_s is the analogous thermal capacitance, R_s is the analogous thermal resistance, C_v is the electrical capacitance, R_v is the electrical resistance, L_v is the electrical inductance, m is the mass of the system, c is the damping coefficient, k is the stiffness, θ is the temperature difference, v is the voltage, x is the mechanical displacement, d represents the piezoelectric coupling coefficient, and ρ represents the pyroelectric coupling coefficient.

For our analysis, however, it is more useful to write these system equations using the analogous terms defined in Section 2.3. We can define these systems in terms of their inertance I, their resistance R, their compliance C, and either their flow f or their effort e variables. We use the subscripts t, e and m to refer to the thermal, electrical and mechanical systems respectively. Using these definitions, along with the ideas from Section 3.1 to introduce the inputs, we can now write the driven system equations in a general form

$$C_t\dot{e}_t + R_t^{-1}e_t - R_t^{-1}\rho^{-1}\int R_e^{-1}e_e\,\mathrm{d}t = -C_t\dot{\mathcal{E}}_t, \tag{4.4}$$

$$C_e\dot{e}_e + R_e^{-1}e_e + I_e^{-1}\int e_e\,\mathrm{d}t + \rho\dot{e}_t - R_e^{-1}d^{-1}\int f_m\,\mathrm{d}t = -C_e\dot{\mathcal{E}}_e, \tag{4.5}$$

$$I_m\dot{f}_m + R_m f_m + C_m^{-1}\int f_m\,\mathrm{d}t + R_m d e_e = -I_m\dot{\mathcal{F}}_m, \tag{4.6}$$

where $\dot{\mathcal{E}}$ represents the input from an effort source and $\dot{\mathcal{F}}$ represents the input from a flow source. The thermal variable θ is now e_t and the thermal parameters are now $C_s = C_t$, and $R_s = R_t$. The electrical variable v is now e_e and the electrical parameters are now $C_v = C_e$, $R_v = R_e$, and $I_v = I_e$. The mechanical variable $\dot{x}$ is now f_m and the mechanical parameters are now $m = I_m$, $c = R_m$, and $k = C_m^{-1}$.

4.1.1 Matrix Representation

As we saw in Section 2.3.4, it is possible to re-write the system equations for a multi-degree-of-freedom mechanical system in a matrix form. Here we will consider each different domain as a separate degree of freedom and use matrices to combine Eqs. (4.4) to (4.6) into a single equation. We introduce the following

$$\dot{\mathbf{q}} = \begin{pmatrix} e_t \\ e_e \\ f_m \end{pmatrix}, \tag{4.7}$$

$$\mathbf{K} = \begin{pmatrix} C_t & 0 & 0 \\ 0 & C_e & 0 \\ 0 & 0 & I_m \end{pmatrix}, \tag{4.8}$$

$$\mathbf{g} = \begin{pmatrix} R_t^{-1} e_t - R_t^{-1} \rho^{-1} \int R_e^{-1} e_e \, \mathrm{d}t \\ R_e^{-1} e_e + I_e^{-1} \int e_e \, \mathrm{d}t + \rho \dot{e}_t - R_e^{-1} d^{-1} \int f_m \, \mathrm{d}t \\ R_m f_m + C_m^{-1} \int f_m \, \mathrm{d}t + R_m d e_e \end{pmatrix}. \tag{4.9}$$

In addition, we define a forcing vector of the inputs from Eqs. (4.4) to (4.6), such that

$$\mathbf{f} = \begin{pmatrix} \dot{\mathcal{E}}_t \\ \dot{\mathcal{E}}_e \\ \dot{\mathcal{F}}_m \end{pmatrix}. \tag{4.10}$$

This allows us to write the system of Eqs. (4.4) to (4.6) as

$$\mathbf{K}\ddot{\mathbf{q}} + \mathbf{g}(\mathbf{q}, \dot{\mathbf{q}}, \ddot{\mathbf{q}}) = -\mathbf{K}\,\mathbf{f}. \tag{4.11}$$

These matrices each carry a specific physical interpretation, although some are more abstract than others. The vector $\mathbf{q}$ in this case deals with a general displacement in the corresponding systems; although, this can only be physically interpreted as a displacement for systems expressed in terms of flow variables. This is a mathematically analogous term for systems expressed in terms of their effort variable. Due to the definitions used, if we took a mechanical system with a unit mass and an electrical system with a unit capacitance, the change in internal energy would be equal for equal values of q.

Similarly, $\mathbf{K}$ has a different physical interpretation depending on whether or not the system is defined in terms of its flow or effort variable. Despite this, the term $\mathbf{K}\ddot{\mathbf{q}}$ exhibits

analogous behaviour, regardless of the choice of variable for each system. For example, the term $C_e\dot{e}_e$, for a system where the boundary conditions are expressed in terms of effort variables, is a conserved quantity—in the electrical case, we can understand this as conservation of charge. This is analogous to the conservation of the momentum term $I_m\dot{f}_m$ for systems where the boundary conditions are expressed in terms of their flow variable.

To further demonstrate this analogous behaviour for general systems described in terms of their effort variable, we take a form of the Lagrangian where

$$\mathcal{L} = \frac{C}{2}e^2 - \frac{I^{-1}}{2}\left(\int e\,\mathrm{d}t\right)^2. \tag{4.12}$$

Although the first term corresponds to the potential energy of the system, it is mathematically analogous to the kinetic energy term in a system described in terms of flow. This becomes more apparent when we use the substitution $\dot{q} = e$, giving

$$\mathcal{L} = \frac{C}{2}\dot{q}^2 - \frac{I^{-1}}{2}q^2. \tag{4.13}$$

Deriving the system equation using the Lagrangian provides a useful check, where

$$\frac{\mathrm{d}}{\mathrm{d}t}\left(\frac{\partial\mathcal{L}}{\partial\dot{q}}\right) - \left(\frac{\partial\mathcal{L}}{\partial q}\right) = 0, \tag{4.14}$$

where

$$\frac{\mathrm{d}}{\mathrm{d}t}\left(\frac{\partial\mathcal{L}}{\partial\dot{q}}\right) = C\dot{e} \tag{4.15}$$

and

$$\left(\frac{\partial\mathcal{L}}{\partial q}\right) = I^{-1}q. \tag{4.16}$$

Re-substituting e back into the equation gives us the system equation for an undamped linear oscillator

$$C\dot{e} + I^{-1}\int e\,\mathrm{d}t = 0. \tag{4.17}$$

It is important to note that no distinction has been made between kinetic or potential energy, and both have instead been considered as energy *stored* in the system. These ideas will be used as a basis for the derivation in Section 4.2.4, where the inputs will be introduced as 'kinetic' energy terms and non-conservative forces will be used to represent energy dissipation.

The vector $\mathbf{f}$, contains the amplitude of the various inputs. At this point, we have not explicitly defined the functional form of the system inputs. This allows us to use $\mathbf{f}$ to represent any arbitrary function.

4.2 Power Bounds for a Multi-Source System

If we can find the expression for the maximum power absorbed (power bound) of a multi-source system driven by a white-noise input, then we can use this as the basis for an effectiveness metric for comparing multi-source energy harvesters. If it is possible to derive an expression for the maximum power absorbed by each system individually, then we can postulate that it is possible to find the maximum power absorbed when these systems are combined. Eq. (4.11) demonstrates that it is possible to describe multi-source energy harvesters in a way that allows for a wide range of functional forms for the system equation. Therefore we will use this equation as the basis for deriving a power-bound for multi-source systems driven by a white-noise input.

4.2.1 Direct Derivation for Stochastic Systems

We can treat the inputs contained in $\mathbf{f}$ as stochastic white noise inputs. These are defined so that $\mathcal{E}$ represents a general white noise input described in terms of effort, such that $\mathrm{E}[\dot{\mathcal{E}}(t)\,\dot{\mathcal{E}}(t+\tau)] = \pi S_{\mathcal{E}}\delta(\tau)$; and $\mathcal{F}$ represents a general white noise input described in terms of flow, defined as $\mathrm{E}[\dot{\mathcal{F}}(t)\,\dot{\mathcal{F}}(t+\tau)] = \pi S_{\mathcal{F}}\delta(\tau)$. S is the power spectral density of an input and represents a constant for white-noise inputs, and δ is the value of the Dirac delta function at time τ. When applied to S, the subscript $\mathcal{E}$ denotes the effort and the subscript $\mathcal{F}$ denotes the flow. This allows us to find the expression for the maximum power absorbed by a multi-source energy harvester, assuming that the inputs are stochastic.

From Eq. (4.11) we can directly derive the power absorbed from all sources. This was done by Langley [36] for an uncoupled mechanical system. Here we demonstrate that his analysis can be extended to our general system. The first step is to pre-multiply Eq. (4.11) by $\dot{\mathbf{q}}^{\mathrm{T}}$ and take the expected result

$$\mathrm{E}[\dot{\mathbf{q}}^{\mathrm{T}}\mathbf{K}\ddot{\mathbf{q}}] + \mathrm{E}[\dot{\mathbf{q}}^{\mathrm{T}}\mathbf{g}(\mathbf{q},\dot{\mathbf{q}},\ddot{\mathbf{q}})] = -\,\mathrm{E}[\dot{\mathbf{q}}^{\mathrm{T}}\mathbf{K}\,\mathbf{f}]. \tag{4.18}$$

The left-hand side of Eq. (4.18) contains terms relating to the expected value of the change in the energy stored in the system with respect to time, which is zero for a

stationary system. This includes the expected value for the power transferred through coupling *within* the system, which is also zero. However, the second term on the left-hand side also contains the expected power dissipated by the system through the resistances. Conservation of energy tells us that this must be equal to the power absorbed from the inputs (given by the right-hand side of the equation). This gives the following result for the power absorbed by the system

$$P = -\,\mathrm{E}[\dot{\mathbf{q}}^{\mathrm{T}}\mathbf{K}\,\mathbf{f}] = -\,\mathrm{E}[\mathbf{f}^{\mathrm{T}}\mathbf{K}\dot{\mathbf{q}}]. \tag{4.19}$$

While Eq. (4.19) gives us an expression for the power absorbed by the system, it contains terms relating to both the system response and the input to the system. However, the ideal expression would be one that only relates to the input, as then we do not need to consider the system response. If we have an expression which does not rely on system response, then we do not need to impose any assumptions on the form of the system response. This allows us to use an arbitrary functional form for the system response, given by $\mathbf{g}$. To find an expression for the power absorbed by the system in terms of the inputs only, we first need to integrate Eq. (4.11) with respect to time. This gives us

$$\mathbf{K}\dot{\mathbf{q}}(t) = -\int_{-\infty}^{t} \mathbf{g}(\tau)\,\mathrm{d}\tau - \int_{-\infty}^{t} \mathbf{K}\mathbf{f}(\tau)\,\mathrm{d}\tau, \tag{4.20}$$

where $\mathbf{g}$ is now taken as a function of time, instead of as a function of the system variables. If we pre-multiply each term in Eq. (4.20) by $\mathbf{f}(t)^{\mathrm{T}}$ and take the expected value, we get the following expression for the power absorbed

$$P = -\,\mathrm{E}[\mathbf{f}(t)^{\mathrm{T}}\mathbf{K}\dot{\mathbf{q}}] = \int_{-\infty}^{t} \mathrm{E}[\mathbf{f}(t)^{\mathrm{T}}\mathbf{g}(\tau)]\,\mathrm{d}\tau + \int_{-\infty}^{t} \mathrm{E}[\mathbf{f}(t)^{\mathrm{T}}\mathbf{K}\mathbf{f}(\tau)]\,\mathrm{d}\tau. \tag{4.21}$$

For a stochastic input $\mathbf{f}(t)$, the response of the system is uncorrelated to future inputs. This also includes the point at time t, since the system does not respond instantaneously. This can be stated mathematically as

$$\mathrm{E}[\mathbf{f}(t)^{\mathrm{T}}\mathbf{g}(\tau)] = 0,\ \tau \leq t. \tag{4.22}$$

Eliminating the first term on the right-hand side of Eq. (4.21) leaves us with

$$P = \int_{-\infty}^{t} \mathrm{E}[\mathbf{f}(t)^{\mathrm{T}}\mathbf{K}\mathbf{f}(\tau)]\,\mathrm{d}\tau, \tag{4.23}$$

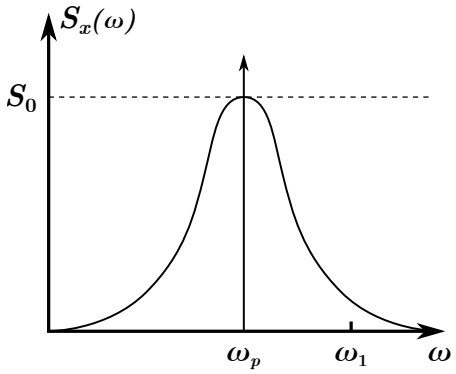

Figure 4.1: Figure showing the equivalent white-noise signal (with a constant power spectral density of S_0) for a narrowband excitation, with a peak power spectral density of S_0 around ω_p. Also shown is a harmonic excitation at ω_p, represented as a Dirac delta function.

and so

$$P = \mathrm{E}[\mathbf{f}^{\mathrm{T}}\mathbf{K}\mathbf{f}]. \tag{4.24}$$

Expanding out Eq. (4.24) gives us the contribution from each individual source

$$P = \frac{\pi S_{\mathcal{E}t} C_t}{2} + \frac{\pi S_{\mathcal{E}e} C_e}{2} + \frac{\pi S_{\mathcal{F}m} I_m}{2}. \tag{4.25}$$

This result is in agreement with Eqs. (3.15) and (3.27). Essentially what we see here is the integral over the power spectral density (mean square average) for the white-noise input to each system, multiplied by the corresponding system parameter. The corresponding system parameter is compliance for systems described in terms of effort, and the corresponding system parameter is inertance for systems described in terms of flow. This power bound is independent of both the configuration of the systems and their domain, as well as the number of sources and boundary conditions. However, the assumptions used require that **f** represents a vector of white noise processes. In addition, the terms in **K** must be linear.

4.2.2 Application to General Systems

Work by Hawes and Langley [31] has demonstrated that for linear systems—and most non-linear systems, although the result is not guaranteed for all non-linear systems—it is possible to extend the power bound described by Eq. (4.24) to a system with narrowband excitation by treating the narrowband input as an equivalent white-noise excitation. This approach is illustrated in Fig. 4.1.

For a linear system, the frequency components of the noise are uncoupled, therefore the power spectral density at a given frequency will never exceed the peak of the narrowband noise. Therefore, treating the narrowband excitation as a white-noise excitation with a value S_0 equal to the peak of the narrowband excitation will provide a bound on the maximum power that can be absorbed. For most non-linear systems this approach will also be valid; however, we can imagine the unfortunate case where the power from a frequency component of the narrowband excitation at ω_1 (i.e. far from the peak) spills into a frequency component close to ω_p. In this case, the power spectral density at ω_p may exceed S_0, meaning that the equivalent white-noise signal no longer represents a bound on the maximum power. Fortunately, such cases tend to be rare and so we can use this equivalent white-noise approach to extend Eq. (4.24) to both linear and non-linear systems with narrowband excitation.

Fig. 4.1 illustrates why Eq. (4.24) is not valid for systems with harmonic excitation. Since the power spectral density for a harmonic excitation is modelled as a Dirac delta function, $S_x(\omega_p) = \infty$. Therefore, using the power spectral density for a harmonic signal in Eq. (4.24) gives an answer that is unbounded, implying that Eq. (4.24) does not represent a bound on the maximum power that a system can absorb from a non-stochastic excitation.

4.2.3 Alternative Derivation for General Systems

If we instead define

$$\hat{\mathbf{g}} = \mathbf{K}\ddot{\mathbf{q}} + \mathbf{g}(\mathbf{q}, \dot{\mathbf{q}}, \ddot{\mathbf{q}}), \tag{4.26}$$

we can rewrite Eq. (4.11) as

$$\hat{\mathbf{g}}(\mathbf{q}, \dot{\mathbf{q}}, \ddot{\mathbf{q}}) = -\mathbf{K}\,\mathbf{f}, \tag{4.27}$$

where $\hat{\mathbf{g}}$ now represents the change in the *total* energy stored in the system over time as well as the power dissipated. Multiplying Eq. (4.27) by $\dot{\mathbf{q}}^{\mathrm{T}}$ and taking the expected result gives

$$\mathrm{E}[\dot{\mathbf{q}}^{\mathrm{T}}\hat{\mathbf{g}}(\mathbf{q}, \dot{\mathbf{q}}, \ddot{\mathbf{q}})] = -\mathrm{E}[\dot{\mathbf{q}}^{\mathrm{T}}\mathbf{K}\,\mathbf{f}]. \tag{4.28}$$

As before, the change in the energy stored over time is zero for a stationary system. The term $-\mathrm{E}[\dot{\mathbf{q}}^{\mathrm{T}}\mathbf{K}\,\mathbf{f}]$ once again represents the expected value for the total power absorbed by the system. Using Eq. (4.19) we can see that

$$P = \mathrm{E}[\dot{\mathbf{q}}^{\mathrm{T}}\hat{\mathbf{g}}(\mathbf{q}, \dot{\mathbf{q}}, \ddot{\mathbf{q}})] = \mathrm{E}[\mathbf{f}^{\mathrm{T}}\mathbf{K}\mathbf{f}]. \tag{4.29}$$

4.2.4 Lagrangian with Non-Conservative Forces

Another method is to use analogous expressions for the energy stored within the system to define a form of the Lagrangian. We can then find the power dissipated through non-conservative forces by first introducing a matrix of the resistances

$$\mathbf{R} = \begin{pmatrix} R_t^{-1} & 0 & 0 \\ 0 & R_e^{-1} & 0 \\ 0 & 0 & R_m \end{pmatrix}. \tag{4.30}$$

Using this matrix, the power dissipated by the system can be treated as a generalised Rayleigh dissipation function, which, assuming linear resistance gives

$$\mathcal{R} = \frac{1}{2}\dot{\mathbf{q}}^{\mathrm{T}}\mathbf{R}\dot{\mathbf{q}}. \tag{4.31}$$

The quantity which is mathematically analogous to a non-conservative force is therefore

$$\mathbf{Q} = \left(\frac{\partial \mathcal{R}}{\partial \dot{\mathbf{q}}}\right). \tag{4.32}$$

Since $\mathcal{L} = T - V$, if we take the quantities analogous to the kinetic energy

$$T = \frac{1}{2}C_t(e_t + \mathcal{E}_t)^2 + \frac{1}{2}\rho e_t^2 + \frac{1}{2}C_e(e_e + \mathcal{E}_e)^2 + \frac{1}{2}R_m d e_e^2 + \frac{1}{2}I_m(f_m + \mathcal{F}_m)^2 \tag{4.33}$$

and the quantities analogous to the potential energy

$$V = \frac{1}{2}(I_e^{-1} - R_t^{-1}\rho)\int e_e^2\,\mathrm{d}t + \frac{1}{2}I_e^{-1}\int e_e^2\,\mathrm{d}t + \frac{1}{2}(C_m^{-1} - R_e^{-1}d)\int f_m^2\,\mathrm{d}t, \tag{4.34}$$

we can then re-write Eq. (4.11) as

$$\frac{\mathrm{d}}{\mathrm{d}t}\left(\frac{\partial \mathcal{L}}{\partial \dot{\mathbf{q}}}\right) - \left(\frac{\partial \mathcal{L}}{\partial \mathbf{q}}\right) + \mathbf{Q} = 0. \tag{4.35}$$

We can then pre-multiply the terms in Eq. (4.35) by $\dot{\mathbf{q}}^{\mathrm{T}}$ and take the expected value to give

$$\mathrm{E}\left[\dot{\mathbf{q}}^{\mathrm{T}}\frac{\mathrm{d}}{\mathrm{d}t}\left(\frac{\partial \mathcal{L}}{\partial \dot{\mathbf{q}}}\right) - \dot{\mathbf{q}}^{\mathrm{T}}\left(\frac{\partial \mathcal{L}}{\partial \mathbf{q}}\right)\right] + \mathrm{E}[\dot{\mathbf{q}}^{\mathrm{T}}\mathbf{R}\dot{\mathbf{q}}] = 0, \tag{4.36}$$

where the first term represents the change in the energy stored in the system over time. From Eq. (4.18) we can see that

$$-\mathrm{E}[\dot{\mathbf{q}}^{\mathrm{T}}\mathbf{K}\mathbf{f}] + \mathrm{E}[\dot{\mathbf{q}}^{\mathrm{T}}\mathbf{R}\dot{\mathbf{q}}] = 0. \tag{4.37}$$

Using Eqs. (4.19), (4.24) and (4.37) we arrive at the same expression for the maximum power absorbed by the system and can show that this is equal and opposite to the power dissipated

$$P = \mathrm{E}[\mathbf{f}^{\mathrm{T}}\mathbf{K}\mathbf{f}] = -\mathrm{E}[\dot{\mathbf{q}}^{\mathrm{T}}\mathbf{R}\dot{\mathbf{q}}]. \tag{4.38}$$

This demonstrates how generalised coordinates can be used to represent different domains, as long as energy-based analogies are used to define the equivalent parameters and variables.

4.3 Non-stochastic Numerical Simulations

Section 4.2.2 highlighted a possible method for calculating the time average input power from a non-stochastic source, providing the input and system response can be measured. By calculating the input power, it should be possible to develop an efficiency metric which is valid for a multi-source system with both stochastic *and* deterministic inputs only, as well as systems with mixed stochastic-deterministic inputs. Using numerical simulations we can validate this theoretical prediction by checking that the input for calculated using Eq. (4.19) does not exceed the power dissipated for a system.

We simulate a single-source system, to confirm that this method for calculating the input power is independent of whether the input is stochastic, deterministic or some combination of the two. It should also be possible to show that this method for calculating the input power is independent of the system configuration for an arbitrary input signal. We can verify this by driving a system with a mixed stochastic-deterministic signal for a variety of system configurations and checking that the time averaged input power matches the power dissipated. The chosen parameters represent a mechanical system, but of course we can extend the result to other systems using physical analogy.

Section 4.3.1 will describe the method for performing these simulations, along with the parameters used. The results will then be included in Section 4.3.2, where a brief comment will be made as to whether or not Eq. (4.19) is a valid method for calculating the input power. (Further discussion of the results from the numerical simulations can be found in Section 4.4.) We will also describe the procedure for calculating the efficiency of energy harvesters.

4.3.1 Methods

These simulations were conducted to examine whether or not the input power from mixed stochastic-deterministic inputs could be calculated in a similar way to purely stochastic or deterministic inputs. For this, a single-source mechanical system was driven with an input signal that contained both stochastic and deterministic components. For the single-source mechanical system, the following system configurations were used: linear, non-linear and bistable.

Single-source simulation

The system used for these simulations is a single-degree-of-freedom (SDOF) mass-spring-damper system with the equation

$$I_m \dot{f}_m + R_m f_m + C_{1m}^{-1} \int f_m \, \mathrm{d}t + C_{3m}^{-1} \left(\int f_m \, \mathrm{d}t \right)^3 = -I_m \dot{\mathcal{F}}_m, \tag{4.39}$$

where C_{1m} represents the linear compliance and C_{3m} can be varied to create non-linearities in the system. The values for the parameters used are as follows: $I_m = 1 \times 10^{-3}\,\mathrm{kg}$, $R_m = 1 \times 10^{-3}\,\mathrm{kg/s}$. For the linear and non-linear case $C_{1m} = 1 \times 10^{2}\,\mathrm{m/N}$, and for the bistable case $C_{1m} = -1 \times 10^{2}\,\mathrm{m/N}$; for the linear case $C_{3m} = 0\,\mathrm{m/N}$, and for the non-linear and bistable case $C_{3m} = 1 \times 10^{9}\,\mathrm{m/N}$. The ensemble average of the system was found over 250 realisations for a duration $T = 20\mathrm{s}$, and time step $\mathrm{d}t = 5 \times 10^{-4}\mathrm{s}$.

The first step was to create the mixed stochastic-deterministic input by generating a white-noise signal with a mean square average of $S_0 = \pi^{-1} \times 10^{-3}\,\mathrm{m^2/s^3}$ over the frequency range 0–ω_{max}, where $\omega_{max} = 2\pi\,\mathrm{d}t^{-1}$. The second step involved generating a sinusoidal signal with a similar mean square average power as the white-noise signal. For this, it was necessary to use an amplitude of $A = \sqrt{1 \times 10^{-2}}$. This sinusoidal signal provides a correlated harmonic component, thus creating a mixed stochastic-deterministic signal. The final step was to add these two signals together.

Several different simulations were carried out using different frequencies to generate the sinusoidal signals. The relative frequency (ratio of the frequency of the sinusoidal input to the resonant frequency of the oscillator) ω/ω_0 was varied between 0.5 and 1.5. Due to resonance, the frequency of the sinusoidal signal affects the input power in the linear case, but not significantly in the non-linear and bistable cases.

Eq. (4.39) was solved using the ode45 function in MATLAB. This is the recommended solver when looking to solve differential equations using MATLAB as it has the highest accuracy.

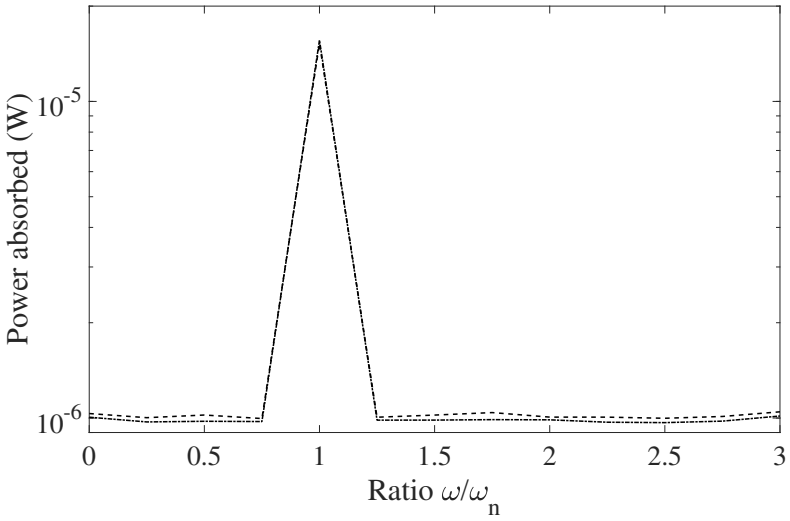

Figure 4.2: The time averaged input power (dot-dashed black line) and time averaged power dissipated (dashed black line) by a linear system as a function of the input frequency. As can be seen, there is a peak as ω/ω_n approaches 1.

Estimating the input power

The input power is estimated using Eq. (4.19), however instead of taking the expected value, the time average is used instead to give

$$P = -\langle\, \dot{\mathbf{q}}^{\mathrm{T}} \mathbf{K}\, \mathbf{f}\, \rangle \tag{4.40}$$

where P is the total power dissipated by the system. By using the time average of the input power, this expression is no longer limited to stochastic systems. For multi-source systems, the dissipated power would be restricted to the power dissipated electrically to give an estimate of the efficiency.

4.3.2 Results

The power dissipated matches the input power calculated by Eq. (4.40). We can see that the introduction of a harmonic component has the a large effect on the linear system shown in Fig. 4.2. There are no obvious peaks in either the non-linear results (shown in Fig. 4.3) or the bistable results (shown in Fig. 4.4), and in fact these approach the power bound for systems driven by a white-noise input.

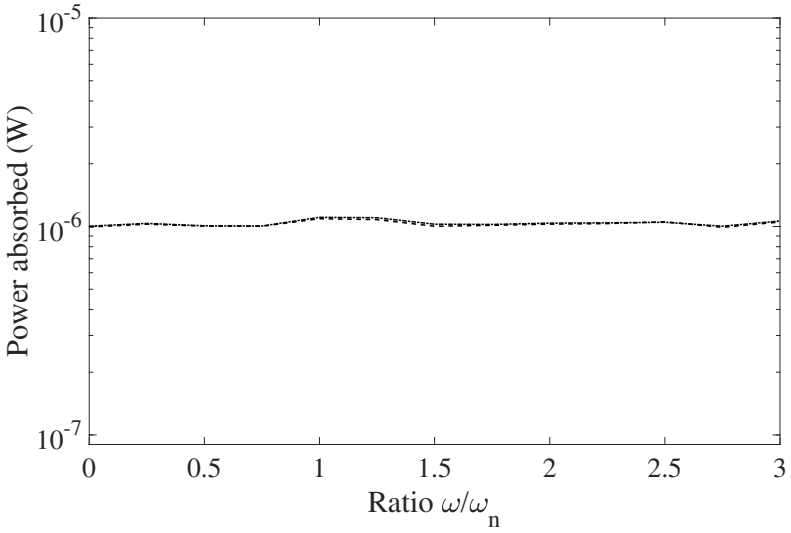

Figure 4.3: The time averaged input power (dot-dashed black line) and time averaged power dissipated (dashed black line) by a non-linear system as a function of the input frequency. The input power is not strongly affected by the frequency of the harmonic component ω. The input power and power dissipated match closely and Eq. (4.40) deals effectively with the non-stochastic input.

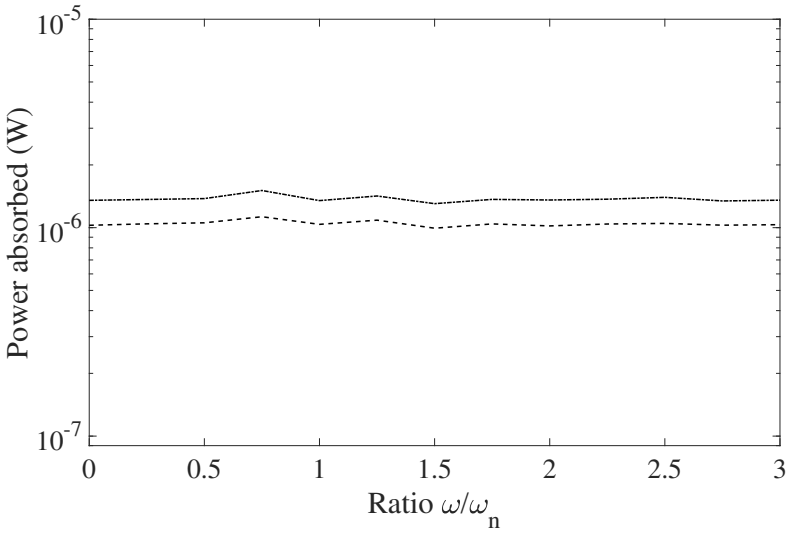

Figure 4.4: The time averaged input power (dot-dashed black line) and time averaged power dissipated (dashed black line) by a bistable system as a function of the input frequency. The frequency response of the system is even flatter than that of the non-linear system. It would seem that using the time average input power as described in Eq. (4.40) is not as accurate for bistable system, but there is still close agreement.

4.4 Discussion

Numerical results

From the numerical results for the linear system shown in Fig. 4.2 we see that the input power estimated using Eq. (4.40) matches well with the dissipated power for non-stochastic signals. Due to conservation of energy, it is physically impossible for the total power dissipated by the system to exceed the total input power. This demonstrates the effectiveness of this expression: it is not based upon particular inputs or configurations, but rather upon fundamental physical principles.

The numerical results for the non-linear and bistable system, shown in Figs. 4.3 and 4.4, also exhibit the behaviour that we would expect from such systems. They are decidedly broadband in their frequency response, with the ensemble average of the non-linear and bistable system responses lacking any strong peaks, even with a harmonic excitation. These systems have a tendency to respond at a range of frequencies for a given input frequency, thus distributing the energy from the harmonic signal over a wider frequency range. The input power from these systems is close to the power bound for white-noise systems Eq. (4.24), as the harmonic component has not strong effect on these systems.

The linear system exhibits a higher input power when the frequency of the harmonic component is close to resonance. This causes the performance to far exceed that of the bistable or non-linear systems. However, when the excitation frequency of the harmonic component is far from resonance, the bistable and non-linear systems exhibit superior performance. This is not a new finding, but it lends weight to the validity of the numerical results, as they conform, not only to what we would predict theoretically, but also what we would expect to see from a real experiment.

Theoretical results

Eq. (4.24) demonstrates that by using these domain neutral analogies, we can perform analysis on multi-degree-of-freedom systems in the same way we would for a SDOF system. We could theoretically extend this analysis to an n-degree-of-freedom system. These degrees of freedom could theoretically describe a system of any domain, providing that the system could be described using equivalent variables and parameters which form an energy-based analogy (see Section 2.3). It is also entirely possible to include extra degrees of freedom to give extra dimensions in one of the domains; for example, if you wanted to model a three-dimensional piezoelectric system, you could simply include

three mechanical degrees of freedom. Despite the flexibility in the nature and number of degrees of freedom, due to assumptions made regarding the inputs, this derivation is only valid for systems with stochastic inputs.

For stochastic systems, the power bound will equal the total input power to the system. To generate a meaningful estimate for the efficiency of a multi-source system, one can therefore simply use Eq. (4.24) as the total power in, comparing it with the power dissipated electrically. However, for systems with a non-stochastic input, no such power-bound exists. By removing assumptions on the functional form of the input and using the time averaged power instead of the expected power, one can use Eq. (4.40) to calculate the input power for a mutli-source energy harvester. Since the power dissipated electrically cannot exceed this value, this represents a practical limit on the useful power that can be generated by the energy harvester. The validity of this approach is confirmed by the numerical simulation results shown in Figs. 4.2 to 4.4, where Eq. (4.40) is used to calculate the input power.

From Eq. (4.29) it becomes obvious that no matter what form the system equations take, the maximum power absorbed by an energy harvester from a white-noise input is entirely dependent on the input. This is logical and demonstrates why this expression is so universal: we are free in our choice of the functional form for the system equations. This also means that this expression for the maximum power absorbed is independent of the form of coupling. This again makes sense if we consider that the coupling describes the transfer of energy *within* the system of systems that make up our multi-source energy harvester. In principle, the fact that Eq. (4.29) is dependent only on the input allows this expression to be used to describe any multi-source energy harvester driven by a white-noise input.

When we examine the Lagrangian of the system in Section 4.2.4. For a mechanical system, examining the first term in Eq. (4.35) shows that the energy from vibrations is transferred to the system through a change in momentum. However, when we use Eq. (4.35) to describe an electrical system expressed using the effort variable, this first term becomes a mathematically analogous term, representing a change in the electrical charge. For the mechanical system, momentum is conserved, and for the electrical system, charge is conserved. Therefore, for a general system we can say that the power absorbed is proportional to the change in the analogous conserved quantity with respect to time. The change in the analogous conserved quantity for a multi-source energy harvester driven by white-noise sources is given by $\mathbf{Kf}$.

An advantage of using power conjugate variables is that the expressions for the change in energy stored in the system over time, power dissipated and power absorbed

are always analogous. This is demonstrated in Sections 4.2.1 to 4.2.3, where we see that, despite using different variables to define the boundary conditions, kinetic and potential energy are mathematically analogous concepts. Whether or not this term relates to the kinetic or potential energy of the system depends on how the boundary conditions are described: the kinetic energy stored in a system is modified and determines power into the system when the boundary conditions are expressed in terms of the flow; whereas, the potential energy determines power into the system when the boundary conditions are expressed in terms of the effort. The kinetic and potential energy more generally represent the energy stored in the system, which is partly why they can be treated as analogous. For stationary systems the expected value for the change in stored energy over time is zero.

4.5 Conclusions

Based on the derivations presented in this chapter, as well as the numerical simulations, the following expression for the efficiency of a multi-source energy harvester is proposed

$$\eta = \frac{\langle P \rangle}{\langle\, \dot{\mathbf{q}}^{\mathrm{T}} \mathbf{K}\, \mathbf{f}\, \rangle}, \tag{4.41}$$

where $\dot{\mathbf{q}}$ is a vector representing the time-derivative of system variable from each domain, f is the vector of inputs from each domain, $\mathbf{K}$ is a matrix containing the corresponding system parameters, and $\langle P \rangle$ is the time averaged power dissipated electrically (thus representing useful power). For a practical system, the steps required to calculate the efficiency are:

- Measure the input for each domain (voltage, acceleration, temperature difference).
- Measure the system state for each domain.
- Measure the appropriate system parameters to populate $\hat{\mathbf{K}}$.
- Multiply the time-derivative of the system variable with the corresponding system parameter and the input signal from each domain.
- Compare this with the electrical power generated.

Since $\langle\, \dot{\mathbf{q}}^{\mathrm{T}} \mathbf{K}\, \mathbf{f}\, \rangle$ represents the actual input power and not a theoretical power bound, it is liable to change depending on the design of the energy harvester. As such, increases in the efficiency may not reflect an increase in the overall performance of the device. For

example, changing the design of a harvester may decrease the total input power, but if the power dissipated electrically remains the same, the efficiency according to Eq. (4.41) would increase, but the actual output would not have improved. However, this limitation is offset by the fact that Eq. (4.41) is valid for any possible configuration or excitation, giving it wide practical applicability. With care—and by examining the value of the power dissipated to ensure that it too increases—it is possible to optimise multi-source energy harvesters using Eq. (4.41).

It is suggested that, for an excitation that is some form of noise, estimating the power bound using the value of power spectral density S_0 for an equivalent white-noise excitation (Section 4.2.2) is valid. The value of S_0 for each domain can be multiplied by the corresponding parameter, as shown in 4.25. Practically we can use the following expression

$$\eta = \frac{\mathrm{E}[P]}{\mathbf{S}\hat{\mathbf{K}}}, \tag{4.42}$$

where $\mathbf{S} = \begin{pmatrix} S_1 & S_2 & \dots & S_n \end{pmatrix}$ is a vector containing the power spectral density for n inputs and $\hat{\mathbf{K}} = \mathbf{K}_{\mathrm{n}\times\mathrm{n}} \cdot \mathbf{1}_{1\times\mathrm{n}}$ is a vector containing the corresponding system parameters, where $\mathbf{1}$ is a vector of ones, and $\mathrm{E}[P]$ is the expected value for the amount of power dissipated electrically (thus representing useful power). In a practical experiment, $\mathrm{E}[P]$ can be treated as the time average over a sufficiently long duration (as in Eq. (4.41)), such that it approaches the expected value. For a practical system, the steps required to calculate the efficiency are:

- Estimate the power spectral density of the input signals.
- Integrate over the power spectral density to find the expected *power*[1] of the input signals.
- Measure the appropriate system parameters to populate $\hat{\mathbf{K}}$.
- Multiply the expected *power* of the input signal with the corresponding system parameter.
- Compare this with the electrical power generated.

However, using the power bound for white-noise inputs is not valid if the input signal contains a mix of stochastic and deterministic components, or if the input is stochastic but not white. The next step is to demonstrate this approach to calculating the efficiency experimentally, which will be discussed in Chapter 5.

[1] Power here is used in the signal processing context.

5

Experimental Work for Multi-source Harvesters

As we saw in Chapter 4, it is possible to develop bounds for the maximum power absorbed from a stochastic source by multi-source energy harvesters which depend only on the input. We predict that these power bounds are independent of the system domain, the form of coupling, and the system configuration (linear and non-linear). We also saw in Chapter 4 that if we could measure the system response, we could also calculate the input power. This input power could be used as the basis for a universal efficiency metric for energy harvesters. In the case of stochastic energy harvesters, the total input power can be found by the total maximum power absorbed by the system. This approach to calculating the efficiency was illustrated with several experiments. These experiments are largely based on the experiment performed in Chapter 3.

Section 5.1 describes the first of these multi-source energy harvester experiments. To illustrate the procedure from Chapter 4, these experiments compared the power absorbed with the power dissipated electrically (from here on referred to as power harvested) from both a mechanical and electrical source individually, and from both sources simultaneously. Section 5.2 describes the second multi-source experiment, where a thermal source was included in addition to the electrical and mechanical source. Section 5.3 highlights the key findings from these experiments and compares the results with those found in the literature.

5.1 Electro-mechanical Experiment

The purpose of these experiments was to demonstrate that the expressions developed in Chapter 4 could be applied to practical systems with at least two sources. Electrical and mechanical sources were chosen, as these are relatively easy to control and measure when compared to, say, thermal or chemical sources. This experiment was intended to validate the trends predicted by the theoretical expressions. Also, this experiment was used to demonstrate how both the input power and dissipated can be found for a multi-source energy harvester, as well as how these can then be used to calculate efficiency.

A piezoelectric vibrational energy harvester is combined with an electromagnetic (EM) energy harvester, represented by a voltage source. The radio frequency (RF) energy harvester is essentially the same as that used in Chapter 3. A piezoelectric patch is then combined in parallel to create an energy harvester capable of using both electrical and mechanical sources. The performance of the multi-source energy harvester is then compared with single source solutions using the following metrics: input power (which for white-noise systems is equal to the power absorbed), power harvested and efficiency.

5.1.1 Setup

Instrumentation

The oscilloscope and data acquisition card (DAQ) used for this experiment are the same as those used for the single-source energy harvester experiments (described in Section 3.2.1). The DAQ provides the electrical input, while the oscilloscope measures the voltage output of the energy harvester. To provide estimates for the power absorbed by the mechanical system, an accelerometer and load cell are attached to the system. The accelerometer (PCB, 353B15) is attached to the end-mass on the harvester. The clamps which hold the piezoelectric patch is attached to a PCB 208C03 load cell, which feeds into an NI 9234 DAQ. The load cell is then attached to the shaker. The output from the load cell is measured by LabView with a sampling rate of $10,000$ Hz.

The mechanical input signal is generated using a computer, amplified and then fed into a shaker. The signal itself is generated in Audacity. The signal is then converted to an electrical signal through the computer's soundcard (Microsoft, High Definition Audio Device). This signal is transmitted to a signal amplifier (Data Physics, SignalForce 100W Power Amplifier) via the headphone socket (AUX to BNC cable). This signal amplifier then drives the shaker, which provides the mechanical input.

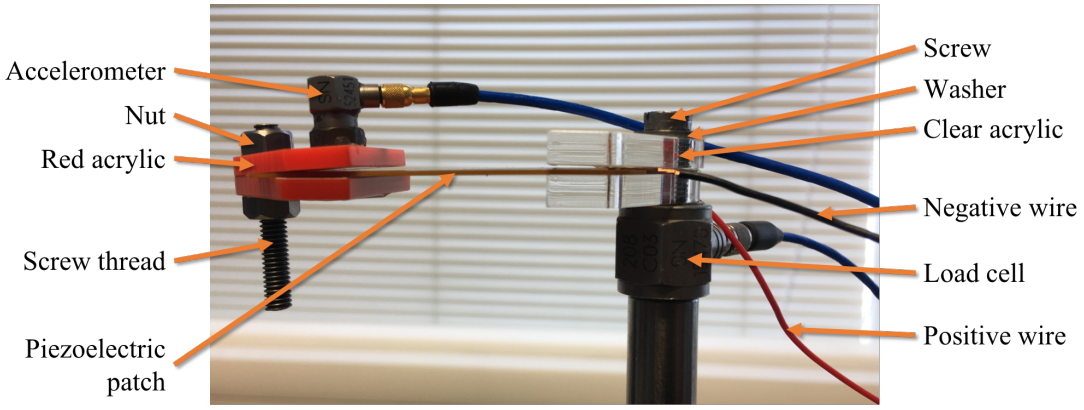

Figure 5.1: The piezoelectric patch is clamped to the shaker at one end using two separate pieces of clear acrylic. The clear acrylic is then screwed onto the load cell, with a washer between the two pieces to keep them roughly parallel. Two pieces of red acrylic are used, along with a screw thread and two nuts, to create the end-mass for the harvester. The clamping pieces and the end-mass provide sources of non-linearity, as there is contact for high amplitude vibrations. An accelerometer is attached to the end-mass using wax. The mass of the entire structure M_{total} attached to the load-cell is 33.7×10^{-3}kg, and for the end-mass $M_{\text{end}} = 17.4 \times 10^{-3}$kg. The patch is excited with a white-noise signal via the shaker, which is attached to the load cell. The wires (black for the negative side, and red for positive) leading from the piezoelectric patch are attached to create the circuit shown in Fig. 5.3.

Mechanical setup

A simple energy harvester is created by attaching an end-mass to a piezoelectric patch (PI ceramics, P-876.A15 DuraAct Patch Transducer) of length 61×10^{-3}m, width 35×10^{-3}m, and thickness 0.4×10^{-3}m. The piezoelectric patch is then clamped to the shaker (shown in Fig. 5.1). The end-mass M_{end} has a mass of 17.4×10^{-3}kg and is made up of two pieces of acrylic held together with two nuts and a screw thread. The total mass of the structure M_{total} attached to the load cell is 33.7×10^{-3}kg.

The method for clamping the piezoelectric patch to the shaker—as well as the method for clamping the end-mass to the piezoelectric patch—creates inherently non-linear behaviour, as at large amplitudes of vibration, the acrylic pieces can come into contact with the piezoelectric patch. The non-linear behaviour of this device was confirmed by measuring the acceleration of the end-mass, whilst the shaker was driven with a sine wave of increasing frequency (upsweep). The frequency response was then found by taking the Fast Fourier Transform (FFT) of the measured acceleration. A representative sample of the frequency response is shown in Fig. 5.2.

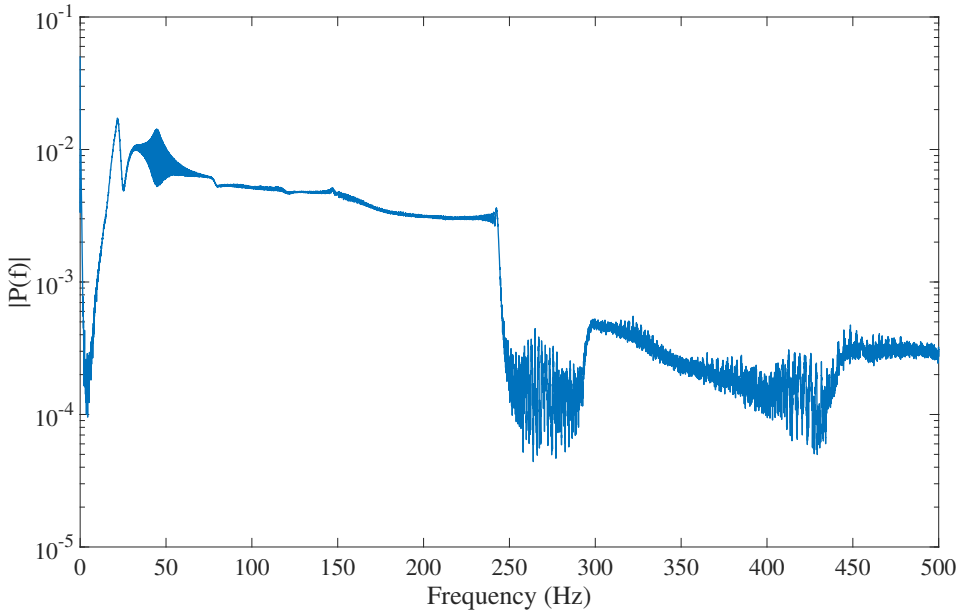

Figure 5.2: The frequency response of the mechanical system shows possible bifurcation above 250 Hz, after a jump in the system response. This suggests that the system is non-linear. The section between 50-250 Hz would also suggest a non-linear system, as linear systems do not typically have flat sections in their frequency response, and we also see possible bifurcation occuring around 50 Hz.

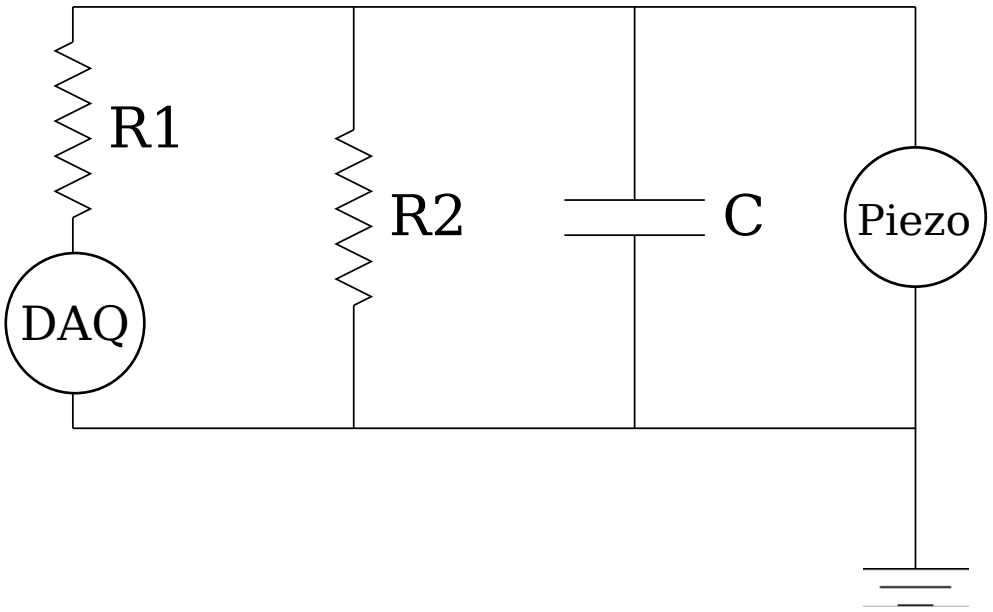

Figure 5.3: Schematic of a parallel resistor-capacitor (RC) circuit with the impedance of the oscilloscope included. The electrical input is represented by 'DAQ' and the mechanical input is represented by 'Piezo'. R1, R2 represent electrical resistors with R2 specifically representing R_e, and C represents the electrical capacitance C_e of the system.

Resistor-capacitor circuit setup

The circuit was set up according to Fig. 5.3, where a piezoelectric patch was attached in parallel with both the voltage source provided by the DAQ and the oscilloscope. An additional $1 \times 10^5 \Omega$ resistor R1 was included in series with the DAQ to reduce the voltage output to a level comparable to that of the piezoelectric patch. There is also a capacitor C and resistor R2 included in parallel which have a value of C_e and R_e respectively. The value of C_e was kept constant at 3.01×10^{-6} F, and the value of R_e was kept constant at $1 \times 10^5 \Omega$. Fig. 5.4 shows a photograph of the real circuit, where we can see an additional resistor in series with the capacitor C. This is not included in the circuit schematic as it is simply intended to stop the capacitor short-circuiting the voltage source and is therefore treated as a property of the capacitor. Therefore, we treat the capacitor as having a parasitic resistance of $1 \times 10^3 \Omega$.

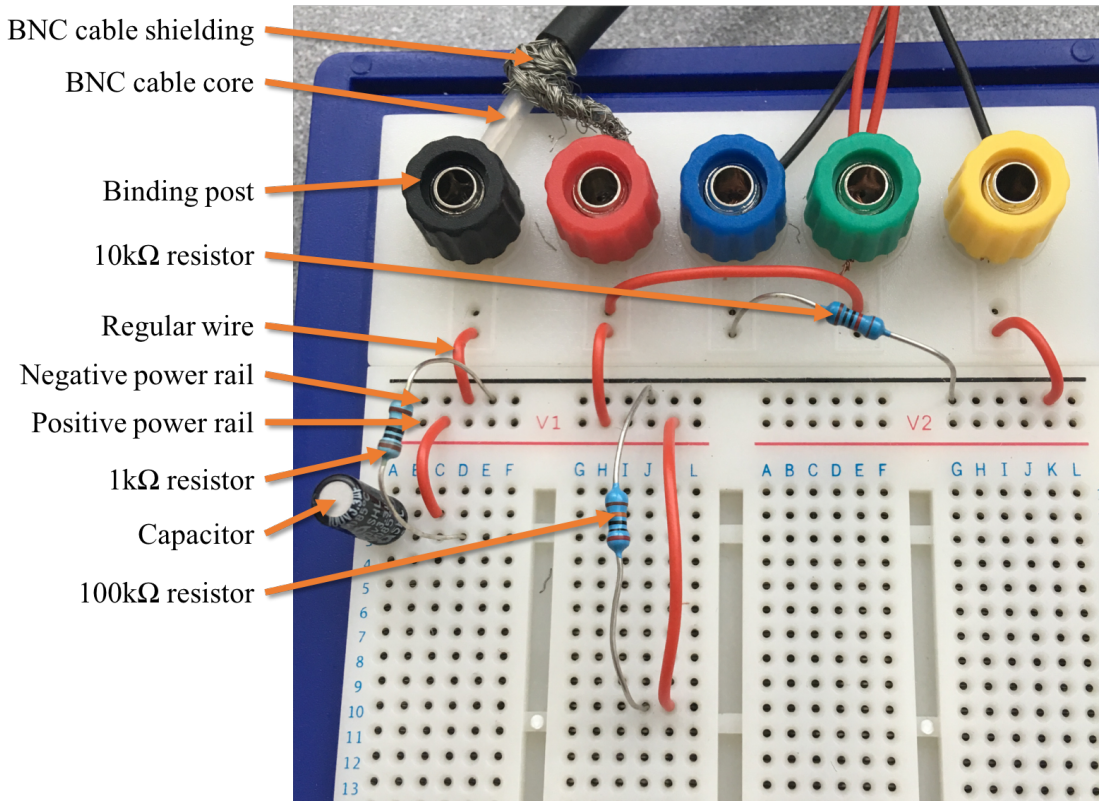

Figure 5.4: Shown here is a photograph of the RC circuit represented by the schematic shown in Fig. 5.3. In the top left we can see the core of the BNC cable (oscilloscope active) attached to the black binding post; this is then connected to the negative power rail (black). The shielding from the BNC cable (oscilloscope ground) is attached to the red binding post; this is then connected to the positive power rail (red). The active wire (black) leading from the analog output channel of the DAQ is attached to the blue binding post, which in turn is connected to the negative power rail using a resistor (R1 from Fig. 5.3). The ground wire (red) from the DAQ analog output channel is connected to the green binding post, which is directly connected to the ground of the oscilloscope. The negative side (black wire) of the piezoelectric patch (as seen in Fig. 5.1) is connected to the yellow binding post, which is then connected to the negative power rail. The positive side (red wire) of the piezoelectric patch is also connected to the green binding post. The circuit components (C and R2) are placed so that they form a bridge between the two power rails, creating a parallel circuit.

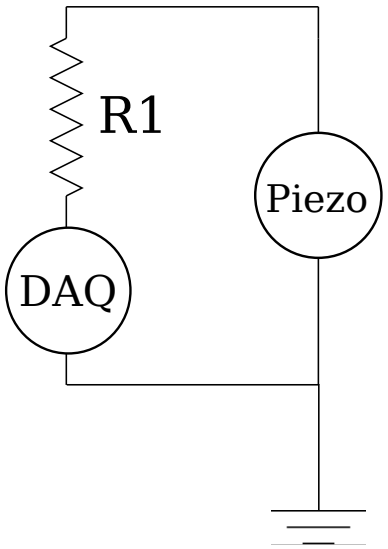

Figure 5.5: Schematic of the circuit setup used to measure the power dissipated directly. The electrical input is represented by 'DAQ' and the mechanical input represented by 'Piezo'. R1 represents an electrical resistor.

Simplified circuit setup

The circuit setup described in the previous sub-section uses a similar setup to the one which was verified for single-source energy harvesters in Fig. 3.1. This circuit included a capacitor, which was necessary to examine the power absorbed as, theoretically, a circuit with zero capacitance is not capable of absorbing power. If we assume that the ratio of electrical power dissipated to the total power dissipated remains constant (which is the case for linear systems), then we can assume that the power dissipated is directly proportional to the power absorbed. Since the mechanical system in this case is non-linear, this is not necessarily the case, but examining the experimental results, this assumption has held for this particular example. We can therefore simplify this circuit and examine the expressions for the power absorbed by a multi-source energy harvester by calculating the power dissipated instead. We can also predict that the power *dissipated* when multiple sources are active simultaneously should be the sum of the power dissipated from each source individually. To verify the above statement, an alternative circuit setup, shown in Fig. 5.5, was used. The $1 \times 10^5 \Omega$ resistor R1 was still included in series with the electromagnetic source, as shown in Fig. 5.6, to keep the voltage provided by the DAQ and the piezoelectric at a similar level.

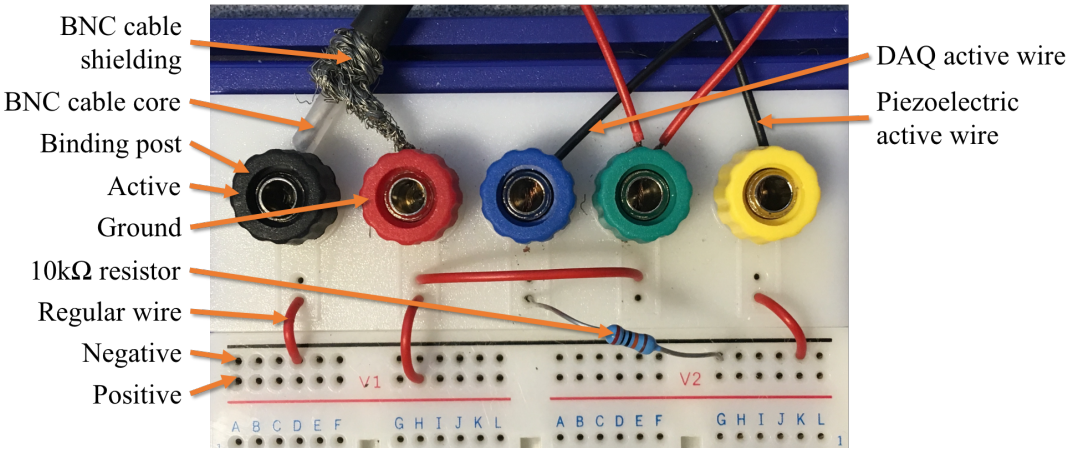

Figure 5.6: This circuit is identical to Fig. 5.4, except for the parallel electrical components, C and R2, have been removed. The oscilloscope, DAQ, resistor and piezoelectric patch are connected in exactly the same way.

5.1.2 Procedure

A white-noise voltage input was created using the same procedure as for the single-source energy harvester experiment. This procedure is described in Section 3.2.2. The standard deviation of the input voltage $S_{\dot{\mathcal{E}}e}$ was varied in a similar fashion to the single-source experiments. The voltage across the circuit represented in Fig. 5.3 was measured for 10 seconds for each value of $S_{\dot{\mathcal{E}}e}$. Three different electro-mechanical experiments were performed:

- In Experiment A, the electrical power (absorbed and dissipated) was measured with the piezoelectric patch disconnected from the circuit. The piezoelectric material was then re-connected to measure the combined mechanical and electrical power, as well as the mechanical power alone.
- In Experiment B, the simplified circuit was used and the piezoelectric patch was attached while measuring the electrical, mechanical, and combined power dissipated.
- In Experiment C, the RC circuit was used and the piezoelectric patch was connected while the electrical, mechanical and combined power (absorbed and dissipated) was measured.

Mechanical noise

For the electro-mechanical experiment, it was necessary to generate a white-noise mechanical acceleration—in addition to the white-noise voltage. The white-noise mechanical acceleration was created using a Gaussian white-noise signal, generated in Audacity, where the amplitude can be adjusted from 0 to 1. The amplitude of the white-noise signal driving the shaker was adjusted until the power harvested from mechanical excitation alone was roughly equal to the power harvested from electrical excitation. In this experiment, the power of this white-noise acceleration input signal was kept constant at $S_{\dot{\mathcal{F}}m}$ of 30.1 $\mathrm{m}^2/\mathrm{s}^3$.

Calculating the power absorbed

The theoretical prediction given by Eq. (4.24) is that the power absorbed from both the mechanical and electrical source simultaneously should be the sum of the power harvested from the two sources separately. To verify this prediction, it was necessary to run each source separately and then both sources simultaneously and compare the power absorbed. In this way, it was possible to sum the power harvested from the sources when tested separately, which could then be compared with the output when both were run simultaneously.

For a practical system, to calculate the power absorbed by the energy harvester from both the mechanical and electrical systems, we need to find the average of the measured power absorbed by both of these systems. For systems driven with white-noise inputs, the derivative of the input mechanical power to the energy harvester from the shaker can be found using the total mass M_{total} of the energy harvester and the input force $\mathcal{E}_m$

$$\frac{\mathrm{d}}{\mathrm{d}t}P_{\text{mech}} = \frac{\dot{\mathcal{E}}_m^2}{M_{\text{total}}}, \tag{5.1}$$

where the input force is measured directly using the load cell shown in Fig. 5.1. Integrating this expression allows us to find the input power

$$P_{\text{mech}} = \frac{1}{M_{\text{total}}}\int_0^t \dot{\mathcal{E}}_m^2 \,\mathrm{d}t, \tag{5.2}$$

which we will use to find the time averaged input power. The electrical power absorbed P_{elec} can be calculated using the expression for the maximum power absorbed from a white-noise effort source, given by Eq. (3.27). For this practical system, we can calculate the total power absorbed as $P_{\text{total}} = P_{\text{mech}} + P_{\text{elec}}$. Although, as we will see,

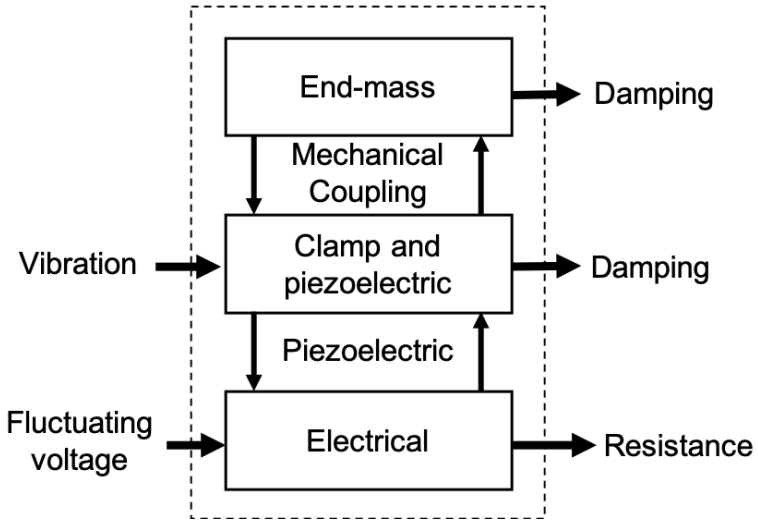

Figure 5.7: Diagram showing the flow of power into and out of the multi-source energy harvester used in the experiment. Also shown is the internal transfer of power.

the electrical power absorbed is negligible when compared to the mechanical power absorbed; therefore, the power dissipated electrically will be used to verify the trends predicted by Eq. (4.24). The power absorbed and dissipated in for the experimental multi-source energy harvester with electrical and mechanical sources can be seen in Fig. 5.7, with a more detailed view of the power flow in the mechanical portion shown in Fig. 5.8.

Calculating the power harvested

We will assume that in the real harvester, the resistor R2 and capacitor C represent some useful energy harvesting circuitry, for example, a power management circuit. We can then view the power dissipated via the resistor $\mathcal{R}_e = R_e^{-1} e_e^2$ as the power harvested by the device. The power dissipated was calculated for: the mechanical source alone, the electrical source alone, and when the two sources were active simultaneously. For the circuit shown in Fig. 5.3, $R_e = 1 \times 10^5 \Omega$. For the circuit shown in Fig. 5.5, the value for R_e was taken as the oscilloscope resistance of $1 \times 10^6 \Omega$.

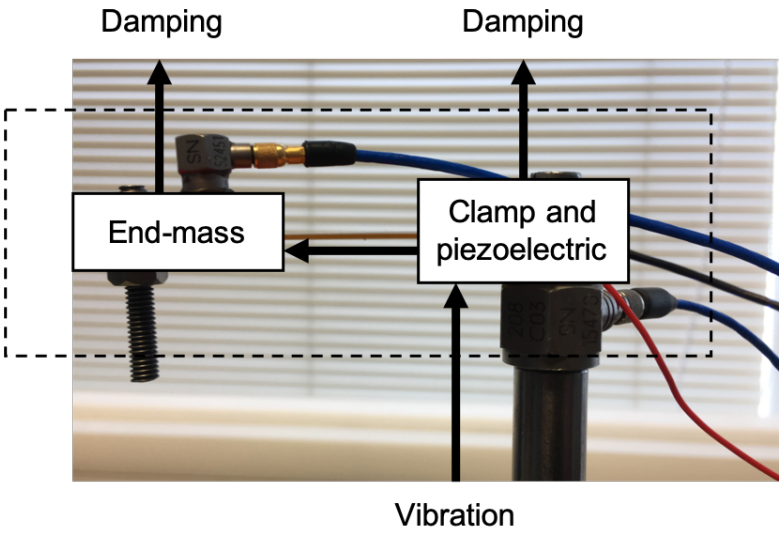

Figure 5.8: Detailed view of the power flow within the harvester. The dashed line represents the mechanical portion of the system. It should be noted that the mechanical system is coupled with the electrical system through the piezoelectric, however, this is not shown here.

5.1.3 Results

Fig. 5.9 shows that the mechanical power absorbed P_{mech} is constant as the mean square voltage is varied; whereas, in Fig. 5.10, we can see that the electrical power absorbed P_{elec} *is* a function of the mean square voltage. Since this is the case, the total power absorbed will also be a function of the mean square voltage as $P_{\text{total}} = P_{\text{mech}} + P_{\text{elec}}$. However, since the standard deviation of the average mechanical power absorbed by the entire system is greater than the maximum value for the electrical power absorbed, this cannot be seen on a graph.

The results from Experiment A are shown in Fig. 5.11 while the results from Experiment B are shown in Fig. 5.12. These results both show the same trends: the power harvested from the electrical source alone varies linearly with $S_{\dot{\mathcal{E}}_e}$, and the power harvested from both sources simultaneously is the sum of the power harvested from each source separately.

The results from Experiment C, shown in Fig. 5.13, shows similar trends to the results from Experiments A and B; however, the experimental result for the combined power harvested is greater than the theoretical value predicted.

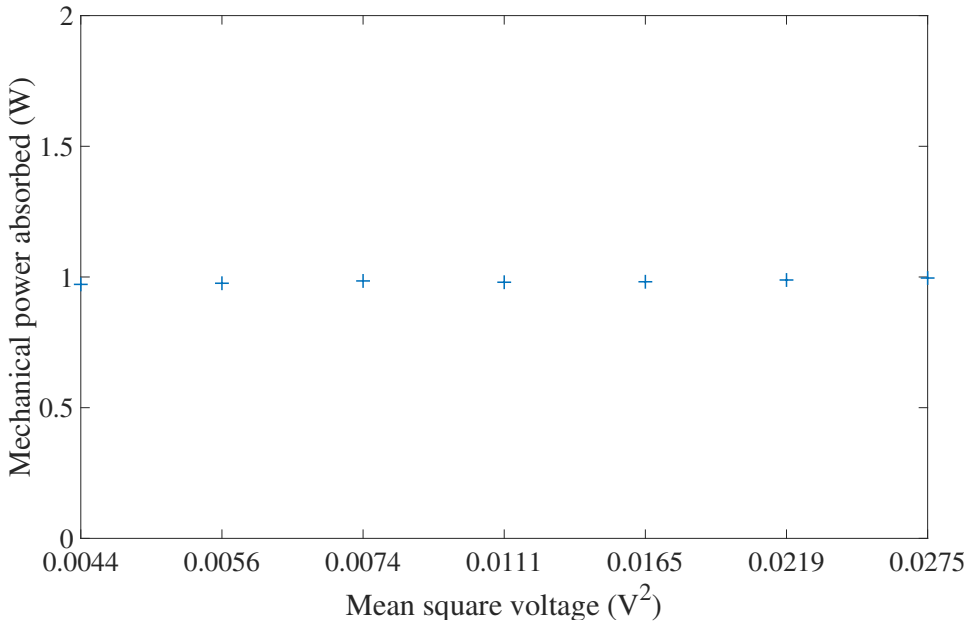

Figure 5.9: Experimental results showing the mechanical power absorbed (pluses). The mechanical power absorbed by the system is not a function of the mean square voltage.

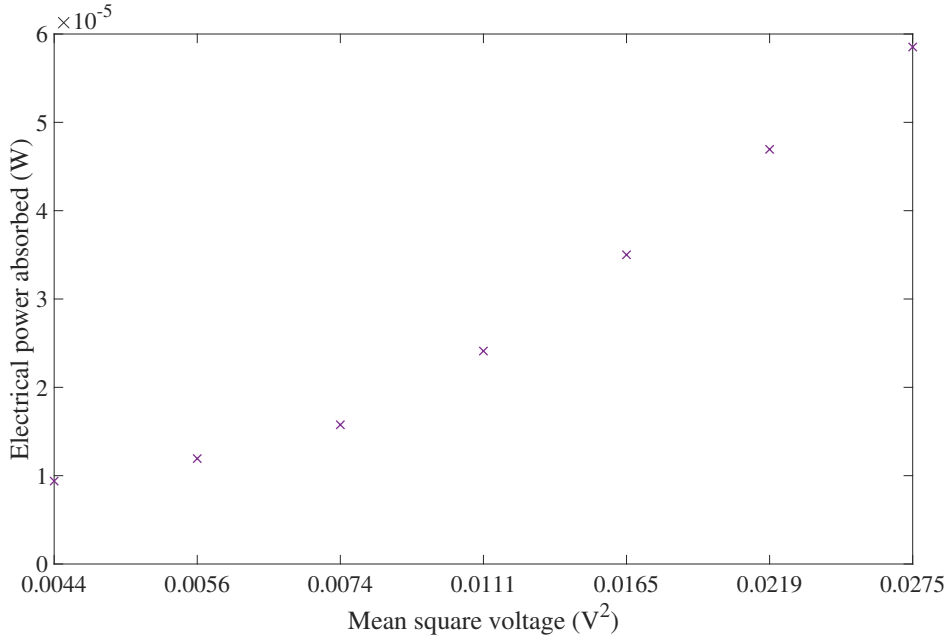

Figure 5.10: Experimental results showing the electrical power absorbed (crosses). The electrical power absorbed by the system is clearly a function of the mean square voltage.

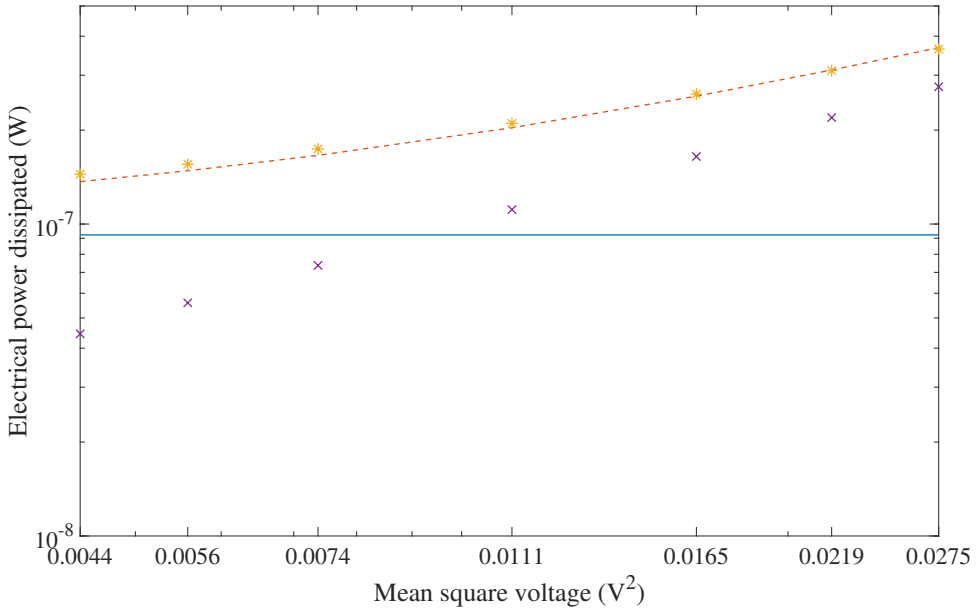

Figure 5.11: Results from Experiment A, showing that the power harvested from two sources simultaneously (asterisks) is approximately the sum of the power harvested from each source individually (dashed line). The power harvested from the mechanical (solid line) and electrical (crosses) sources individually is also shown. These results were measured using the circuit shown in Fig. 5.3.

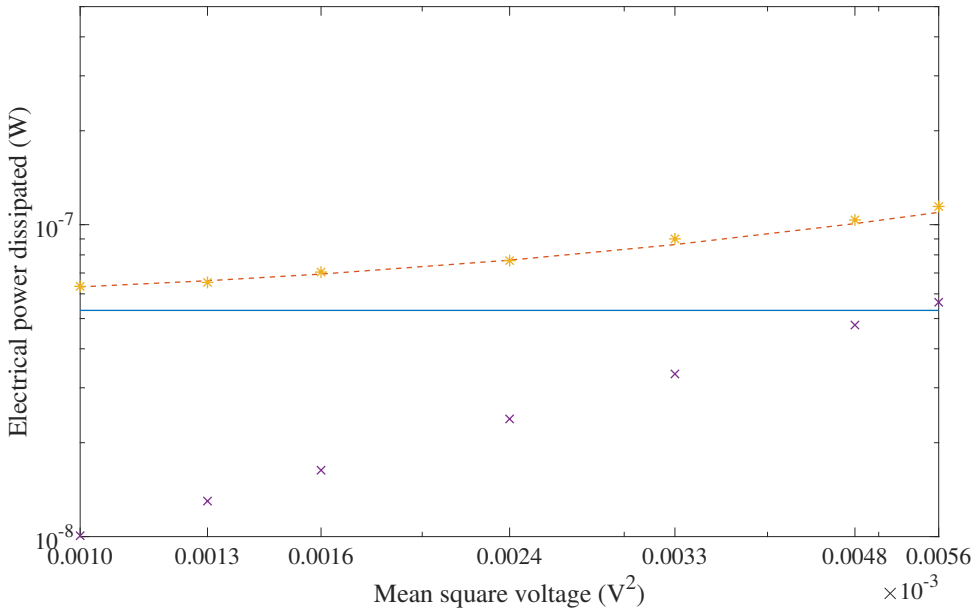

Figure 5.12: Results from Experiment B, which match the trends shown in Fig. 5.11. These were measured using the circuit shown in Fig. 5.5.

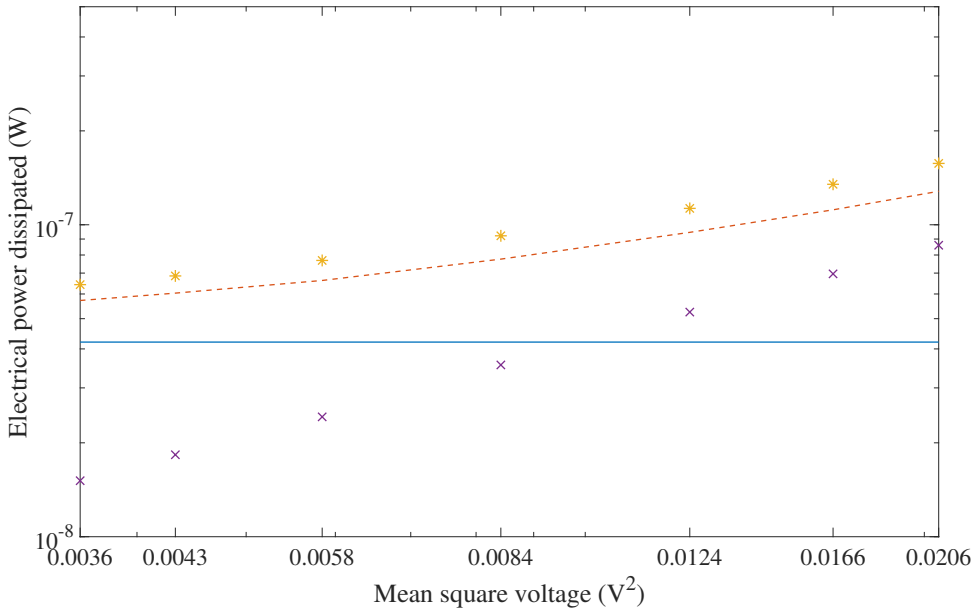

Figure 5.13: Results from Experiment C, showing similar trends to Fig. 5.11, except for there is an offset between the measured results for the power harvested from two sources simultaneously (asterisks) and the theoretical prediction (dashed line). The theoretical prediction is again found by taking the sum of the power harvested from the mechanical (solid line) and electrical (crosses) sources individually. These were measured using the circuit shown in Fig. 5.3.

5.1.4 Discussion

The results shown in Fig. 5.9 and Fig. 5.10 show that the ratio of the capacitance affects the proportion of the power absorbed by electrical systems when compared to the overall power absorbed by the multi-source energy harvester. Treating the mass and capacitance as analogous (as shown in Chapter 4), we compare the ratio of the electrical power absorbed to the total power absorbed to the ratio of the capacitance and the total inertance (mass plus capacitance). The ratio of the capacitance and the total inertance is roughly 10^{-5}, and a quick examination of Fig. 5.10 and Fig. 5.9 reveals approximately the same difference in the power absorbed. This result would also suggest that these system parameters not only determine how much power is absorbed, but also strongly influence how the energy is distributed and stored in the system.

This result has the potential to explain the offset seen in the results for the power harvested in Experiment C, shown in Fig. 5.13. In Experiment C, there are in fact two capacitances: the capacitor C in the circuit; and the piezoelectric patch, which acts as a capacitor at low frequencies. This would cause power absorbed from the electrical source to be split among the capacitor and the piezoelectric patch. Therefore, the power dissipated through the resistor R2 may be lower when the system is driven by the electrical source, as some of the electrical power is absorbed by the piezoelectric material. However, we do not see this effect when the two sources are active. This is possibly because the piezoelectric patch becomes saturated with its own charge as the vibration absorbed by the mechanical system is converted to electricity. By comparing Fig. 5.9 with Fig. 5.10, we see that the piezoelectric patch can gain far more power in this way. Caveat: this is a theory that is inferred from observed results and relationships, but not necessarily demonstrated by them.

An alternative theory is that some of the electrical energy is dissipated across the capacitor. Otherwise the balance of the power dissipated in the electrical and mechanical systems could be affected by the combination of both the piezoelectric and attached circuitry. This would change the proportion power dissipated electrically (with respect to the total power dissipated), meaning that the total power dissipated when the two sources are active simultaneously was *not* the sum of the power dissipated when the sources are activated separately.

Whatever the case may be, we can see that this effect is removed by eliminating either the capacitor or the piezoelectric patch from the system when measuring the power harvested from the electrical source. In Experiment A, we eliminate the capacitance

of the piezoelectric patch by disconnecting it when examining the electrical source. In Experiment B, we eliminate the capacitance of the circuit.

The results from Experiments A and B, shown in Figs. 5.11 and 5.12, demonstrate that the sum of the power harvested from each source individually is approximately equal to the power harvested from the two sources simultaneously. This agrees with the result predicted by the expression for the maximum power absorbed by a multi-source energy harvester Eq. (4.24). These experimental results also demonstrate the theoretical result Eq. (4.29) by showing that the results for Experiment A and B do not depend on the electrical circuit used. Also, the non-linearity present in the mechanical system informs us that the theoretical results are valid for systems with a mix of linear and non-linear subsystems.

We can now apply Eq. (4.41) to a particular design of energy harvester. For our energy harvester, we use the RC circuit shown in Fig. 5.3. We can treat the harvester as a single-source mechanical energy harvester by only driving it with vibrations. Similarly, we can treat the harvester as a single-source electromagnetic energy harvester by using only the voltage source. We can then compare the efficiency from each of these single-source energy harvesters with the efficiency of the multi-source energy harvester. Following the procedure described in Section 4.5, it was necessary to first measure the inputs and find the mean square average for the mechanical input $S_{\mathcal{E}m} = 0.033\text{kg}^2\text{m}^2/\text{s}^3$ and the mean square average for the voltage input $S_{\dot{\mathcal{E}}e} = 19.4\text{V}^2/\text{s}$. The corresponding system parameter for the mechanical system was $I_m = M_{\text{total}} = 33.7 \times 10^{-3}\text{kg}$ and $C_e = 3.01 \times 10^{-6}\text{F}$ for the electrical system. Using these values it was possible to calculate the absorbed power: 0.979W for the mechanical system and $5.84 \times 10^{-5}\text{W}$ for the electrical system. We can then compare the power absorbed with the measured power harvested for each harvester: $9.23 \times 10^{-8}\text{W}$ from the mechanical single source, $2.76 \times 10^{-7}\text{W}$ from the electrical single source, and $3.64 \times 10^{-7}\text{W}$ from the multi-source energy harvester (both sources combined).

From Table 5.1 it becomes clear that despite the large amount of mechanical power absorbed, the device converts barely any of this into useful energy. The electrical energy harvester on the other hand performs significantly better. Using both sources gives a device roughly four times as efficient as the mechanical energy harvester, but far less efficient than the electrical energy harvester. Despite the drop in efficiency, the multi-source energy harvester still produces more power than the electrical energy harvester. This highlights the care that must be taken when optimising devices using either Eq. (4.41) or Eq. (4.42): using efficiency alone may lead to a device with a lower output. The higher efficiency of the electrical device still tells us something about where

Table 5.1: A comparsion of the power absorbed, power harvested and efficiency for single-source and multi-source energy harvesters explored

RC Harvester	Power absorbed (W)	Power harvested (W)	Efficiency (%)
Mechanical	0.979	9.23×10^{-8}	9.43×10^{-6}
Electrical	5.84×10^{-5}	2.76×10^{-7}	0.473
Combined	0.979	3.64×10^{-7}	3.72×10^{-5}

potential improvements lie. As the efficiency of the power harvested from the electrical source is far higher, we may assume that this is better optimised, and that the mechanical part of the harvester could use a re-design. This is certainly true for this particular harvester as no effort has been made to optimise the mechanical portion, whereas the electrical circuit is directly connected to a voltage source.

5.2 Thermo-electro-mechanical Experiment

This experiment is an extension of the previous experiment. In this experiment, a thermal source was included to demonstrate that the different coupling (pyroelectric and piezoelectric) had no effect on the results predicted. This was an important finding from Chapter 4. Therefore, an attempt was made to create a stochastic thermal source. Creating a stochastic thermal source proved challenging; however, it provided an interesting case, as it represents a process with a non-stationary mean. Another challenge was calculating the thermal power absorbed—this would have involved estimating the thermal capacitance and thermal input—and so only the power harvested is examined. Also, since the accelerometer and load cells both use piezoelectric material, the thermal source affects their readings, thus making it impossible to measure the mechanical power absorbed using this experimental setup. As shown in the previous section, examining the power harvested can still reveal trends in the power absorbed.

5.2.1 Thermal Setup

For this experiment, a similar setup to that described in Section 5.1.1 was used. It was not necessary to modify the mechanical part of the setup, since the piezoelectric material already displays the pyroelectric effect. In addition, the electrical setup used is the same as shown in Fig. 5.3. However, it was necessary to change the values for the resistors and

capacitor used as the voltage generated through the pyroelectric effect was not as high as the voltage from the other two sources. Therefore, the resistance values for R1 and R2 were changed to $1 \times 10^6\Omega$. The value of the capacitor C was changed to 8×10^{-8}F. A hairdryer was used to provide a thermal source, as shown in Fig. 5.14. A thermocouple was inserted into the end-mass to measure the temperature of the system.

5.2.2 Procedure

This time three sources were used: electrical, mechanical and thermal. The electrical and mechanical inputs were created in the same way as before, only this time, the input power for both sources was kept constant. The power harvested from the mechanical-electrical combination of sources was measured six times (for a duration of five seconds) without the thermal source present. The power harvested from the mechanical and electrical sources simultaneously was fairly consistent, but, during commissioning, it was found that there was considerable variation in the power harvested from the thermal source. This was despite attempts to keep the mean square average of the thermal fluctuations constant.

In order to achieve a reasonably consistent thermal input, the system would have ideally been allowed to reach steady-state. Unfortunately, reaching a steady state would have led to excessive temperatures in the piezoelectric patch. This could cause damage, which, in the best case scenario could mean damage to the epoxy or de-bonding between the epoxy and the piezoelectric material. In the worst case scenario, the piezoelectric could have become de-poled. To avoid damage to the piezoelectric patch, the experiment was conducted while the piezoelectric patch was still heating. By adjusting the hairdryer it was possible to at least keep a fairly steady rate of heating, as shown in Fig. 5.15.

Since the thermal input was non-stationary, it was hoped that reducing the time between subsequent experiments would reduce the variation in the thermal input, and so the following procedure was adopted:

1. Measure the power harvested from the thermal source alone.
2. Activate the electrical and mechanical sources and measure the power harvested from all three sources simultaneously.
3. De-activate the electrical and mechanical sources and measure the power harvested from the thermal source alone.
4. Repeat these steps until there are six results for the power harvested for the thermal source alone and for all three sources simultaneously.

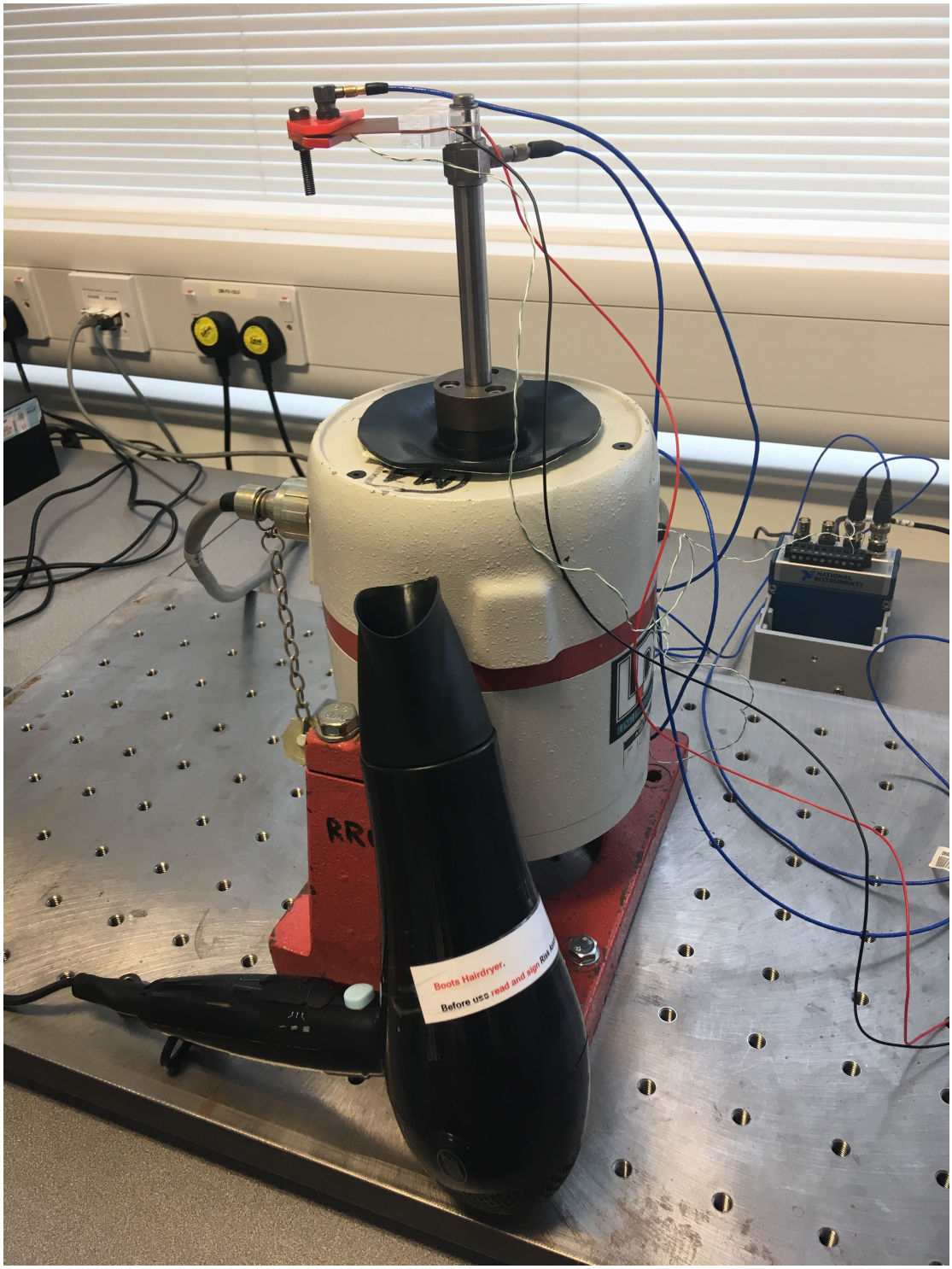

Figure 5.14: Photograph showing the mechanical setup from Fig. 5.1 with the thermocouple (green and white wires) inserted into the end-mass. The hairdryer shown provides the temperature fluctuations.

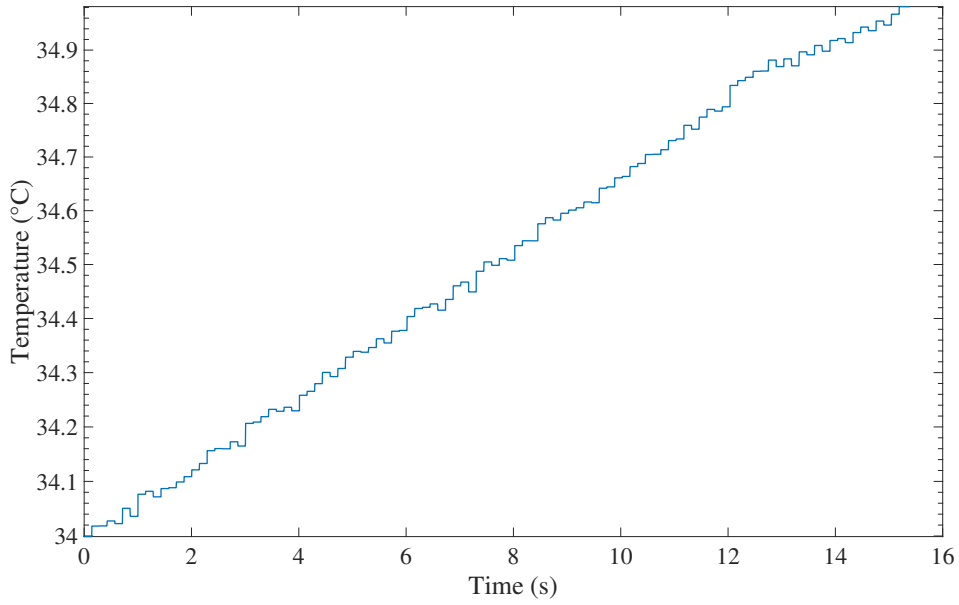

Figure 5.15: Typical temperature history for the energy harvester. The temperature was recorded by thermocouple inserted into the end-mass. We can see that although the overall rate of heating was fairly consistent, there was still some variation present.

Generating thermal noise

The stochastic thermal input was generated using a hairdryer, the idea being that the turbulent airflow would create convection currents. It was hoped that these convection currents would contain pockets of cool and hot air. The turbulent nature should then provide a stochastic thermal source. Pointing the hairdryer directly at the piezoelectric patch did not provide a sufficiently noisy thermal source, instead it was necessary to offset it slightly so that the airflow from the hairdryer passed by the side of the harvester. This still led to heating of the piezoelectric patch, as shown in Fig. 5.15, however the heating signal was considerably noisier. It should be noted that this was a largely qualitative process, and it is suggested that any future experiments seek to somehow control the variation present in the thermal source. The hairdryer was set at the highest heat setting, but the lowest fan setting.

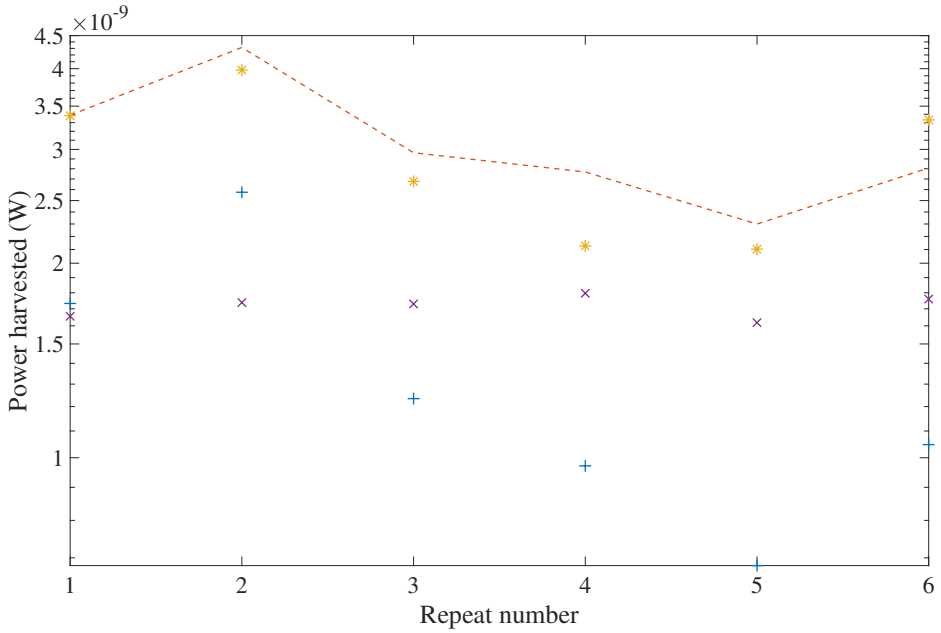

Figure 5.16: Experimental results showing the time-averaged power from each source for the six repeats. The pluses represent the power harvested from the thermal source separately. The crosses represent the power harvested from the mechanical and electrical sources simultaneously. The asterisks represent the power harvested from the thermal, mechanical and electrical sources simultaneously. The dashed line represents the theoretical prediction (sum of the thermal power and the combined mechanical and electrical power).

5.2.3 Results

Due to the variability of the thermal source, the average power harvested from each combination of sources (thermal; mechanical and electrical; thermal, mechanical and electrical) was taken over six repeats. To give the theoretical prediction shown in Fig. 5.16, the power from the mechanical and electromagnetic sources simultaneously was summed with the power from the thermal source individually. When the average is taken over all six repeats, the theoretical prediction agrees with the measured result when all three sources are active simultaneously, as can be seen in Table 5.2.

5.2.4 Discussion

The results shown in Fig. 5.16 demonstrate that the difference in coupling between the pyroelectric and piezoelectric effect does not significantly effect how power is absorbed by the system. This matches the theoretical predictions featured in Chapter 4.

Table 5.2: The power harvested from each combination of sources, averaged over the six repeats

Combination of sources	Time-averaged power harvested (W)
Thermal source (experimental)	1.37×10^{-8}
Mechanical and electrical sources (experimental)	1.72×10^{-8}
Sum of sources (theoretical)	3.10×10^{-8}
All three sources (experimental)	2.93×10^{-8}

A surprising result is that the expression Eq. (4.24) is still valid for a source with non-stationary mean. We can see from Fig. 5.15 that the thermal source is clearly non-stationary. However, Fig. 5.16 still shows similar trends to Figs. 5.11 and 5.12, where only stationary inputs are present. This is possibly due to the variance remaining relatively stationary, although efforts should be made to quantify this. This result opens up an avenue for future research to investigate whether we can apply the same expression for the maximum power absorbed to both stationary and non-stationary systems, and, if so, understand why this is possible.

5.3 Conclusions

The results from electro-mechanical Experiment A and Experiment B (Figs. 5.11 and 5.12) both demonstrate that the power harvested from two sources is the sum of the power harvested from the individual sources for white-noise inputs. This is also confirmed in experimental findings by Hansen et al. [28], Guo et al. [27], Xu et al. [80], Tan and Panda [72], Xu and Wang [79], Pan et al. [52] and Lee et al. [38]. The novelty of this work lies in showing that this is due to the fact that the power absorbed from two sources is the sum of the power absorbed from the individual sources. The results from Experiment C, shown in Fig. 5.13, demonstrate that, for certain system configurations, the power harvested from two sources is *not* the sum of the power harvested from the individual sources; however, since the input provided by the DAQ and the shaker was not changed for these experiments, it is likely that the absorbed power will have been the same between experiments A, B and C.

Fig. 5.9 shows that even within a structure, the amount of mechanical power absorbed by various parts of the structure is related to the mass. In this case, the mechanical power absorbed by the end-mass was half that absorbed by the structure as a whole.

This supports the expressions for the maximum power absorbed by a single-source mechanical system, given by Eq. (3.15). Using analogies, we can speculate that this result can be used to find the distribution of absorbed power in any system.

The results from the thermo-electro-mechanical experiment, shown in Fig. 5.16, give further confidence in the results for the electro-mechanical experiments, shown in Figs. 5.11 and 5.12. These results all suggest that the power harvested from multiple sources is the sum of the contributions from each individual source. Furthermore, Fig. 5.16 suggests that, for a practical system, the inputs do not necessarily need to have a stationary mean for Eq. (4.24) to hold true. This is an unexpected result and goes beyond the theoretical predictions, though further work is needed to lend validity to this result.

6 Conclusions and Further Work

This thesis develops a method for assessing the efficiency of energy harvesters. The method developed in this thesis for estimating efficiency is simple and robust, requiring only that the input to the system is measured, along with the system response, useful power output and a single system parameter. The method presented is valid regardless of the nature or number of inputs, or the configuration of the system, or the domain of the energy harvester. This method was derived analytically, and validated both numerically and experimentally.

The main finding from the literature review was that, beyond mechanical systems, the lack of a universal framework for describing energy harvesters had made it difficult to compare the performance of different designs. The difficulty of assessing different designs inevitably makes it more challenging for researchers to choose which designs to focus on. Not being able to compare designs also makes it difficult for anyone looking to commercialise energy harvesters or use them for industrial applications.

The reasons behind the lack of a general performance framework were the absence of a unified language to describe energy harvesters, and the wide variety of designs. The lack of any unified language for describing energy harvesters has typically meant that any efficiency measures or effectiveness metrics were limited to a particular domain, for example vibrational or electromagnetic energy harvesters. Another consequence of researchers using domain-specific language was that research on multi-source harvesters has arisen in two separate areas and—judging by the references—neither area is aware of the existence of the other. Within each domain, the variety of different system configurations and inputs meant that efficiency metrics were largely only valid for a few specific examples, with many papers defining their own efficiency measures which were limited to a single design. The approaches employed in this thesis to overcome these problems can be largely categorised as: (a) using a comprehensive system of

analogies to develop a domain-neutral framework for describing the behaviour of energy harvesters, and (b) developing expressions which are valid for arbitrary inputs and system configurations.

As mentioned, the key novel contribution of this thesis is a universal method for the comparison of multi-source energy harvester efficiency. This is something that does not currently exist in the literature and has the potential to significantly aid in the further design of energy harvesting devices by allowing researchers to benchmark and compare designs. This thesis also demonstrates how expressions for the maximum power that can be absorbed by an energy harvester from stochastic inputs can be used to compare different designs.

The key conclusions and a summary of the work related to the three main themes of the thesis will be provided in this chapter. Section 6.1 summarises the work on creating a domain-neutral framework for describing and comparing energy harvesters. Section 6.2 summarises the theoretical work exploring how to calculate a practical measure of efficiency. Section 6.3 summarises the experimental work undertaken to validate the theoretical findings presented. Section 6.4 suggests further avenues of enquiry.

6.1 Domain-Neutral Language for Describing Systems

As previously mentioned, a lack of unified—in particular, domain-neutral—language creates barriers when it comes to sharing research. This has resulted in research on multi-source energy harvesting occurring in two separate areas. Since each area uses different and domain-specific terminology, the abstracts, keywords, and titles used in papers from each area have little in common. This has led to virtually no cross-referencing. At best this means that potential collaboration is limited, and at worst could lead to the duplication of effort. Choosing to use domain-neutral language has the potential to make the field of energy harvesting more unified.

Creating and understanding the system equations for multi-source energy harvesters is made more complicated by the particular way the physical behaviour is expressed in each domain. This becomes very apparent when dealing with coupled thermal systems, as the variables used to describe these systems are not power conjugate variables, which means that the equations used to describe thermal systems cannot be manipulated in the same way as the equations for describing electrical and mechanical systems. In addition, the equations describing mechanical systems are often expressed using displacement, whereas electrical systems tend to be described using current, which makes examining electromechanical coupling harder than it needs to be. In Chapter 2,

we define a dimensionally consistent set of analogies, which makes it possible to describe each system using the same functional form. This allows us to immediately determine whether or not two systems will display similar behaviour. Essentially, using analogies allows us to express thermal, electrical and mechanical systems in a mathematically consistent fashion, which enables the subsequent analysis.

Being able to express each coupled system using the same functional form has a great benefit when analysing these systems: we can treat the entire multi-source system as if it were a single-degree-of-freedom system. Essentially, because each term in each system is mathematically analogous, we can combine them into a matrix form (see Section 4.1.1 for details). Again, since the terms are all mathematically analogous, they relate to the power transfer in the system in the same way. Provided the system of analogies is defined consistently, it is possible to transform and manipulate the expressions for each system in the same way. Combining the multi-source systems in this way allows us to assume arbitrary forms for the system configuration—eliminating dependence on factors such as coupling or whether the system is non-linear. This approach not only significantly simplifies our analysis, but it allows us to further generalise our approach to an arbitrary number of degrees of freedom.

Combining the various systems into a matrix form relies on the fact that kinetic energy and potential energy are mathematically analogous. The key difference lies in whether a system is driven by a flow or an effort source: in a system driven by a flow source, it is kinetic energy that is absorbed by the system; in a system driven by an effort source, it is potential energy that is absorbed. When we use the Lagrangian to derive the system equation in Section 4.2.4—where the generalised coordinates are taken to represent the separate energy domains—we see that it makes no difference if we switch the parameters relating to the kinetic and potential energy, as long as we are consistent in how we change the corresponding variables. This incorporates the idea of duality as well, where we can readily move between describing a system in terms of flow or effort variables. This has the advantage of allowing us to move between impedance analogies or mobility analogies, depending on which one is the most convenient. The system of analogies described in this thesis gives us the freedom to use flow or effort variables to describe the system, without having to worry that our choice will somehow influence the analysis.

The conclusions from the work on defining a system of analogies are:

- Introducing domain-neutral language and a dimensionally consistent system of analogies allows different types of energy harvester to be directly compared to one another.
- Using this system of analogies enables the creation of a matrix representation of n-degree-of-freedom multi-domain energy harvesters.
- This matrix representation and domain-neutral set of analogies can be used as a theoretical framework for describing the behaviour of multi-source energy harvesters.

6.2 A Practical Measure for Efficiency

In the energy harvesting literature (discussed in Chapter 1) for vibrational harvesters, we can find early examples of effectiveness measures that generalised well across linear harmonic energy harvesters; however, these measures were not valid for the non-linear and stochastic energy harvesting solutions which came afterwards. In Section 4.2.1 for stochastic systems, it was possible to eliminate terms which were related to the system response when deriving the expression for the maximum power absorbed by a system from a white-noise excitation. This meant that it was not necessary to make any assumptions regarding the system response, which in turn made it possible to derive an expression for the maximum power absorbed by the system which was independent of the system configuration.

The applicability of these expressions to linear and non-linear systems with either narrowband excitation or harmonic excitations was discussed in Section 4.2.2. For linear systems excited with narrowband noise, treating the excitation as an equivalent white-noise signal will always provide an upper bound on the power that can be absorbed. For non-linear systems, this approach is not guaranteed to provide an upper bound, but will still work in the majority of cases. For both linear and non-linear systems, the power absorbed from a harmonic excitation can not be bounded. To still provide an efficiency measure for systems with non-stochastic inputs, it is necessary to measure the system response and use this to calculate the power into the system.

In Section 4.2.3, further derivations demonstrated that it was possible to assume an arbitrary functional form for the system equation (including any coupling) and still arrive at the same expression for the power absorbed. This involved grouping the entire

system equation into a single function on the system variables and arriving at a point where it could be demonstrated that the predicted response was the same as if the system had been left as separate terms. This not only demonstrated that these expressions were independent of the system configuration, but also valid for most forms of coupling as these expressions depend on the input *only*.

There is an important limitation however: these expressions require that the *causal* system element be linear, and that the systems cannot be coupled through this element. The causal element in electrical systems driven by effort is the capacitance and the causal element in mechanical system driven by flow is the mass. It is clear which element this is, as it is the element that appears in the expression for the power absorbed, and is related to the derivative of the system variable with respect to time. Non-linearity, or coupling through the causal element would affect how the inputs appear in the system equation and could therefore result in different expressions for the power absorbed by the system.

The conclusions from the theoretical work are:

- An approach was developed for calculating the practical efficiency of an energy harvester that was independent of the number or domain of sources, the nature of the input signal, and any static coupling.
- For non-stochastic systems, the power input can be used as the basis for an efficiency metric for comparing energy harvester performance.
- For systems with stochastic inputs, in most cases the upper bound for a white-noise excitation can be used as the basis for calculating efficiency.
- This is the first time effort variables have been used as the generalised coordinate (conventionally displacements are used) in a Lagrangian for describing the behaviour of an energy harvesting system.

6.3 Summary of Experimental Work

For single-source energy harvesters driven by noise, the theoretical expressions suggest that the power absorbed varies linearly with a single system parameter which corresponds to either the kinetic or the potential energy. This was relatively simple to confirm experimentally—all that was required was to vary the appropriate system parameter and check that this caused a linear variation in the power absorbed. The experiment, detailed in Section 3.2, used an electrical system with a voltage input. This required the capacitance to be varied, as the voltage relates to the potential energy of the system.

By using a range of capacitors, it was possible to vary the capacitance of the system, while keeping the input power from the voltage signal the same. Varying the capacitance indeed led to a linear variation in the power absorbed. Performing this experiment provided confidence in the experimental setup used for to examine the behaviour of a multi-source energy harvester.

For multi-source energy harvesters, the theory developed in Chapter 4 suggests that the power input to the entire system is the sum of the power input from each individual source. As such, an experiment was carried out to investigate the power absorbed by a multi-source energy harvester for a varying number of white-noise sources. The two-source experiment is described in Section 5.1 and the three-source experiment is described in Section 5.2. The power absorbed by each source individually was compared with the power absorbed when both sources were active simultaneously. Unfortunately, the variation in the results for the mechanical power absorbed was greater than the electrical power absorbed. We can see this by comparing the relative magnitude of the results for the mechanical power absorbed, shown in Fig. 5.9, with the results for the electrical power absorbed, shown in Fig. 5.10. This difference in the magnitude of the power absorbed from each source made it difficult to check the theoretical prediction, since the sum of the mechanical and electrical power was not significantly greater than the mechanical power absorbed. Nonetheless, the difference in magnitude of the power absorbed—through its similarity to the difference in magnitude of the value of the capacitance and the total mass—did confirm that mass and capacitance could be treated as analogous when describing how energy is distributed within the system.

It was, however, possible to see the predicted trends in the power dissipated electrically, shown in Figs. 5.11 and 5.12. By assuming that the proportion of power dissipated electrically compared to the total power dissipated remained constant—independent of the magnitude of the electrical input signal—it was possible to infer that the power dissipated electrically is directly proportional to the power absorbed. The power dissipated electrically when multiple sources are active is the sum of the power dissipated from each source individually, which implies that the same is true for the power absorbed, especially for linear systems.

One of the key findings from Chapter 4 was that the expression for the input power an energy harvester, given by Eq. (4.41) is valid for arbitrary input signals. This also allows the same expression to be used for calculating the efficiency of systems where the input is a mix of stochastic and deterministic signals. The simplest way to validate this was numerically. The numerical simulation, described in Section 4.3, showed that the input power from the mixed stochastic-deterministic input signal (when calculated

using the input and system response) was the same as the power dissipated. Thus this is a valid approach to calculating the input power to the system.

The multi-source experiments in Section 5.1 were used to illustrate the procedure for estimating and comparing the efficiency of several energy harvesting designs. Once the input power (or the maximum power absorbed for stochastic systems) and the average power harvested had been calculated, it was possible to find the efficiency. The efficiency for several energy harvesters was then compared by treating the individual results in the multi-source experiments as separate harvesters. By comparing the efficiency it could be seen that while the electrical harvester absorbed far less power, this was the most efficient method; and that combining the electrical harvester with the mechanical improved its output considerably, but decreased the overall efficiency. This measure of efficiency can be applied to virtually any energy harvester, thus providing a clear means of comparison.

The conclusions from the experimental work are:

- The analogies used in this thesis represent the physical reality.
- In terms of power absorbed, mass and capacitance determine the distribution of the absorbed power in the system, despite the fact that one relates to kinetic energy, and the other to potential energy.
- The experimental results were used to demonstrate the procedure for calculating the efficiency of energy harvesters.
- Additionally, numerical simulations have shown that the expressions for the power absorbed derived in Chapter 4 are valid for arbitrary input signals.

6.4 Further Work

This work has focused primarily on developing a practical method for assessing the efficiency of energy harvesters. As such there were a number of theoretical questions which remain unanswered and could form the basis for future investigations.

Throughout the derivations presented in both Sections 3.1 and 4.2, it was assumed that the system element relating to the input signal (e.g. capacitance or mass) would be linear. We can describe said element as the *causal element*. While it is hard to imagine a system with a non-linear mass occurring on Earth, we may occasionally find systems with a non-linear capacitance or inductance. It would therefore be useful to examine how a non-linear causal element would affect the power absorbed, and if it is possible to derive a useful expression for the power-absorbed by such a system.

Another assumption is that the system is not coupled through the causal elements. Again, this is unlikely in systems where each degree of freedom is considered as a separate domain; however, if we consider a beam attached to a base using two springs, where the center of mass is not aligned with the center of rotation, we would see dynamic coupling. There would be very definite coupling in the causal elements, and so any translational energy supplied to the system would result in some rotational energy being absorbed as well. Does this add to the overall energy absorbed, or does it lead to energy being stored (and therefore unused) in the rotational degree of freedom? Deriving the expression for the power absorbed by a system with dynamic coupling could provide a possible mechanism for increasing the effective power absorbed and is a question that could be explored in more detail.

The combined thermo-electro-mechanical experiment described in Section 5.2 hints at the idea that perhaps these expressions can be applied to non-stationary systems. It would be worth developing analytical expressions for the power-absorbed by non-stationary systems. On this theme, it would be worth further examining the power absorbed from arbitrary inputs. And finally, the power absorbed from inputs which vary with time in either frequency content or intensity would be an interesting avenue to explore.

Using the framework described in this thesis, it would be useful to perform a comprehensive comparison of energy harvesting designs. This could reveal which of the current designs are the most efficient, enabling researchers to focus their efforts on fruitful areas. Such a review would allow future researchers to benchmark their designs against those already found in the literature and determine quickly whether their design represented an improvement.

Bibliography

[1] A. Alomari, A. Batra, M. Aggarwal, and C. R. Bowen. A multisource energy harvesting utilizing highly efficient ferroelectric PMN-PT single crystal. *Journal of Materials Science: Materials in Electronics*, 27(10):10020–10030, 2016.

[2] S. R. Anton and H. A. Sodano. A review of power harvesting using piezoelectric materials (2003-2006). *Smart Materials and Structures*, 16(3), 2007.

[3] A. F. Arrieta, P. Hagedorn, A. Erturk, and D. J. Inman. A piezoelectric bistable plate for nonlinear broadband energy harvesting. *Applied Physics Letters*, 97(10): 1–3, 2010.

[4] J. Bae, Y. J. Park, M. Lee, S. N. Cha, Y. J. Choi, C. S. Lee, J. M. Kim, and Z. L. Wang. Single-fiber-based hybridization of energy converters and storage units using graphene as electrodes. *Advanced Materials*, 23(30):3446–3449, 2011.

[5] J. Baker, S. Roundy, and P. Wright. Alternative Geometries for Increasing Power Density in Vibration Energy Scavenging for Wireless Sensor Networks. In *3rd International Energy Conversion Engineering Conference*, number 3, pages 1–12, Reston, Virigina, aug 2005. American Institute of Aeronautics and Astronautics.

[6] S. Bandyopadhyay and A. P. Chandrakasan. Platform architecture for solar, thermal, and vibration energy combining with MPPT and single inductor. *IEEE Journal of Solid-State Circuits*, 47(9):2199–2215, 2012.

[7] S. P. Beeby, R. N. Torah, M. J. Tudor, P. Glynne-Jones, T. O'Donnell, C. R. Saha, and S. Roy. A micro electromagnetic generator for vibration energy harvesting. *Journal of Micromechanics and Microengineering*, 17(7):1257–1265, 2007.

[8] A. Betz. *Introduction to the theory of flow machines*. London : Pergamon, Oxford, 1966.

[9] A. Bokulich. Maxwell, Helmholtz, and the unreasonable effectiveness of the method of physical analogy. *Studies in History and Philosophy of Science Part A*, 50(1):28–37, 2015.

[10] B. S. Borowy and Z. M. Salameh. Optimum Photovoltaic Array Size for a Hybrid Wind/PV System. *IEEE Transactions on Energy Conversion*, 9(3):482–488, 1994.

[11] W. Borutzky. *Bond Graph Modelling of Engineering Systems*. Springer New York, New York, NY, 2011.

[12] R. C. L. Bosworth. LXXXIII. The thermal Ohm, Farad and Henry. *The London, Edinburgh, and Dublin Philosophical Magazine and Journal of Science*, 37(274): 803–808, 1946.

[13] R. C. Buchanan. *Ceramic Materials for Electronics: Third Edition*. Marcel Dekker, Cincinnati, Ohio, 2004.

[14] I. J. Busch-Vishniac. *Electromechanical Sensors and Actuators*. Mechanical Engineering Series. Springer New York, New York, NY, 1999.

[15] D. Choi, K. Y. Lee, M. J. Jin, S. G. Ihn, S. Yun, X. Bulliard, W. Choi, S. Y. Lee, S. W. Kim, J. Y. Choi, J. M. Kim, and Z. L. Wang. Control of naturally coupled piezoelectric and photovoltaic properties for multi-type energy scavengers. *Energy and Environmental Science*, 4(11):4607–4613, 2011.

[16] A. Collado and A. Georgiadis. Conformal hybrid solar and electromagnetic (EM) energy harvesting rectenna. *IEEE Transactions on Circuits and Systems I: Regular Papers*, 60(8):2225–2234, 2013.

[17] J. Colomer, J. Brufau, P. Miribel, A. Saiz-Vela, M. Puig, and J. Samitier. Novel autonomous low power VLSI system powered by ambient mechanical vibrations and solar cells for portable applications in a 0.13μ technology. *PESC Record - IEEE Annual Power Electronics Specialists Conference*, pages 2786–2791, 2007.

[18] J. Colomer-Farrarons, P. Miribel-Català, A. Saiz-Vela, and J. Samitier. A Multi-harvested Self-Powered System in a Low-Voltage Low-Power Technology. *IEEE Transactions on Industrial Electronics*, 58(9):4250–4263, 2011.

[19] F. Cottone, H. Vocca, and L. Gammaitoni. Nonlinear energy harvesting. *Physical Review Letters*, 102(8):1–4, 2009.

[20] M. Dini, A. Romani, M. Filippi, and M. Tartagni. A Nano-Current Power Management IC for Low Voltage Energy Harvesting. *IEEE Transactions on Power Electronics*, 31(6):1–1, 2015.

[21] A. Georgiadis, A. Collado, S. Via, and C. Meneses. Flexible hybrid solar/EM energy harvester for autonomous sensors. *IEEE MTT-S International Microwave Symposium Digest*, pages 6–9, 2011.

[22] M. Ghandchi Tehrani and S. J. Elliott. Extending the dynamic range of an energy harvester using nonlinear damping. *Journal of Sound and Vibration*, 333(3):623–629, 2014.

[23] P. Glynne-Jones, M. J. Tudor, S. P. Beeby, and N. M. White. An electromagnetic, vibration-powered generator for intelligent sensor systems. *Sensors and Actuators, A: Physical*, 110(1-3):344–349, 2004.

[24] P. L. Green, K. Worden, K. Atallah, and N. D. Sims. The benefits of Duffing-type nonlinearities and electrical optimisation of a mono-stable energy harvester under white Gaussian excitations. *Journal of Sound and Vibration*, 331(20):4504–4517, 2012.

[25] C. Grossman, H.-G. Roos, and Martin Stynes. *Numerical Treatment of Partial Differential Equations*. Springer Science & Business Media, Heidelberg, 2007.

[26] N. J. Guilar, T. J. Kleeburg, A. Chen, D. R. Yankelevich, and R. Amirtharajah. Integrated solar energy harvesting and storage. *Very Large Scale Integration (VLSI) Systems, IEEE Transactions on*, 17(5):627–637, 2009.

[27] X. Z. Guo, Y. D. Zhang, D. Qin, Y. H. Luo, D. M. Li, Y. T. Pang, and Q. B. Meng. Hybrid tandem solar cell for concurrently converting light and heat energy with utilization of full solar spectrum. *Journal of Power Sources*, 195(22):7684–7690, 2010.

[28] B. J. Hansen, Y. Liu, R. Yang, and Z. L. Wang. Hybrid Nanogenerator for Concurrently Harvesting Biomechanical and Biochemical Energy. *ACS Nano*, 4(7): 3647–3652, 2010.

[29] A. Harb. Energy harvesting: State-of-the-art. *Renewable Energy*, 36(10):2641–2654, 2011.

[30] D. H. Hawes. *Nonlinear Stochastic Vibration Analysis for Energy Harvesting and Other Applications*. PhD thesis, University of Cambridge, 2016.

[31] D. H. Hawes and R. S. Langley. Analysis of the power flow in nonlinear oscillators driven by random excitation using the first Wiener kernel. *Journal of Sound and Vibration*, 412:256–269, 2018.

[32] B. Jaffe, W. R. Cook, and H. Jaffe. *Piezoelectric Ceramics*. Elsevier, 1971.

[33] H. W. Kim, A. Batra, S. Priya, K. Uchino, D. Markley, R. E. Newnham, and H. F. Hofmann. Energy harvesting using a piezoelectric "cymbal" transducer in dynamic environment. *Japanese Journal of Applied Physics, Part 1: Regular Papers and Short Notes and Review Papers*, 43(9 A):6178–6183, 2004.

[34] J. Kymissis, C. Kendall, J. Paradiso, and N. Gershenfeld. Parasitic power harvesting in shoes. *Digest of Papers. Second International Symposium on Wearable Computers (Cat. No.98EX215)*, pages 2–9, 1998.

[35] R. S. Langley. Can An Undamped Oscillator Dissipate Energy? *Journal of Sound and Vibration*, 206(4):624–626, 1997.

[36] R. S. Langley. A general mass law for broadband energy harvesting. *Journal of Sound and Vibration*, 333(3):927–936, 2014.

[37] R. S. Langley. Bounds on the vibrational energy that can be harvested from random base motion. *Journal of Sound and Vibration*, 339:247–261, 2015.

[38] J. H. Lee, K. Y. Lee, M. K. Gupta, T. Y. Kim, D. Y. Lee, J. Oh, C. Ryu, W. J. Yoo, C. Y. Kang, S. J. Yoon, J. B. Yoo, and S. W. Kim. Highly stretchable piezoelectric-pyroelectric hybrid nanogenerator. *Advanced Materials*, 26(5):765–769, 2014.

[39] M. Lee, R. Yang, C. Li, and Z. L. Wang. Nanowire-quantum dot hybridized cell for harvesting sound and solar energies. *Journal of Physical Chemistry Letters*, 1 (19):2929–2935, 2010.

[40] S. Lee, S. H. Bae, L. Lin, S. Ahn, C. Park, S. W. Kim, S. N. Cha, Y. J. Park, and Z. L. Wang. Flexible hybrid cell for simultaneously harvesting thermal and mechanical energies. *Nano Energy*, 2(5):817–825, 2013.

[41] H. Lhermet, C. Condemine, M. Plissonnier, R. Salot, P. Audebert, and M. Rosset. Efficient Power Management Circuit: From Thermal Energy Harvesting to Above-IC Microbattery Energy Storage. *IEEE Journal of Solid-State Circuits*, 43(1): 246–255, 2008.

[42] J. C. Maxwell. *An Elementary Treatise on Electricity*. Cambridge University Press, Cambridge, 2011.

[43] S. Meninger, J. O. Mur-Miranda, R. Amirtharajah, A. P. Chandrakasan, and J. H. Lang. Vibration-to-Electric Energy Conversion. *IEEETransactions on Very Large Scale Integration (Vlsi) Systems*, 9(1):64–76, 2001.

[44] P. D. Mitcheson, T. C. Green, E. M. Yeatman, and A. S. Holmes. Architectures for vibration-driven micropower generators. *Journal of Microelectromechanical Systems*, 13(3):429–440, 2004.

[45] P. D. Mitcheson, P. Miao, B. H. Stark, E. M. Yeatman, A. S. Holmes, and T. C. Green. MEMS electrostatic micropower generator for low frequency operation. *Sensors and Actuators, A: Physical*, 115(2-3 SPEC. ISS.):523–529, 2004.

[46] P. D. Mitcheson, E. K. Reilly, T. Toh, P. K. Wright, and E. M. Yeatman. Transduction Mechanisms and Power Density for MEMS Inertial Energy Scavengers. 278 (April 2016):275–278, 2006.

[47] P. D. Mitcheson, E. M. Yeatman, G. K. Rao, A. S. Holmes, and T. C. Green. Energy Harvesting from Human and Machine Motion for Wireless Electronic Devices. 96 (9):1457–1486, 2008.

[48] S. O. Reza Moheimani and A. J. Fleming. *Piezoelectric Transducers for Vibration Control and Damping*. Advances in Industrial Control. Springer-Verlag, London, 2006.

[49] F. Narita and M. Fox. A Review on Piezoelectric, Magnetostrictive, and Magnetoelectric Materials and Device Technologies for Energy Harvesting Applications. *Advanced Engineering Materials*, 20(5):1–22, 2018.

[50] T. T. Nguyen, T. Feng, P. Häfliger, and S. Chakrabartty. Hybrid CMOS rectifier based on synergistic RF-piezoelectric energy scavenging. *IEEE Transactions on Circuits and Systems I: Regular Papers*, 61(12):3330–3338, 2014.

[51] K. Niotaki, F. Giuppi, A. Georgiadis, and A. Collado. Solar/EM energy harvester for autonomous operation of a monitoring sensor platform. *Wireless Power Transfer*, 1(01):44–50, 2014.

[52] C. Pan, Z. Li, W. Guo, J. Zhu, and Z. L. Wang. Fiber-based hybrid nanogenerators for/as self-powered systems in biological liquid. *Angewandte Chemie - International Edition*, 50(47):11192–11196, 2011.

[53] C. Pan, W. Guo, L. Dong, G. Zhu, and Z. L. Wang. Optical fiber-based core-shell coaxially structured hybrid cells for self-powered nanosystems. *Advanced Materials*, 24(25):3356–3361, 2012.

[54] J. A. Paradiso and T. Starner. Energy scavenging for mobile and wireless electronics. *IEEE Pervasive Computing*, 4(1):18–27, 2005.

[55] C. Park and P. H. Chou. AmbiMax : Autonomous Energy Harvesting Platform for Multi-Supply Wireless Sensor Nodes AmbiMax : Autonomous Energy Harvesting Platform for Multi-Supply Wireless Sensor Nodes. In *IEEE SECON 2006 proceedings*, pages 168–177, 2006.

[56] H. M. Paynter. Analysis and Design of Engineering Systems: class notes for M.I.T. course 2.751, 1961.

[57] S. P. Pellegrini, N. Tolou, M. Schenk, and J. L. Herder. Bistable vibration energy harvesters: A review. *Journal of Intelligent Material Systems and Structures*, 24 (11):1303–1312, 2013.

[58] C. D. Richards, M. J. Anderson, D. F. Bahr, and R. F. Richards. Efficiency of energy conversion for devices containing a piezoelectric component. *Journal of Micromechanics and Microengineering*, 14(5):717–721, 2004.

[59] E. Romero. Energy Harvesting for Autonomous Biomedical Devices. *Proceedings of the ASME 2012 10th International Conference on Nanochannels, Microchannels, and Minichannels*, pages 1–5, 2012.

[60] S. Roundy. *Energy Scavenging for Wireless Sensor Nodes with a Focus on Vibration to Electricity Conversion*. PhD thesis, The University of California, Berkeley, 2003.

[61] S. Roundy. On the effectiveness of vibration-based energy harvesting. *Journal of Intelligent Material Systems and Structures*, 16(10):809–823, 2005.

[62] S. Roundy and Y. Zhang. Toward self-tuning adaptive vibration-based microgenerators. In Said F. Al-Sarawi, editor, *Proc. SPIE 5649, Smart Structures, Devices, and Systems*, number 2, page 373. SPIE, feb 2005.

[63] S. Roundy, P. K. Wright, and K. S. J. Pister. Micro-Electrostatic Vibration-to-Electricity Converters. *Microelectromechanical Systems*, 2002:487–496, 2002.

[64] S. Roundy, E. S. Leland, J. Baker, E. Carleton, E. Reilly, E. Lai, B. Otis, J. M. Rabaey, P. K. Wright, and V. Sundararajan. Improving power output for vibration-based energy scavengers. *IEEE Pervasive Computing*, 4(1):28–36, 2005.

[65] F. K. Shaikh and S. Zeadally. Energy harvesting in wireless sensor networks: A comprehensive review. *Renewable and Sustainable Energy Reviews*, 55:1041–1054, 2015.

[66] W. Shockley and H. J. Queisser. Detailed balance limit of efficiency of p-n junction solar cells. *Journal of Applied Physics*, 32(3):510–519, 1961.

[67] J. Siang, M. H. Lim, and M. Salman Leong. Review of vibration-based energy harvesting technology: Mechanism and architectural approach. *International Journal of Energy Research*, 42(5):1866–1893, 2018.

[68] H. A. Sodano, E. A. Magliula, G. Park, and D. J. Inman. Electric Power Generation from Piezoelectric Materials. In *Proceedings of the 13th International Conference on Adaptive Structures and Technologies*, pages 153–161, 2002.

[69] H. A. Sodano, G. Park, and D. J. Inman. Estimation of electric charge output for piezoelectric energy harvesting. *Strain*, 40(2):49–58, 2004.

[70] H. A. Sodano, D. J. Inman, and G. Park. Comparison of piezoelectric energy harvesting devices for recharging batteries. *Journal of Intelligent Material Systems and Structures*, 16(10):799–807, 2005.

[71] C. Y. Sue and N. C. Tsai. Human powered MEMS-based energy harvest devices. *Applied Energy*, 93:390–403, 2012.

[72] Y. K. Tan and S. K. Panda. Energy Harvesting From Hybrid Indoor Ambient Light and Thermal Energy Sources for Enhanced Performance of Wireless Sensor Nodes. *IEEE Transactions on Industrial Electronics*, 58(9):4424–4435, sep 2011.

[73] M. Tanaka, R. Suzuki, Y. Suzuki, and K. Araki. Microstrip antenna with solar cells for microsatellites. *Proceedings of IEEE Antennas and Propagation Society International Symposium and URSI National Radio Science Meeting*, 2(I):5–6, 1994.

[74] M. Umeda, K. Nakamura, and S. Ueha. Energy Storage Characteristics of a Piezo-Generator using Impact Induced Vibration. *Japanese Journal of Applied Physics*, 36(5B):3146–3151, 1997.

[75] C. Vankecke, L. Assouère, A. Wang, P. Durand-Estèbe, F. Caignet, J. M. Dilhac, and M. Bafleur. Multisource and battery-free energy harvesting architecture for aeronautics applications. *IEEE Transactions on Power Electronics*, 30(6):3215–3227, 2015.

[76] A. A. Vives. *Piezoelectric Transducers and Applications*. Springer Berlin Heidelberg, Berlin, Heidelberg, 2008.

[77] Z. L. Wang, X. Wang, J. Song, J. Liu, and Y. Gao. Piezoelectric nanogenerators for self-powered nanodevices. *IEEE Pervasive Computing*, 7(1):49–55, 2008.

[78] C. B. Williams and R. B. Yates. Analysis of a micro-electric generator for microsystems. *Sensors and Actuators*, 52:8–11, 1996.

[79] C. Xu and Z. L. Wang. Compact hybrid cell based on a convoluted nanowire structure for harvesting solar and mechanical energy. *Advanced Materials*, 23(7): 873–877, 2011.

[80] C. Xu, X. Wang, and Z. L. Wang. Nanowire structured hybrid cell for concurrently scavenging solar and mechanical energies. *Journal of the American Chemical Society*, 131(16):5866–5872, 2009.

[81] Y. Yang, H. Zhang, J. Chen, S. Lee, T. C. Hou, and Z. L. Wang. Simultaneously harvesting mechanical and chemical energies by a hybrid cell for self-powered biosensors and personal electronics. *Energy and Environmental Science*, 6(6): 1744–1749, 2013.

[82] Y. Yang, H. Zhang, S. Lee, D. Kim, W. Hwang, and Z. L. Wang. Hybrid energy cell for degradation of methyl orange by self-powered electrocatalytic oxidation. *Nano Letters*, 13(2):803–808, 2013.

[83] Ya Yang, H. Zhang, Guang Zhu, S. Lee, Z.-H. Lin, and Z. L. Wang. Flexible Hybrid Energy Cell for Simultaneously Harvesting Thermal, Mechanical, and Solar Energies. *ACS Nano*, 7(1):785–790, jan 2013.

[84] H. Yu, Q. Yue, J. Zhou, and W. Wang. A Hybrid Indoor Ambient Light and Vibration Energy Harvester for Wireless Sensor Nodes. *Sensors*, 14(5):8740–8755, 2014.

[85] F. Zahra El Fatnani, D. Guyomar, F. Belhora, M. Mazroui, Y. Boughaleb, and A. Hajjaji. A new concept to harvest thermal energy using pyroeletric effect and Rayleigh-Benard convections. *European Physical Journal Plus*, 131(8), 2016.

[86] H. Zhang, S. Zhang, G. Yao, Z. Huang, Y. Xie, Y. Su, W. Yang, C. Zheng, and Y. Lin. Simultaneously Harvesting Thermal and Mechanical Energies based on Flexible Hybrid Nanogenerator for Self-Powered Cathodic Protection. *ACS Applied Materials and Interfaces*, 7(51):28142–28147, 2015.

[87] H. Zhong, Z. Wu, X. Li, W. Xu, S. Xu, S. Zhang, Z. Xu, H. Chen, and S. Lin. Graphene based two dimensional hybrid nanogenerator for concurrently harvesting energy from sunlight and water flow. *Carbon*, 105:199–204, 2016.

[88] Y. Zi, L. Lin, J. Wang, S. Wang, J. Chen, X. Fan, P. K. Yang, F. Yi, and Z. L. Wang. Triboelectric-pyroelectric-piezoelectric hybrid cell for high-efficiency energy-harvesting and self-powered sensing. *Advanced Materials*, 27(14):2340–2347, 2015.